LAYER-BY-LAYER NANOCOATINGS WITH FLAME RETARDANT AND OXYGEN BARRIER PROPERTIES: MOVING TOWARD RENEWABLE SYSTEMS

A Dissertation

by

GALINA S. LAUFER

Submitted to the Office of Graduate Studies of
Texas A&M University
in partial fulfillment of the requirements for the degree of

DOCTOR OF PHILOSOPHY

Approved by:

Chair of Committee,	Jaime Grunlan
Committee Members,	Terry Creasy
	Hae-Kwon Jeong
	Nicole Zacharia
Head of Department,	Jerald Caton

December 2012

Major Subject: Mechanical Engineering

ABSTRACT

Numerous studies have focused on enhancing the flame retardant behavior of cotton and polyurethane foam. Some of the most commonly used treatments (e.g., brominated compounds) have raised concerns with regard to toxicity and environmental persistence. These concerns have led to significant research into the use of alternative approaches, including polymer nanocomposites prepared from more environmentally benign nanoparticles. These particles migrate to the surface from the bulk during fire exposure to form a barrier on the surface that protects the underlying polymer. This theory of fire suppression in bulk nanocomposites inspired the use of layer-by-layer (LbL) assembly to create nanocoatings in an effort to produce more effective and environmentally-benign flame retardant treatments.

Negatively charged silica nanoparticles of two different sizes were paired with either positively charged silica or cationic polyethylenimine (PEI) to create thin film assemblies. When applying these films to cotton fabric, all coated fabrics retained their weave structure after being exposed to a vertical flame test, while uncoated cotton was completely destroyed. Micro combustion calorimetry confirmed that coated fabrics exhibited a reduced peak heat release rate, by as much as 20% relative to the uncoated control. Even so, this treatment would not pass the standard UL94 vertical flame test, necessitating a more effective treatment.

Positively- charged chitosan (CH) was paired with montmorillonite (MMT) clay to create a renewable flame retardant nanocoating for polyurethane foam. This coating

system completely stops the melting of a flexible polyurethane foam when exposed to direct flame from a butane torch, with just 10 bilayers (~ 30 nm thick). The same coated foam exhibited a reduced peak heat release rate, by as much as 52%, relative to the uncoated control. This same nanobrick wall coating is able to impart gas barrier to permeate plastic film.

Multilayered thin films were assembled with "green" food contact approved materials (i.e., chitosan, polyacrylic acid (PAA) and montmorillonite clay). Only ten CH-PAA-CH-MMT quadlayers (~90 nm thick) cause polylactic acid (PLA) film to behave like PET in terms of oxygen barrier. A thirty bilayer CH-MMT assembly (~100 nm thick) on PLA exhibits an oxygen transmission rate (OTR) below the detection limit of commercial instrumentation ($\leq$0.005 $cm^3/(m^2 \cdot day \cdot atm)$). This is the same recipe used to impart flame retardant behavior to foam, but it did not provide effective FR to cotton fabric, so a very different recipe was used.

Thin films of fully renewable electrolytes, chitosan and phytic acid (PA), were deposited on cotton fabric in an effort to reduce flammability through an intumescent effect. Altering the pH of aqueous deposition solutions modifies the composition of the final nanocoating. Fabrics coated with highest PA content multilayers completely extinguished the flame and reduced peak heat release (pkHRR) and total heat release of 60% and 76%, respectively. This superior performance is believed to be due to high phosphorus content that enhances the intumescent behavior of these nanocoatings.

DEDICATION

To my family, who offered me unconditional love, support and encouragement throughout the course of my graduate studies.

ACKNOWLEDGEMENTS

I would like to thank many people who have helped me through the completion of this dissertation. The first is my advisor, Dr. Jaime Grunlan, who is the true embodiment of a mentor. I am very thankful for his guidance, encouragement and enthusiasm for my project over the years. I also thank my committee members, Dr. Creasy, Dr. Jeong, and Dr. Zacharia for their valuable insight.

My sincere thanks goes to my fantastic undergraduate assistants, Rico Martinez and Christopher Kirkland, whose hard work and dedication helped to keep my research run smoothly and efficiently. I also acknowledge the former and current graduate students of the Polymer Nanocomposites Lab, Dr. Morgan Priolo, Dr. Yong Tae Park, Dr. Yu-Chin Li, Dr. You-Hao Yang, Gregory Moriarty, David Hagen, Amanda Cain, and Bart Stevens for the stimulating discussions and for all the fun we have had in the last four years. I also thank Brennan Bailey for lots of emotional support and always being there for me. I truly appreciate your friendship.

Finally, I would like to thank my mother for her unconditional love and support. I owe everything to you. My deepest gratitude goes to husband, Jon, for inspiring and believing in me even when I did not have faith in myself. No word can express how thankful I am for your love and support. I would also like extend my gratitude to Jon's family for their love, prayers and encouragement.

NOMENCLATURE

AFM	Atomic Force Microscopy
ASTM	American Society for Testing and Materials
BL	Bilayer
CNT	Carbon Nanotube
CH	Chitosan
DWNT	Double-Walled Carbon Nanotube
HRR	Heat Release Rate
LbL	Layer-by-layer
MCC	Microscale Combustion Calorimeter
MMT	Montmorillonite
OTR	Oxygen Transmission Rate
PA	Phytic Acid
PAA	Poly(acrylic acid)
PAAm	Poly(allylamine)
PEI	Branched Polyethylenimine
PET	Poly(ethylene terephthalate)
pkHRR	Peak Heat Release Rate
PLA	Poly(lactic Acid)
PNC	Polymer Nanocomposites
POSS	Polyhedral Oligomeric Silsesquioxane

PSP	Poly(sodium phosphate)
PS	Polystyrene
QCM	Quartz Crystal Microbalance
QL	Quadlayer
SEM	Scanning Electron Microscopy
SWNT	Single-Walled Carbon Nanotube
TEM	Transmission Electron Microscopy
TGA	Thermogravimetric Analysis
UV-Vis	Ultraviolet-Visible Light Spectroscopy

TABLE OF CONTENTS

Page

Page

Page

LIST OF FIGURES

FIGURE Page

FIGURE Page

FIGURE Page

FIGURE Page

LIST OF TABLES

CHAPTER I

INTRODUCTION

1.1 Background

The flammability of upholstered furniture and bedding is a subject of growing interest because of the risk posed by such items in the event of fire.[1-2] These objects are easily ignited and can fuel intense fires with significant smoke and toxic gas. Although the number of house fires has significantly declined in the United States in recent years, according to the National Fire Protection Association, there were 369,500 house fires in 2010, resulting in 13,350 civilian injuries and 2,640 civilian deaths, and almost $7 billion in direct damage. Brominated compounds are one of the most commonly used flame retardant (FR) treatments, but there have been concerns raised with regard to their toxicity and environmental persistence.[3-4] These concerns have led to significant research into the use of alternative FR chemistries and approaches, including polymer nanocomposites prepared from more environmentally benign nanoparticles (e.g., clays[5-11] and carbon nanotubes[12-14]). Unfortunately, while being relatively non-toxic, nanoparticles often require high levels of loading, leading to additional cost, processing difficulties and deterioration of intrinsic polymer mechanical properties.[8, 15] Despite these challenges, flame retardant nanotechnology can be more useful (or friendly) if implemented directly on the surface of the polymer as a protective barrier,[16-17] which provides the same mechanisms of protection as it does for bulk nanocomposites,[6, 18] but

eliminates the challenges associated with processing or undesirable changes in mechanical behavior.

Layered silicates have been intensely studied as an environmentally-friendly alternative to the use of halogenated compounds in flame retardant treatments.[5, 7-8] One proposed mechanism for flame retardancy of nanocomposites is the formation, during combustion, of an inorganic barrier on the surface that protects the underlying polymer from oxygen and reduces heat transfer. This physical barrier is made of nanoparticles that migrated to the surface from the bulk.[19-20] It was this theory of fire supression in bulk nanocomposites that inspired the use of layer-by-layer assembly to create dense nanocoatings in an effort to produce more effective and environmentally-benign FR treatments.

Thin assemblies of polymer and clay, deposited onto cotton fibers using layer-by-layer (LbL) assembly, were recently reported as a more environmentally-friendly FR treatment.[17] Colloidal silica is another inorganic additive known to reduce flammability [21-23] and has also been successfully incorporated into the LbL process.[24-26] LbL deposition consists of building multilayered thin films by consecutive adsorption of oppositely charged polyelectrolytes and/or nanoparticles onto a substrate, as shown in Figure 1.1.[27-29] Steps 1 – 4 are continuously repeated until the desired number of bilayers (BL) (*i.e.*, cationic-anionic pairs of layers) is achieved. The thickness of each BL is typically 1-100 nm and can be controlled at the nanoscale by altering pH,[30-31] molecular weight of the components,[32] ionic strength,[33] and temperature.[31, 34] This versatile process has been used to grow films with antireflective,[35-37] oxygen barrier,[38]

sensing,[39-41] electrochromic,[42-44] antimicrobial,[45-47] and drug delivery [48-49] properties. With LbL assembly, nanoparticles are deposited directly onto the surface of the substrate as a thin layer, which allows protection to be imparted without the challenges associated with processing or adversely modifying mechanical behavior. These qualities result in a highly effective, environmentally-friendly nanocoating for fire suppression.

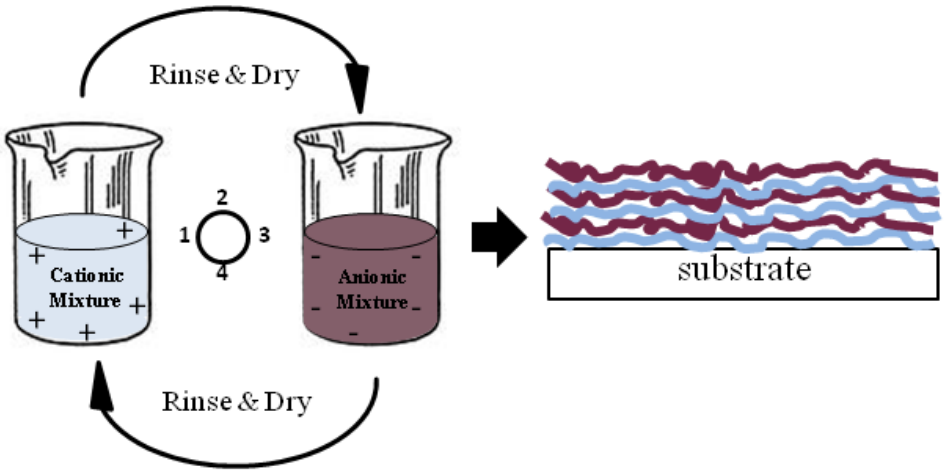

Figure 1.1. Layer-by-layer deposition process used to prepare functional thin films from aqueous mixtures. Steps 1 – 4 are repeated until the desired number of bilayers are generated on a substrate.

1.2 Objectives and Dissertation Outline

Cotton fabric and polyurethane foam are the model substrates used throughout the flame retardant part of this dissertation because they are commonly used for apparel, home furnishings, and industrial products, and they are highly flammable.[50-51] By coating these substrates with a flame retardant nanocoating, we intend to eliminate melt dripping of the foam and to slow down or eliminate the burning process of the fabric to

reduce injury and property damage as a result of exposure to fire. The objective of this portion of my research is to develop and examine the efficacy of flame retardant nanocoatings deposited onto the three-dimensional surfaces of cotton fabric and open-celled polyurethane foam via layer-by-layer assembly. These thin coatings serve as a protective barrier against direct flame and heat. The ultimate goal of this work is to create a conformal coating for complex substrates and extinguish flame on the coated substrate when exposed to fire.

This work with clay also led to the development of gas barrier layers. Clay is well known to reduce the oxygen permeability of bulk composites,[52] but barrier layers made with LbL assembly have been shown to rival SiOx and metalized film.[53] In the present work, polyethylene terephthalate (PET) and polylactic acid (PLA) were chosen as model substrates. PET is already widely used for food packaging applications due to its transparency and a relatively low oxygen transmission rate. PLA is a starch-based polymer that is biodegradable and compostable,[54-55] but it has poor oxygen barrier properties relative to petroleum-based PET, which significantly limits its use in packaging.[56-57] The objective of the oxygen barrier part of my research is to develop a clay-based high oxygen barrier coating using LbL assembly of only food-contact approved materials. These coatings, resembling nanobrick walls, where clay platelets act as bricks held together by polymeric mortar, create highly impermeable layers. These assembled thin films could be used for a variety of food packaging applications, including microwaveable foil replacement.

Chapter II provides a brief review of the flame retardant, oxygen barrier, and layer-by-layer assembly literature. The combustion of polymers and the flame retardant methods and mechanisms are first presented, followed by flame retardant strategies. The tortuosity in clay-based nanocomposites is also described. The second part of this review covers the basics of LbL assembly, with special emphasis on the use of natural materials.

Chapter III describes negatively charged colloidal silica of two different sizes, paired with either polyethylenimine (PEI) or positively charged silica, as the components of multilayer assemblies. The influence of silica size as well as nature of the cationic component (polymer vs. inorganic nanoparticle) on growth and mass composition was examined using ellipsometry and quartz crystal microbalance (QCM), respectively. The conformal nature of these coatings was confirmed using transmission electron microscopy (TEM) and scanning electron microscopy (SEM). Additionally, the flammability of the coatings on cotton fabrics was investigated using a vertical flame test (ASTM D6413) and a micro combustion calorimeter (MCC).

Chapter IV examines the use of fully renewable and environmentally-friendly materials in flame retardant nanocoatings. Chitosan (CH) and montmorillonite clay (MMT) are the components of these renewable assemblies. Films were grown with CH at pH 3 and 6 and characterized on silicon wafer before depositing them onto flexible polyurethane (PU) foam. Small scale torch burn testing and a cone calorimeter (ASTM E-1354/ISO 5660) were used to evaluate the flammability of the coated foam.

Chapter V describes two types of coatings developed with food contact approved materials with high oxygen barrier. The first coating is a chitosan-clay nanobrick wall

film, like that described in Chapter IV. In the second system, polyacrylic acid (PAA) was added to the CH-MMT assembly, creating a CH-PAA-CH-MMT quadlayer system. Both of these coatings were deposited on PET and PLA film and tested for oxygen transmission rate at 23°C/0% RH and 38°C/ 90% RH. Light transmission through this coating was measured using UV-Vis spectroscopy.

Chapter VI describes the first intumescent nanocoating created via LbL assembly using renewable materials. Chitosan and phytic acid (PA) are nitrogen and phosphorus-rich components that were used to create this coating. The effect of the solution's pH on the coating growth and composition was examined using ellipsometry and QCM. Coatings with different PA concentration were evaluated for their flammability on cotton fabric.

Chapter VII provides some conclusions and direction for future research. This dissertation investigates flame retardant nanocoatings via passive (silica or clay-based) or active (intumescent) mechanisms of protection, as well as using renewable, food contact approved materials to create nanocoatings with high oxygen barrier (see Figure 1.2). Creating high oxygen barrier with renewable, food contact safe polyelectrolytes only (i.e., without clay) remains to be studied. To further improve flame retardant coatings on cotton, and make it more commercially viable, the durability of the coating needs to be improved using crosslinking to withstand multiple wash cycles. Finally, the synergistic influence of colloidal silica in intumescent coating assemblies could improve FR performance with fewer layers.

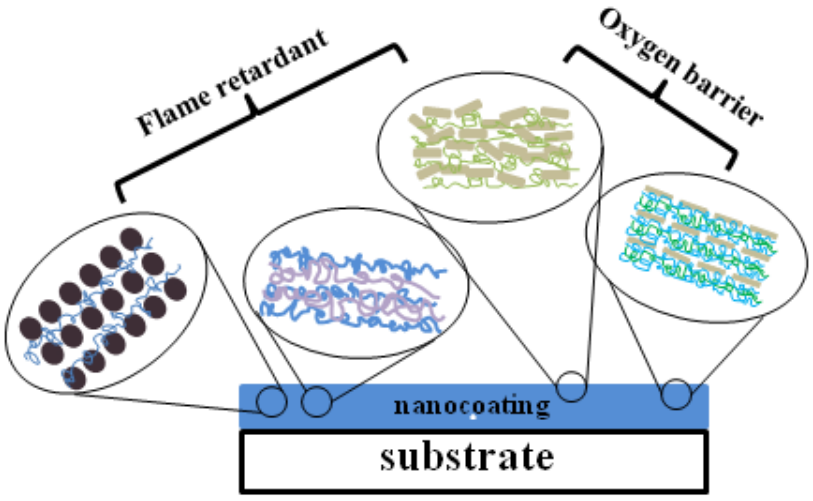

Figure 1.2. Schematic overview of coatings with flame retardant (left to right: colloidal silica-based, intumescent, clay-chitosan) and oxygen barrier (chitosan-based bilayer and quadlayer systems) properties.

CHAPTER II

LITERATURE REVIEW

2.1 Thermal Decomposition of a Polymeric Material

Polymeric material yields volatile gases, smoke and carbonaceous char, after it has been exposed to significant heat. There are both physical and chemical changes that occur when heat is applied. Physical changes include melting and charring, while chemical processes are responsible for generating flammable volatiles.[58] The overall burning process is schematically shown in Figure 2.1. The heat and gases flow back and forth between fire and composite, increasing the temperature in the combustion zone, and as a result accelerate decomposition of the material. The process then continues as long as the heat flow to the polymer is sufficient to sustain burning or until the material is completely degraded.[59] Sometimes, if the above heat requirements are satisfied by thermal oxidation (in gas or condensed phase), a self-sustaining degradation process can occur, even after the heat supply from the ignition source is removed.[60]

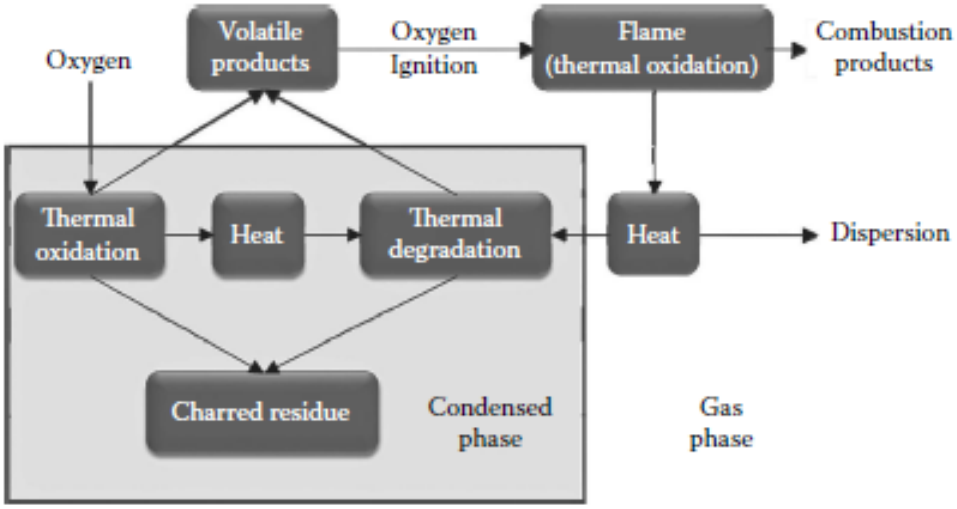

Figure 2.1. Self-sustained polymer combustion cycle.[60]

Due to their unique structures, different polymeric materials decompose via different routes. When heated, the polymer chain breaks down into small fragments, which can then escape into the vapor phase.[61] In general, polymer degradation occurs by four mechanisms: random-chain scission, end-chain scission, chain-stripping, and other processes such as crosslinking.[62] In random chain scission, polymer chains break at random points along their length. In end-chain scission, the chains release groups from their ends most easily. A third process, in which groups that easily release are attached to the backbone as side chains, is known as chain stripping. The other mechanism of degradation is a crosslinking process, which is related to the formation of char. This happens when the polymer chain goes through carbonization instead of undergoing chain scission to form volatiles.[63]

The nature of the volatile products depends on the chemical and physical properties of the polymer. Figure 2.2 shows the range of chemical and physical changes that can occur when a polymer is exposed to heat. Some of these changes are simple phase transformations (solid→ liquid → gas). Thermoplastic materials form a viscous melt, but they may also decompose before melting. Viscous melt can decompose into either liquid or gaseous fragments. Liquid components will decompose further until they are small enough to be vaporized. Polyurethanes (especially flexible foams) decompose by three different mechanisms: breakdown of urethane molecules into gaseous isocyanates, which are released as a yellow smoke, a concerted reaction involving a six-membered cyclic transition state, and a cleavage-recombination mechanism.[64-67] Cellulose materials, like wood or cotton, decompose into three types of products: laevoglucosan, char, and a series of high molecular weight tar.[68] These varied thermal degradation mechanisms between different materials have a significant influence on fire behavior.

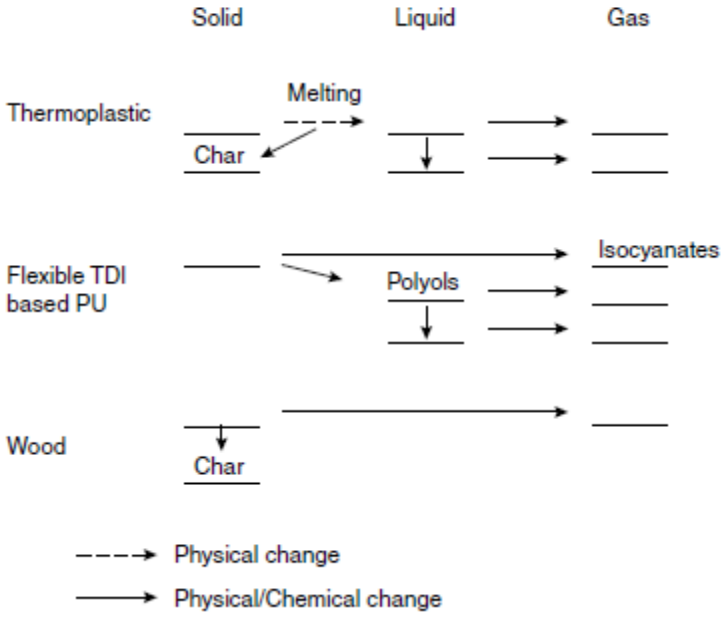

Figure 2.2. Physical and chemical changes that occur during polymer thermal decomposition.[58]

2.2 Flame Retardant Strategies

Flame retardant behavior can be divided into two different modes of action that break the polymer combustion cycle. A retardant can stop the combustion cycle in the condensed phase or gas phase.[69] A condensed-phase mechanism occurs when a FR chemically interacts with the polymer to generate char. Another form of the condensed phase mechanism is incorporation of filler into the polymer matrix, which dilutes the amount of combustible material and reduces the burn temperature of the composite.[70] In the gas phase, flame retardants reduce the amount of heat returned to the polymer surface and, as the temperature of the surface decreases, the pyrolysis is retarded.[71] The

flammability behavior of a polymer is usually evaluated with cone calorimetry, which measures ignition time, mass loss, and heat release rate.

2.2.1 Polymer Nanocomposites

Composites made with nanosize filler are referred to as polymer nanocomposites (PNC). Nanoparticles used in polymer composites are often described by the number of nanoscale dimensions, as shown in Figure 2.3. There are layered materials (2D) like montmorillonite clay (MMT),[6, 72] layered double hydroxides (LDH),[73] layered zirconium phosphate,[74] tube/rods (1D) like carbon nanotubes,[75] and spherical/colloidal solids (0D) like polyhedral oligosilsesquioxane (POSS) or colloidal silica.[76-78] Interfacial interaction between polymer and particle greatly affects the degradation of nanocomposites. A strong interaction allows particles to act as restriction sites for the movement of a polymer chain, making the scission chain harder at lower temperature, and moving the degradation temperature of the material to higher temperature.[79] Since nanoparticles have high surface area-to-volume ratio, for the same particle concentration, they will have a greater interfacial area than microparticles. [80-81] This large interfacial area causes a significant amount of the polymer to come into direct contact with particles and its properties become much different from the bulk polymer.[82]

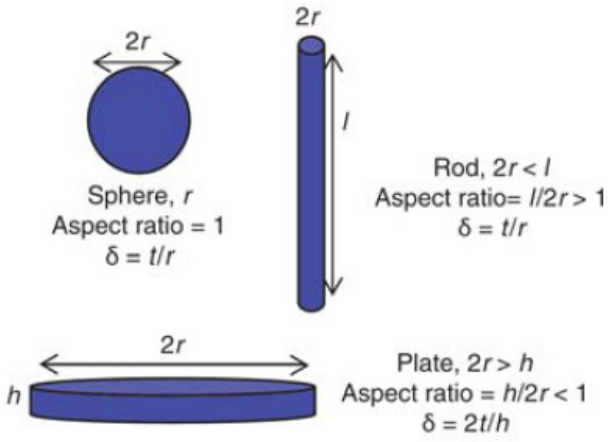

Figure 2.3. 2D (platelet), 1D (rod), and 0D (sphere) nanoparticles and definitions of their aspect ratios.[83]

The objective of PNC fabrication is to uniformly disperse and distribute the filler within the polymer. The final structure will depend on the processing techniques utilized. Simple physical mixing of a polymer and nanoparticles does not typically result in a PNC, but rather creates a conventional composite with relatively poor mechanical and thermal properties because of phase separation.[80] For clay-filled composites the intercalation method is most popular and it can be divided into intercalation of polymer from solution, in-situ intercalative polymerization and melt intercalation.[84] Intercalation from solution means clay is first swollen in a solvent and then mixed with a polymer. Polymer chains displace the solvent and intercalate within the layers of clay.[85-86] For the polymerization intercalation, clay is swollen in a monomer solution, then polymerization occurs and polymer chains are forced into the space between clay sheets, thus separating them and making them intercalated or exfoliated.[87-

[88] The melt method involves annealing a mixture of the polymer and clay above the softening point of the polymer.[89-90] There are three main morphologies of clay-polymer nanocomposites that can be obtained, as shown in Figure 2.4.[91] If the polymer cannot intercalate into the silicate sheets, a conventional composite is obtained. Intercalated structures are formed when there is a polymer chain separating the silicate layers, resulting in ordered structure. When clay platelets are completely dispersed in a polymer matrix, exfoliated composites are formed. The exfoliated structure is favorable to many properties due to its isotropic behavior.[15]

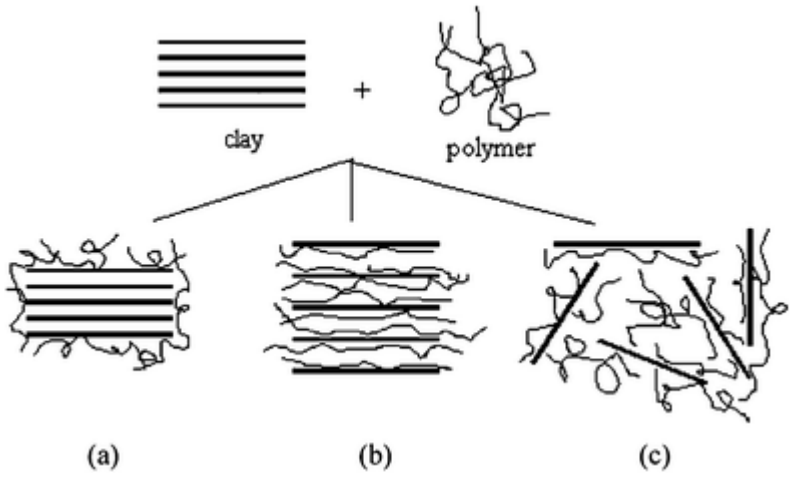

Figure 2.4. Schematic representation of conventional (a), intercalated (b) and exfoliated (c) clay filled composites.[72]

Incorporating layered silicates into polymers was first reported over forty years ago,[92] but it wasn't until 1997 that a detailed investigation of the flame retardant properties of polymer/clay was reported, which inspired numerous further studies in this field.[93] Montmorillonite clay (MMT) is the most studied layered silicate for polymer

nanocomposites.[94-96] In addition to improving antiflammable properties,[97] it has been used to enhance mechanical[94] and gas barrier[72, 98] properties. MMT is a member of the smectite family in which an individual clay platelet is composed of one central layer of Al^{3+} or Mg^{2+} octahedra sandwiched between two layers of Si^{4+} tetrahedral, as shown in Figure 2.5.[99] The thickness of each individual clay platelet is approximately one nanometer.

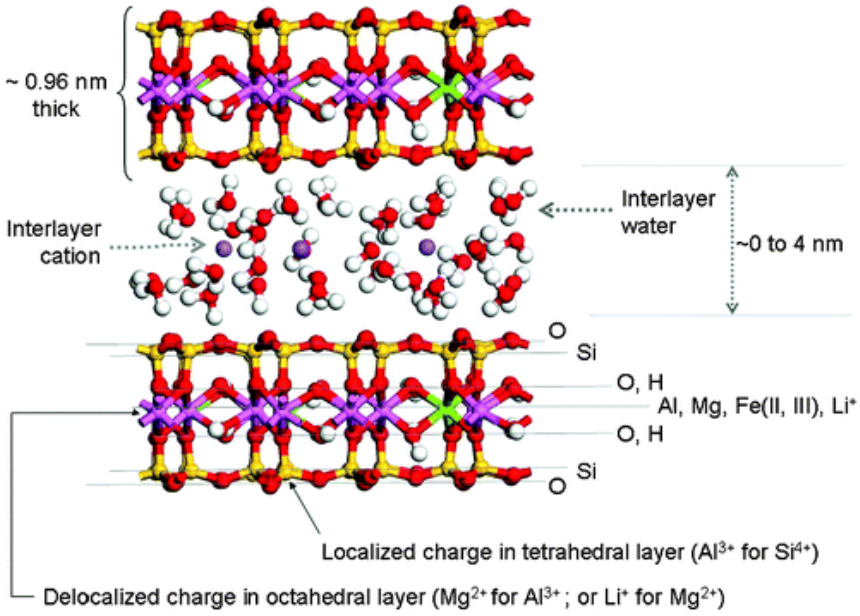

Figure 2.5. Structure of smectite clay.[99]

In addition to clay, carbon nanotubes (CNT) are becoming more commonly used in PNC.[100-102] Carbon nanotubes are long cylinders of covalently bonded carbon atoms and have a very high aspect ratio.[75] The two basic types of CNT are single-wall carbon nanotubes (SWNT) and multiwall carbon nanotubes (MWNT) (Figure 2.6). CNTs have

remarkable mechanical,[103] electrical[101] and thermal[102] properties that make them good candidates for filler in PNC. One major drawback is that CNTs are often held together in bundles by very strong Van der Waals interactions, which makes their dispersion within a polymer matrix problematic.[104] Despite this dispersion issue, CNT is the second most investigated nanofiller for reducing the flammability of polymers.[12, 76]

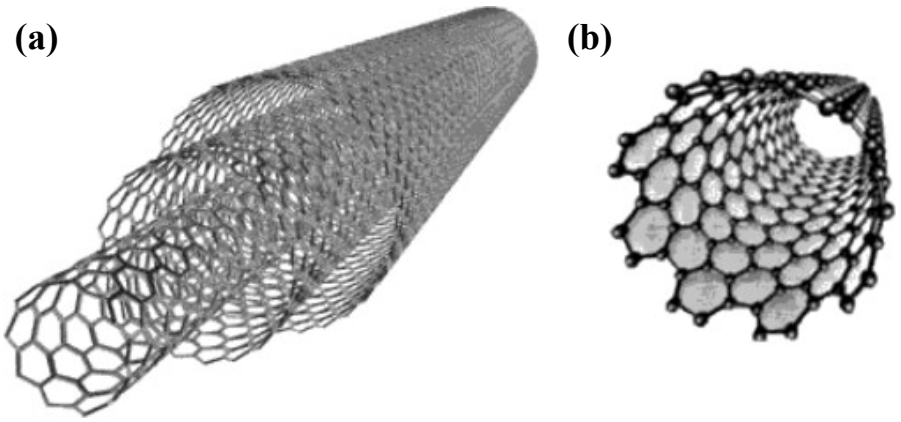

Figure 2.6. Schematic representation of multi-walled (a) and single-walled (b) carbon nanotubes.[105]

Together, layered silicates and carbon nanotubes represent almost half of the ongoing studies on PNC.[83] There are many other FR additives that have been used to reduce flammability of polymer composites. Layered double hydroxide (LDH) is another commonly used 2D inorganic material. The LDH structure is referred to as natural hydrotalcite and it is very similar to layered silicates (Figure 2.7).[106] The flame-retardant characteristics of LDH originate from their chemistry, which involves endothermic decompositions with the formation of water vapor and metal oxide residue. This residue

reduces the oxygen supply to the composite and thus hinders the burning process.[107] Similarly to other inorganic additives, it is hard to achieve good dispersion of LDH within the composite due to strong interactions between its layers.[108]

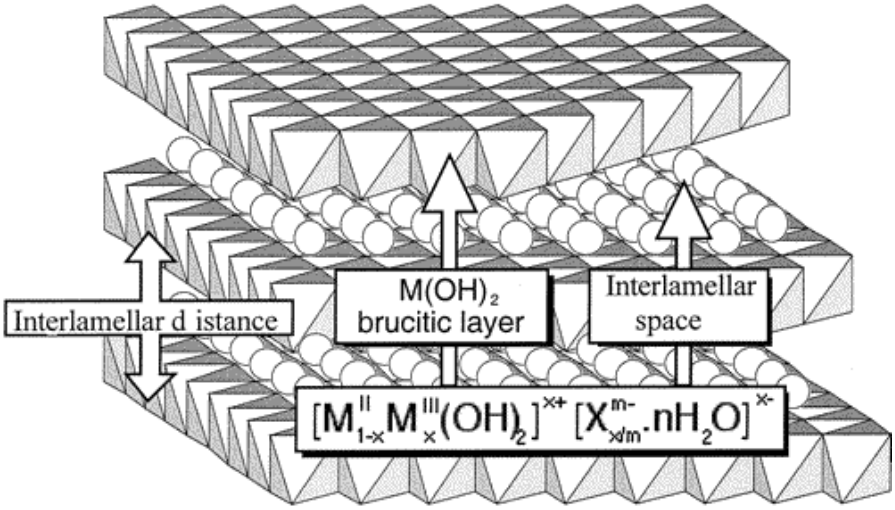

Figure 2.7. Schematic of LDH structure.[106]

Polyhedral oligomeric silsesquioxane (POSS) is one example of a zero dimensional nanoparticle, whose general structure is shown in Figure 2.8. POSS is an inorganic-organic hybrid, containing an inorganic siloxane-like core, $Si_{18}O_{12}$, and organic substituents that can be modified with various groups.[77] It is believed that POSS migrates to the surface of the composites during combustion to form a ceramic-like layer. This insulating layer slows oxygen permeation and protects the underlying composite from further degradation.[109] Due to the structure of POSS, it can reinforce polymer chain segments and control chain motions by maximizing surface area and interaction with polymers in composites.[109-110] In addition to reducing flammability,

incorporation of POSS is known to improve mechanical behavior.[111] Colloidal silica particles also have a large interfacial area and are known to reduce flammability. [22-23, 112] The flame-retardant mechanism of the silica nanoparticles, similar to POSS, is linked to the coagulation of the particles near the sample surface to form a protective barrier for evolved degradation products.

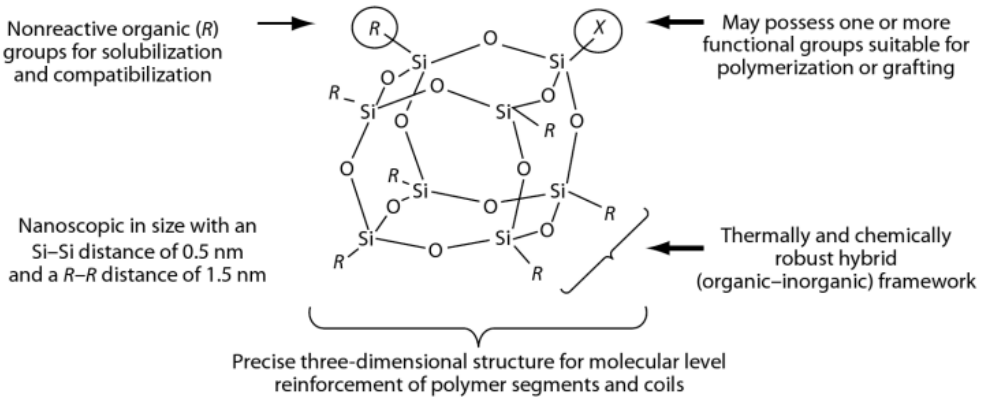

Figure 2.8. General structure of POSS molecule (http://hybridplastics.com).

Metal hydroxides, such as aluminum trihydroxide (ATH) and magnesium hydroxide, can undergo endothermic decomposition to produce water upon heating above 200 °C. This energy absorption is one of the key reasons these materials are flame retardant. As water releases into the vapor phase it dilutes the concentration of combustible gases produced by polymer decomposition, and limits the heat being fed back to the surface of the polymer.[113] These minerals can reflect the heat when they accumulate on the surface. All inorganic hydroxides are relatively nontoxic, but they

generally require more than 50 % by weight of the substrates to pass the various fire tests.[114]

All PNC with inorganic fillers use a similar method to reduce flammability. In general, the nanoparticles reduce mass loss rate by slowing the rate of polymer pyrolysis, which in turn lowers the heat release rate when the polymer burns. The reason for the lowered mass loss rate is the protective barrier formed when the polymer nanocomposites decompose. Nanopartices are pushed by the numerous bubbles of degradation products and migrates to the surface of the polymer matrix.[19, 115] As a result, a protective inorganic barrier is formed on top of the composite surface that provides thermal insulation for the condensed phase, as shown in Figure 2.9.[6, 18]

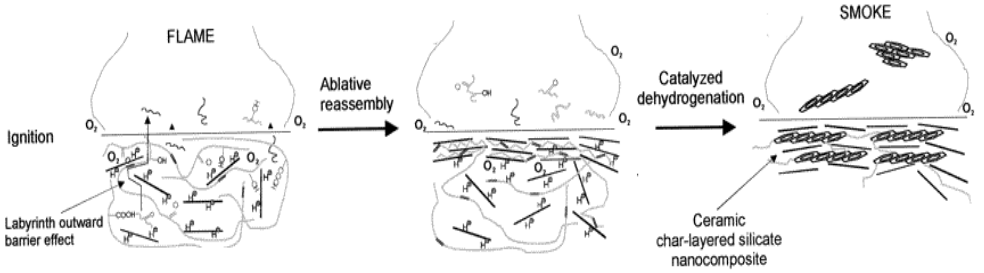

Figure 2.9. Schematic representation of combustion mechanism of PNC.[18]

Another proposed FR mechanism for nanocomposites involves formation of a three-dimensional nanofiller network structure that is formed after filler concentration has reached a critical loading or a threshold value.[76] The threshold value is determined by the percentage and dispersion of the nanoparticles and they can only form the network with good dispersion. This network structure limits the movements of polymer

chains and as a result improves the melt viscosity of polymer nanocomposites. Also, the network structure can reduce the oxygen access to the composite and to the flammable volatiles. With poor dispersion, particles form isolated domains that are too far from each other to form an effective network. In a fire, polymer between these domains burns out very quickly because the regions between the isolated islands are exposed to a constant heat flux, as shown in Figure 2.10. 2D and 1D nanoparticles like clay and CNT can provide denser and more intact char layer than 0D spherical nanoparticles,[116] but spherical particles can also hinder the polymer chains thermal motion. Physical crosslinking between nanoparticles allows the nanocomposite to retain its original shape during combustion.

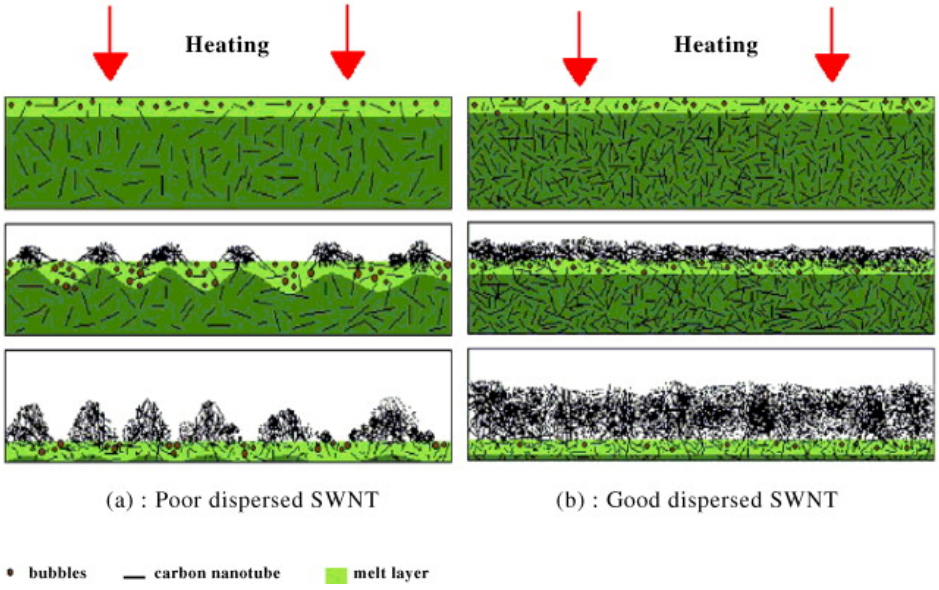

Figure 2.10. Schematic representation of the PNC with poorly dispersed filler (a) and a continuous filler network (b).[117]

In addition to improving flame retardant properties, finely dispersed fillers can also dramatically reduce oxygen permeability of polymer nanocomposites, which is determined by the adsorption rate of gas molecules into the polymer matrix and the diffusion rate of those molecules through the matrix.[52, 118-119] One of the ways dispersed filler improves the barrier properties of a composite is by creating a tortuous path for gas diffusion.[120] Inorganic platelets are impermeable to most gas molecules, forcing them to travel around rather than taking a straight path through the composite, as shown in Figure 2.11. The result is a longer diffusion path for an oxygen molecule through the film in the presence of fillers.[52, 121] The increased diffusion length, referred to as a tortuous path, was first modeled by Nielsen.[122] This model assumes that fillers are shaped like rectangular platelets, that are evenly dispersed throughout the matrix, and supposes that the tortuous path is the only factor influencing the gas diffusion rate. In practice, the Nielsen model is valid only for small loading percentages (< 10 wt%). Improvements on this model include adjustments for random positioning of the filler throughout the matrix,[123-124] as well as filler shape, size and orientation.[119, 125-127]

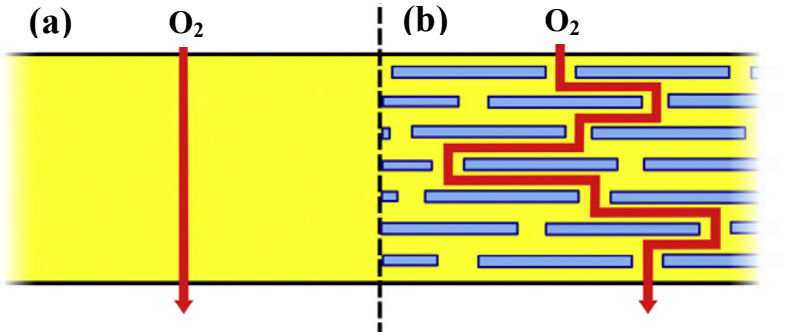

Figure 2.11. Oxygen diffusion path through neat polymer (a) and particles/platelets filled polymer (b).[57]

Clay and other silicate materials are the most studied nanofillers for polymer composites. Incorporation of clay into a polymer matrix has been shown to enhance the gas barrier properties relative to the neat polymer,[128-130] but it is very difficult to obtain complete exfoliation. High loading of nanofillers results in particle aggregation, which limits the achievable diffusion path tortuosity and results in deterioration of other properties like transparency and mechanical strength. In contrast to bulk composites, constructing films using layer-by-layer (LbL) assembly of polymer and clay has been shown to exhibit an oxygen transmission rate (OTR) below 5 x 10^{-3} $cm^3/(m^2 \cdot day \cdot atm)$ (Fig. 2.12 (a)).[38, 131] It is believed the major factor contributing to this low OTR is the extremely high level of clay orientation, with platelets deposited perpendicular to the diffusion direction (Fig. 2.12 (b)). These films contain more than 80 wt% clay and remain completely transparent.

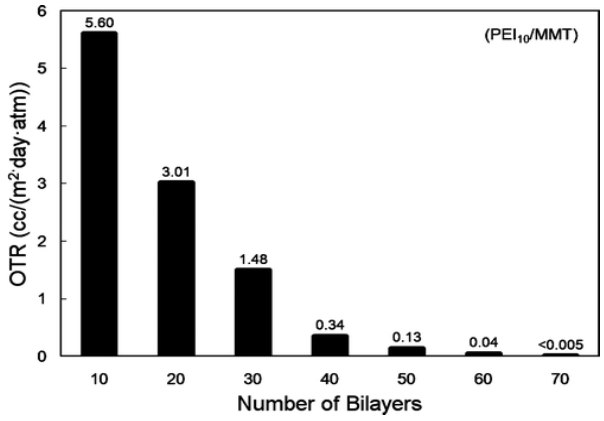

(a)

Figure 2.12. Oxygen transmission rate as a function of the number of PEI-MMT bilayers deposited on PET (a), and a TEM cross-sectional image of a 40-bilayer PEI-MMT film (b).[131]

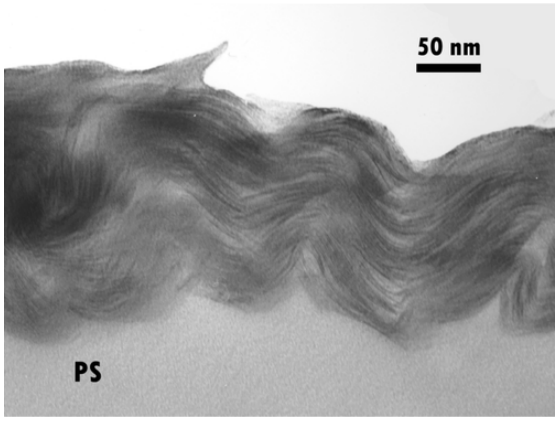

(b)

Figure 2.12. Continued

2.2.2 Other Flame Retardants

2.2.2.1 Halogen Containing FR. The effectiveness of halogen containing flame retardants improves in the order of F< Cl< Br < I.[132] Fluorine and iodine form the strongest and weakest bonds with carbon, respectively, and do not interfere with thecombustion process, so they are not used in practice. Halogen containing FR interrupt the combustion process by interfering with the radical chain mechanism in the gas phase. High energy OH• and H• radicals are replaced with lower energy Br• or Cl• radicals.[60] Bromine is the most effective because its bond to carbon begins to degrade around 290°C, compared to 380°C for C-Cl bond, making Br• radicals more easily available to interfere with combustion. It is also believed that these radicals are released over a narrow temperature range so they are available in high concentration.[60] Chlorine containing FR releases its free radicals over a wide temperature range, which lowers its concentration and makes it less effective.

An alternative theory has been proposed that explains the action of halogens in physical terms.[133] According to this theory, only the total amount of halogen and not its nature is important.[134] When burning polymer is converted to gaseous fuel, the role of the halogens is to increase the total mass of vaporizing material without an equivalent increase in heat flux from the flame.[135] Both approaches, the radical trap theory described above and this physical theory, complement each other. Halogens can inhibit the ignition of polymers, but they will not be very efficient in preventing combustion when the external heat flux is large enough to vaporize most of the polymeric material.

2.2.2.2 Phosphorus containing FR. Environmental concern over the use of halogen-based FR has led to the increased use of phosphorus-based FR.[3, 136] These phosphorus-based compounds can be used as additives, or incorporated into the polymer chain during its synthesis, and can act in the condensed phase by enhancing char [137-138] and in the gas phase by reducing energy of the flame.[132] Phosphorus-based FR are particularly effective in polymers with high oxygen content, such as cellulose. In the presence of P-containing compounds the degradation path of cellulose is altered, flammable gas generation is reduced and dehydration of the cellulose occurs, which promotes char formation.[139-141]

With most phosphorus-containing FR, thermal decomposition leads to the production of phosphoric acid, which condenses to produce pyrophosphate structures and releases water (Fig. 2.13).[142] The pyrophosphoric acid further dehydrates the polymer, forming a carbonaceous layer with a glassy coating. This protective layer shields the underlying polymer from attack by oxygen and heat.[143] Phosphorus-based

flame retardants can also volatilize into the gas phase to form active radicals (PO_2•, PO• and HPO•) and act as scavengers of H• and OH• radicals. Volatile phosphorated compounds are among the most effective combustion inhibitors because phosphorus-based radicals are, on average, five times more effective than bromine and 10 times more effective than chlorine radicals.[144]

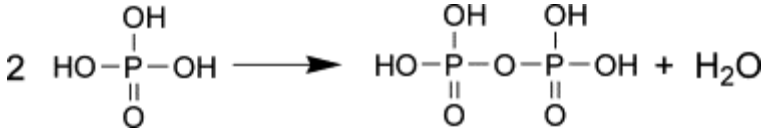

Figure 2.13. Pyrophosphate formation from phosphoric acid condensation.[105]

2.2.2.3 Intumescent FR. Intumescent systems are a subset of FR technology commonly used to protect various construction materials like steel and wood.[145-147] An intumescent system typically requires three components bound together with a binder: a source of carbon (char former), an acid source and a blowing agent that decomposes to cause foaming of the system.[148] Typical examples of components used in intumescent systems are summarized in Table 2.1. During intumescence, the acid is released and esterifies the carbon-rich components at temperatures slightly above the acid release temperature. This mixture of materials then melts prior to, or during, esterification. The ester decomposes via dehydration, resulting in the formation of a carbon-inorganic residue. Gases, released from decomposition of the blowing agent, cause the carbon residue to foam. At the end of the reaction, solidification occurs in the form of multicellular foam (Fig. 2.14).[149] This multicellular layer acts as an insulator, protecting

the underlying material from heat and flame and limiting the diffusion of oxygen into the material.[150]

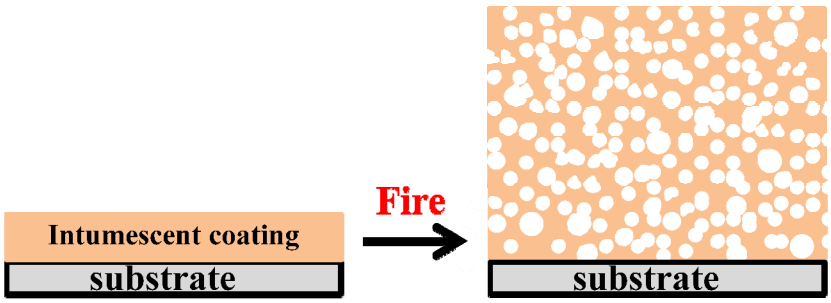

Figure 2.14. Schematic of intumescent coating expansion to form a highly porous, foam-like structure.

Table 2.1. Examples of components in intumescent systems.[149]

(a) Acid source	**(b) Carbonization agent**
Inorganic acid source (phosphoric, sulfuric, boric)	Starch, dextrins, char-former polymers
Ammonium salts (phosphates, borates, sulfates, halides)	
Phosphates of amine or amide (melamine phosphate)	**(c) Blowing agents**
Organophosphorus compounds (tricresyl phosphate, alkyl phosphates)	Urea, melamine, dicyandiamide

2.2.2.4 Miscellaneous FR. Boron containing molecules also have been used to reduce flammability of polymers and nanocomposites (Fig. 2.15(a)).[151-152] The flame retardant mechanism of boron containing molecules is believed to be due to formation of

a borate glass on the surface, which acts as a barrier.[153] Boronic acids are known to release water, which leads to formation of boroxine or boronic acid anhydride that can also form a boroxine glass and lead to high char formation.[154] Nitrogen-based flame retardants have low smoke evolution during combustion, low toxicity and are suitable for recycling.[155] The most important type of organic nitrogen flame retardant is melamine and its derivatives (Fig. 2.15(b)). The main applications for melamine are polyurethane flexible foams,[156] melamine cyanature for nylons,[157-158] and melamine phosphates for polyolefins.[159-160] Hydroxycarbonates are another class of FR additives that are less widely utilized, but serve as an alternative to metal hydroxides (Fig. 2.15(c)). In addition to releasing water at high temperatures, some carbonates (e.g., magnesium carbonate or magnesium hydroxycarbonate) also break down endothermically due to release of carbon dioxide.[161] The temperature range for water and carbon dioxide release for hydroxycarbonates is wider than it is for ATH (200-550 °C versus 180-220 °C), which suggests that they may have similar or better flame retardant properties.[162]

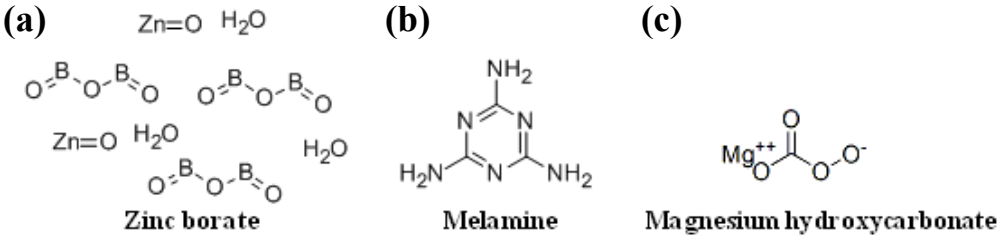

Figure 2.15. Examples of boron-rich (a), nitrogen-rich (b) and hydroxycarbonate (c) molecules used as flame retardant additives.

2.2.3 Layer-by-Layer Assembly

As mentioned in Chapter I, layer-by-layer assembly has become a popular method for construction of multilayer thin films that combines ambient processing and nanoscale control over film structure. Since the pioneering work of Iler in 1966,[163] the polyelectrolyte multilayer concept has been extended by Decher and coworkers in the early 1990s to the deposition of natural materials (e.g., proteins and DNA) and particles.[164-166] Typical LbL deposition consists of building multilayered thin films by consecutive adsorption of oppositely charged polyelectrolytes and/or nanoparticles onto a substrate, as shown in Figure 1.1. This simple procedure is then repeated to deposit a given number of cationic and anionic pairs, known as bilayers (BL). LbL deposition allows for various materials to be incorporated into a film, including conventional polyelectrolytes,[167-168] dendrimers,[169-170] colloidal nanoparticles,[25, 171] porphyrins,[172-173] clay,[174-176] quantum dots,[177-178] nanotubes and nanowires,[179-181] and organic dyes.[182-183] LbL assembly does not require harsh chemical conditions, so it is suitable for using renewable materials. Because many naturally occurring materials have charged sites on their surface, they can be incorporated into LbL structures. This has been demonstrated by assembling films of charged polysaccharides, [184-186] proteins,[187-188] DNA,[189] polypeptides,[190-191] viruses,[192-193] and various enzymes.[194-195]

Chitosan is a renewable polymer that has been used in LbL films for more than a decade.[196] The most distinguishing property of chitosan is biocompatibility, which makes it possible for chitosan to interact with biomolecules without degrading them. Chitosan has been used as a matrix to build devices with tailored properties including

sensing,[197-198] drug and gene delivery,[199] anticoagulant,[200] and antimicrobial.[201-202] Chitosan has been the matrix for several enzymes to preserve their activity.[203-204] One example of a glucose biosensor based on LbL of chitosan and glucose oxidase (GOD), on a Prussian blue film, is shown in Figure 2.16.[205] In addition to flat surfaces, LbL can be applied to three dimensional substrates. Lu et al. used cationic chitosan and anionic carboxymethyl chitosan to build stimuli responsive drug carrying hollow microspheres, as shown in Figure 2.17. Hydrodynamic diameters of the hollow chitosan-based capsules can be controlled by the ionic strength of the media.[206]

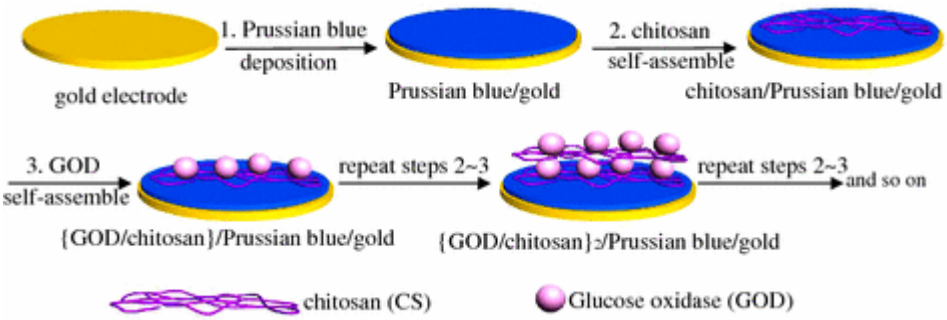

Figure 2.16. Schematic of the preparation process of a glucose biosensor.[205]

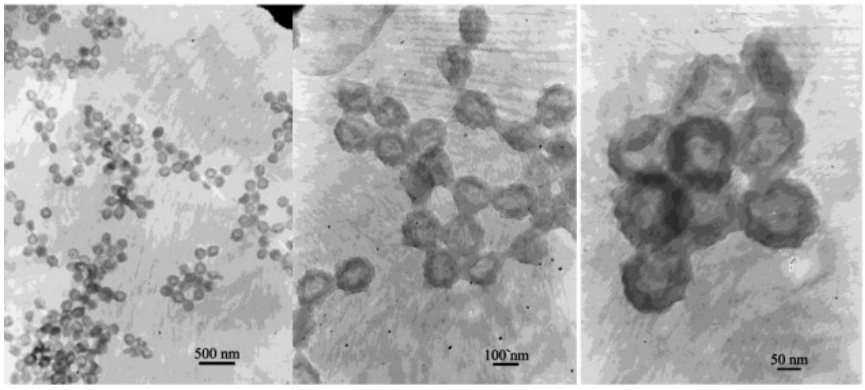

Figure 2.17. TEM images of hollow chitosan microspheres.[206]

Collagen is another natural material that has been deposited using LbL assembly.[207-208] Figure 2.18 shows an AFM surface image of a multilayer film of collagen (COL) and hyaluronic acid (HA). This film's structure is more complex than a simple adsorption of alternatively charged layers. Because collagen is a fibril like material, the growth mechanism involves an increase of fiber diameters due to HA covering previously deposited collagen fibers, allowing new incoming collagen molecules to adsorb again along the HA-coated fibers.[209]

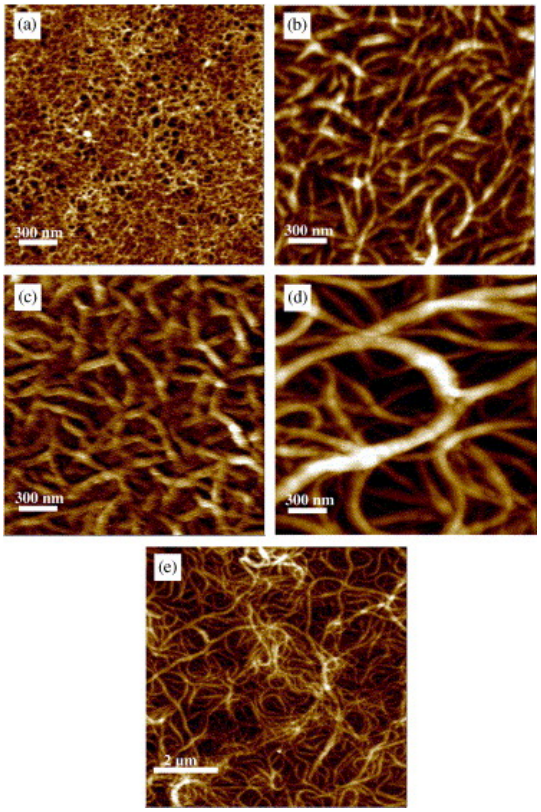

Figure 2.18. AFM height images of a collagen layer (a), PEI/$(HA/COL)_1$ (b), PEI/$(HA/COL)_5$ (c) and PEI/$(HA/COL)_{12}$ (d and e) multilayered films deposited on a glass slide.[209]

Collagen can also be paired with cellulose nanowiskers (CNW) (Figure 2.19 (a)). Due to the presence of the collagen amide group and -OH groups of CNW, this film is able to build through hydrogen bonding rather than electrostatic attraction. Figure 2.19 (b) shows the surface morphology of a 10 BL film grown on a glass substrate. This image clearly shows that the CNW are densely packed and homogeneously adsorbed on the surface, which has also been observed in assemblies of PEI and clay.[131] All of these results suggest that high density and uniform distribution of nanoparticles on the surface are characteristics of LbL assembly.

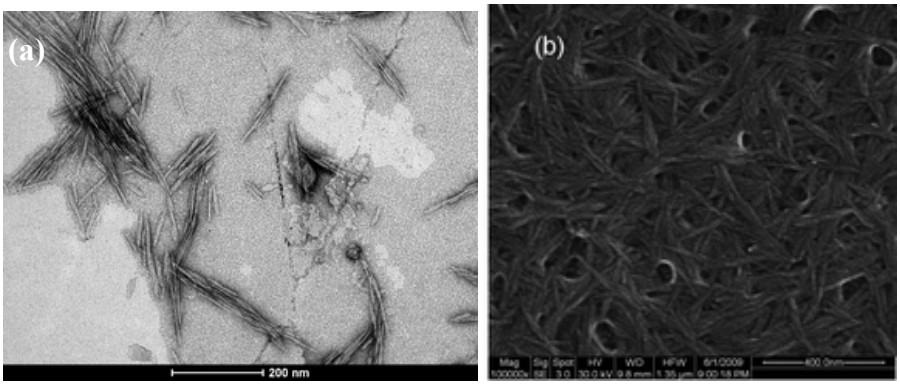

Figure 2.19. TEM image of the cellulose nanowiskers (a) and 10-bilayer collagen/cellulose nanowisker film.[210]

The combination of densely packed nanoparticles in LbL films, with the ability to coat three dimensional substrates, has led to the idea of creating a flame retardant coating for cotton fabric.[17] Cotton fabric was coated with polyethylenimine (PEI) and sodium montmorillonite clay. Figure 2.20 shows uncoated fabric and fabric coated with five bilayers of PEI-MMT before and after flame exposure. Each individual yarn was

protected by the clay-based coating, whereas the ashes from the control fabric show little structure. These studies lay the groundwork for the natural materials-based antiflammable (Chapter III, IV and VI) and oxygen barrier (Chapter V) systems presented in this dissertation.

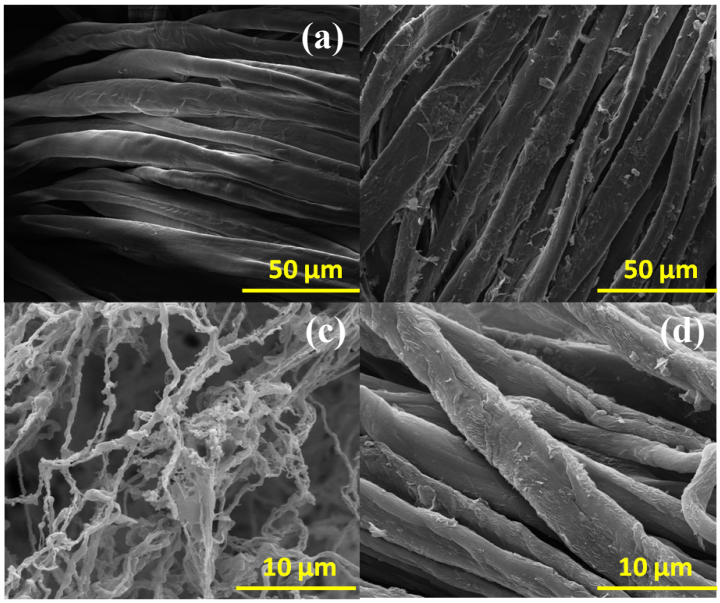

Figure 2.20. SEM images of uncoated fabric before (a) and after (c) the vertical flame test. SEM images of fabric coated with 5 BL of PEI-MMT before (b) and after (d) vertical flame testing.[17]

CHAPTER III

GROWTH AND FIRE RESISTANCE OF COLLOIDAL SILICA-BASED THIN FILM ASSEMBLIES*

3.1 Introduction

Layered silicates have been investigated extensively as an environmentally-friendly alternative to the use of halogenated compounds in flame retardant applications.[5, 7-8] Combining smectite clays with polyelectrolytes in thin films on cotton reduces burn time, afterglow and peak heat release rate.[17] Colloidal silica is another inorganic additive known to reduce flammability [21-23] and has been successfully incorporated into the LbL process.[24-26] The proposed mechanism for this flame retardant behavior is aggregation of particles on the surface of nanocomposites that forms an insulating layer, which limits heat transfer.[112] Despite improving thermal stability, adding nanoparticles is known to increase viscosity and modify mechanical properties of the final polymeric material, making their use prohibitive for many practical applications.[79, 211] With LbL assembly, nanoparticles are deposited directly onto the surface of the substrate as a thin layer, which allows the mechanism of protection to remain without the challenges associated with processing or adversely modifying mechanical behavior.

---

*Reprinted with permission from Laufer, G.; Carosio, F.; Martinez, R.; Camino, G.; Grunlan, J. C. Growth and fire resistance of colloidal silica-polyelectrolyte thin film assemblies. *J. Coll Interf Sci* **2011**, 356, 69-77.

In this chapter, the flammability of cotton fabric is shown to be reduced by depositing bilayers of polyethylenimine and colloidal silica (or positive and negative silica only) via LbL assembly. Growth trends and surface structure of films with varying composition revealed that when PEI is present as the cationic component, thicker and heavier coatings are produced due to better deposition of silica nanoparticles. Ten and 20 BL coatings were evaluated with respect to microstructure and flammability. Microscopic images revealed that 20 BL films were cracking and flaking in all of the systems. As a result, fabrics coated with 10 BL exhibited better flame retardant behavior (i.e., reduced heat release rate and increased post-burn char). Heat release rate was reduced by all coated samples, but a 10 BL coating of PEI- Ludox SM reduced peak heat release by 20% and heat release rate by 17%. Pre-soaking the cotton in an aqueous NaOH solution before LbL deposition further improves this behavior due to increased negative charge on the surface of the cellulosic fibers.[212] This work demonstrates a simple method for uniformly depositing thin films on the complex surface of cotton fibers and the efficacy of colloidal silica as an alternative to inorganic clay platelets for flame retardant fabric.

3.2 Experimental

3.2.1 Materials

Anionic deposition solutions consisted of 1.0 wt% colloidal silica, with particle diameters of 27±5 or 8±3 nm (tradename Ludox TM and Ludox SM, respectively) (Aldrich, Milwaukee, WI), in deionized water (18.2MΩ). Cationic solutions were

prepared by adding 0.1wt% of branched polyethylenimine (PEI), with molecular weight of 25,000 g/mol (Aldrich, Milwaukee, WI), or 1 wt% of CS with 12±2 nm diameter (tradename Ludox CL) (Aldrich, Milwaukee, WI) to deionized water. Specifications of Ludox particles are summarized in Table 3.1. The pH of the PEI was adjusted to 10 with hydrochloric acid (HCl). Single-side-polished (1 0 0) silicon wafers (University Wafer, South Boston, MA) were used as a substrate for film thickness characterization. For the presoaking solution, sodium hydroxide (NaOH) was added to deionized water until pH 10 was achieved. Cotton fabric was supplied by the USDA Southern Regional Research Center (New Orleans, LA). The fabric was a balanced weave with approximately 80 threads per inch in both the warp and fill direction, with a weight of 119 g/m^2.

Table 3.1. Properties of colloidal silica dispersions.

	Ludox SM	**Ludox TM**	**Ludox CL**
Particle size (nm)	8±3	27±5	12±2
Particle surface charge	Negative	Negative	Positive
Counterion	Na^+	Na^+	Cl^-
Chloride content (wt%)	-	-	0.03
Sodium content (wt%)	0.56	0.21	-

3.2.2 Layer-by-Layer Deposition

Prior to deposition, the silicon wafers were rinsed with acetone and deionized water, and then dried with filtered air. In the case of cotton, it was dried in the oven for 1 hour at 70 °C prior to deposition. All films were deposited on a given substrate (Si wafer of cotton fabric) using the procedure shown schematically in Figure 1.1. The substrates

were alternately dipped into positive and negative mixtures. Initial dips were 5 min and each subsequent dip was 1 min. Each dip was followed by rinsing with deionized water and, in case of silicon wafer, drying with air. For NaOH treated cotton, it was soaked in a pH 10 solution for 1 minute prior LbL deposition. Fabrics were wringed out to expel liquid as an alternative to the traditional drying step. After the desired number of bilayers was achieved, fabrics were dried at 70 °C in an oven for 2 hours before testing.

3.2.3 Characterization of Film Growth, Structure and Properties

Film thickness was measured with a PHE-101 Discrete Wavelengh Ellipsometer (Microphotonics, Allentown, PA). The 632.8 nm laser was used at an incidence angle of 65°. The weight per deposited layer was measured with a Maxtek Research Quartz Crystal Microbalance (RQCM) (Infinicon, East Syracuse, NY), with a frequency range of 3.8−6 MHz, in conjunction with 5 MHz quartz crystals. Cross sections of the films were imaged with a JEOL 1200 EX transmission electron microscope (Mitaka, Tokyo, Japan), operated at 110 kV. Samples were prepared for imaging by embedding a piece of fabric supporting the LbL film in epoxy and sectioning it with a microtome equipped with a diamond knife. Surface images of control and coated fabrics before and after the flame test were acquired with a Quanta 600 FE-SEM (FEI Company, Hillsboro, OR).

The thermal stability of uncoated and coated fabrics was measured with a Q50 Thermogravimetric Analyzer (TA Instruments, New Castle, DE). Each sample weighed approximately 20 mg and was run under air from room temperature to 600 °C, at a heating rate of 20 °C/min. Vertical flame tests were conducted on coated and virgin fabrics according to ASTM D6413-08 using an Automatic Vertical Flammability

Cabinet, model VC-2 (Govmark, Farmingdale, NY). Micro combustion calorimeter, model MCC-1 (Govmark), tests were performed at the University of Dayton Research Institute (Dayton, OH). Samples were tested at a 1 °C/sec heating rate under nitrogen from 200 to 600 °C using method A of ASTM D7309, without additional conditioning prior to testing.

3.3 Results and Discussion

3.3.1 Film Growth and Microstructure

The growth of four different colloidal silica-based assemblies (PEI-Ludox SM, PEI-Ludox TM, Ludox CL- Ludox SM, and Ludox CL- Ludox TM) was monitored with ellipsometry, as shown in Figure 3.1 (a). All four systems grow linearly as a function of bilayers deposited. When polyethylenimine is one of the two components, the films grow at a much higher rate as compared to all-silica films. It is possible that PEI provides better adsorption conditions for silica particles due to its flatter (or smoother) deposition and low modulus. PEI is commonly used as a primer layer for LbL deposition due to its adhesive characteristics.[213-215] In all cases, with or without PEI, the average thickness of a bilayer is significantly smaller than a single silica particle diameter. It has been reported that at the initial stages of growth, nanoparticles form isolated domains, which lead to incomplete surface coverage.[216] This effect may be exaggerated for all-silica assemblies due to relatively weak adhesion between layers. A combination of this inhomogeneous film growth and seating of colloidal particles in the interstitial spaces of the preceding layer is believed to account for this thin growth.

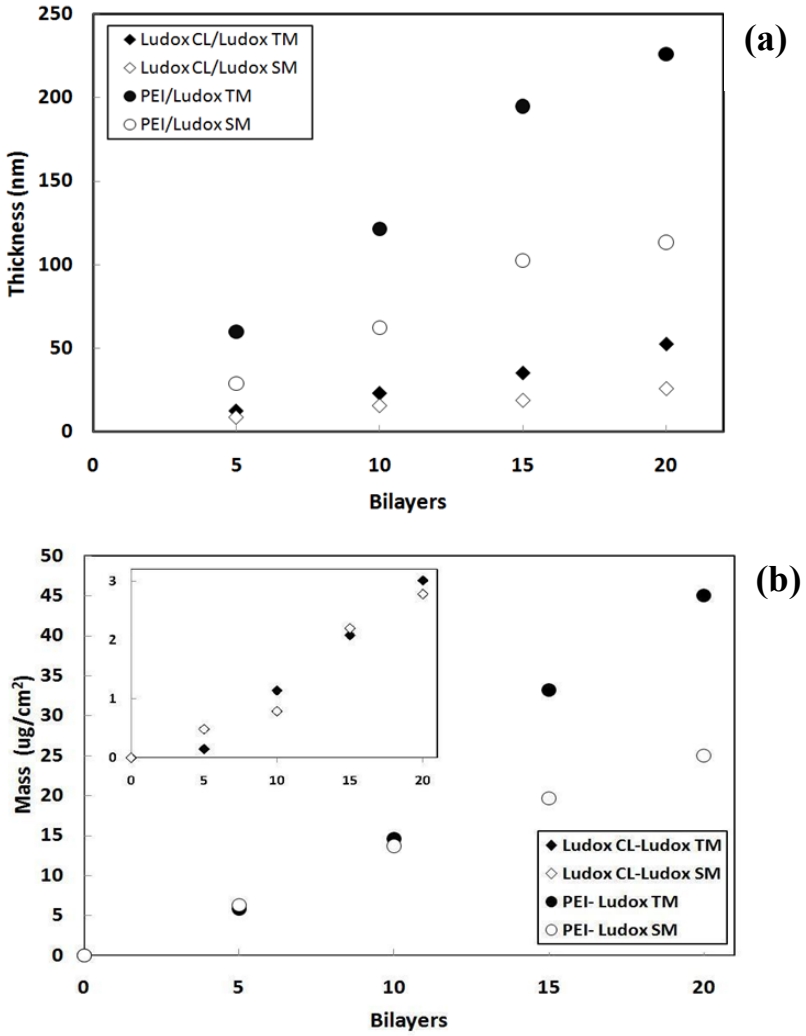

Figure 3.1. Thickness (a) and mass (b) of four different silica-based LbL assembly compositions as function of bilayers deposited. The inset of (b) shows the much lighter (thinner) growth of the all-silica systems.

To further investigate film growth, a quartz crystal microbalance was used to measure mass increase per layer deposited, as shown in Figure 3.1 (b). The growth behavior of all systems is similar to the linear trend observed with ellipsometry, with the growth rate of PEI-silica being larger than that of silica-silica. The weight of a 5 BL PEI-

silica system is more than a 20 BL all-silica film. From Table 3.2, it can be seen that silica is the main ingredient contributing to weight, with PEI being less than 10 wt% in the film. Not only is silica a higher density material, its thickness per layer is much greater. It has already been observed that PEI only deposits ~3.5 nm per layer at pH 10.[131] Table 3.2 also shows that films with smaller silica particles (Ludox SM) always result in higher density. A tighter packing of particles around the cotton fiber should reduce the surface of the fiber exposed to flame. As expected, coatings made with this smaller silica, exhibit better flame retardant properties than coatings made with the larger Ludox TM (see the tables on pages 43 and 49 respectively).

Table 3.2. Composition and density of colloidal silica assemblies.

	cation (wt%)	anion (wt%)	density (g/cm^3)
Ludox CL/Ludox SM	75	25	1.36
Ludox CL/Ludox TM	58	42	1.06
PEI/Ludox SM	7.9	92.1	1.72
PEI/Ludox TM	8.1	91.9	1.45

3.3.2 Deposition on Cotton Fabric

Figure 3.2 shows cross sections of single cotton fibers coated with 20 BL of Ludox CL- Ludox TM (Fig. 3.2 (a)) and 20 BL of PEI-Ludox TM (Fig.3.2 (b)). These systems are highlighted because the relatively large particle diameters are easier to visualize. Lack of coating thickness uniformity observed in these images is likely the result of fibers touching one another during LbL deposition and loss of coating during

sectioning due to the weakly charged cellulose surface, which causes the assemblies to attach to the surface more weakly than to more highly charged, smooth surfaces (e.g., Si wafer). Additionally, the difference in modulus between the cellulosic substrate and silica-based coatings may contribute to some cracking and flaking. Because coating deposited on fiber's surface is less than 250 nm thick, it does not modify the aesthetics and feel of the fabric.

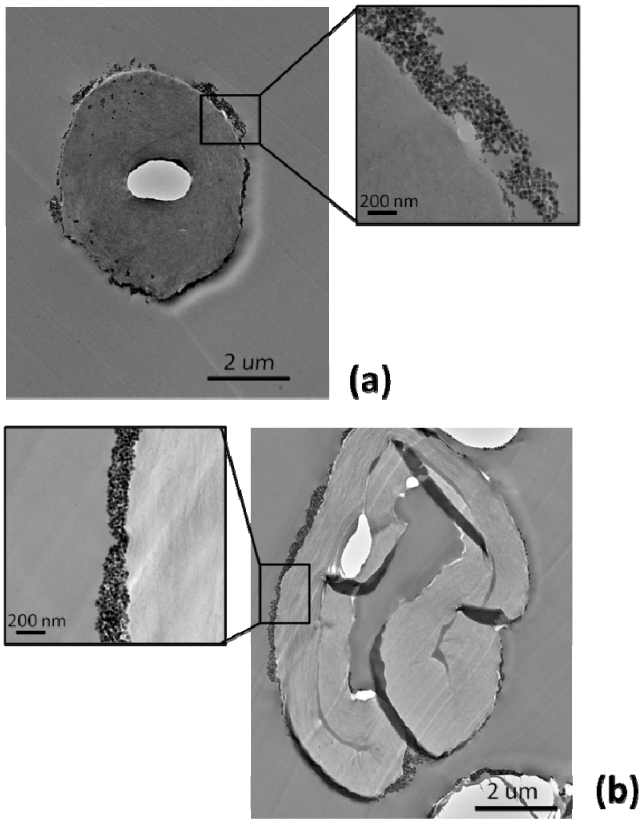

Figure 3.2. TEM cross section of cotton fiber with 20 BL Ludox CL-Ludox TM (a) and 20 BL PEI-Ludox TM (b) coatings.

Figure 3.3 shows the difference in fiber coverage between 10 and 20 BL coatings. Fibers coated with 10 BL of Ludox CL-Ludox TM (Fig. 3.3(a)) are fully covered, but uncoated spots are observed on the fiber's surface with 20 BL (Fig. 3.3(b)). A similar trend is observed with the PEI-Ludox TM system, where the 10 BL coating (Fig. 3.3(c)) looks heavier than the 20 BL coated fibers (Fig. 3.3(d)). This suggests that a 20 BL coating is too heavy to be held by weak charges on the cotton fiber's surface. It is expected that fabric coated with 10 BL will exhibit better flame retardant properties due to this more complete coverage of the fibers. It should also be noted that PEI-containing coatings (Fig. 3.3(c) and (d)) appear much thicker than all-silica coatings (Fig. 3.3(a) and (b)). This observation supports the ellipsometric thicknesses data (Fig. 3.1(a)) and suggests the PEI-based coatings will exhibit better anti-flammable behavior.

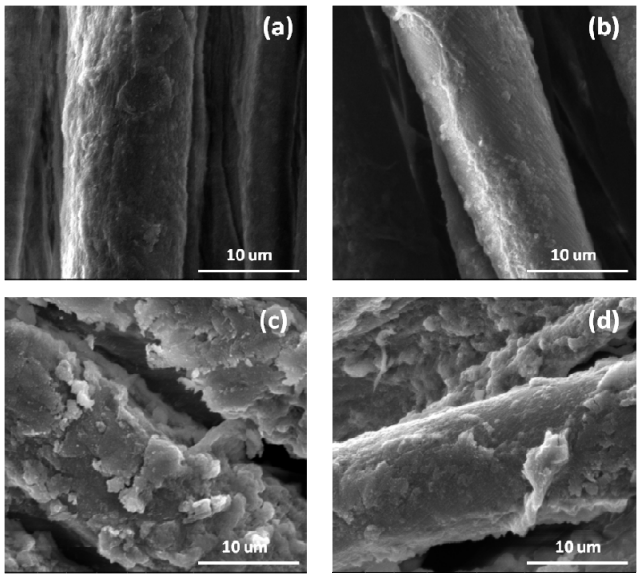

Figure 3.3. SEM images of cotton fabric coated with 10 BL (a) and 20 BL (b) Ludox CL-Ludox TM, and10 BL (c) and 20 BL (d) PEI-Ludox TM.

As discussed above, cotton's low surface charge is one of the contributing factors to flaking of the coating. Untreated cotton has non-cellulose compounds such as waxes, pectins, and proteins on its outer surface that diminish surface charge.[217] This surface charge can be increased, and the contaminants removed, by exposing the cotton fabric to an aqueous NaOH solution at pH 10.[212] At pH 10 this solution is relatively dilute, so there is no damage to the fibers. This NaOH treatment allows the initial layers to better anchor themselves to the fabric and provide improved adhesion for subsequent layer deposition. Figure 3.4 shows the difference in fiber coverage for untreated and NaOH pretreated 10 BL PEI-Ludox SM (Fig. 3.4(b)). The treated fabric clearly exhibits a heavier and more evenly distributed coating (and higher weight gain for 10 BL in Table 3.3), which ultimately provides greater residue in the TGA (see Table 3.3).

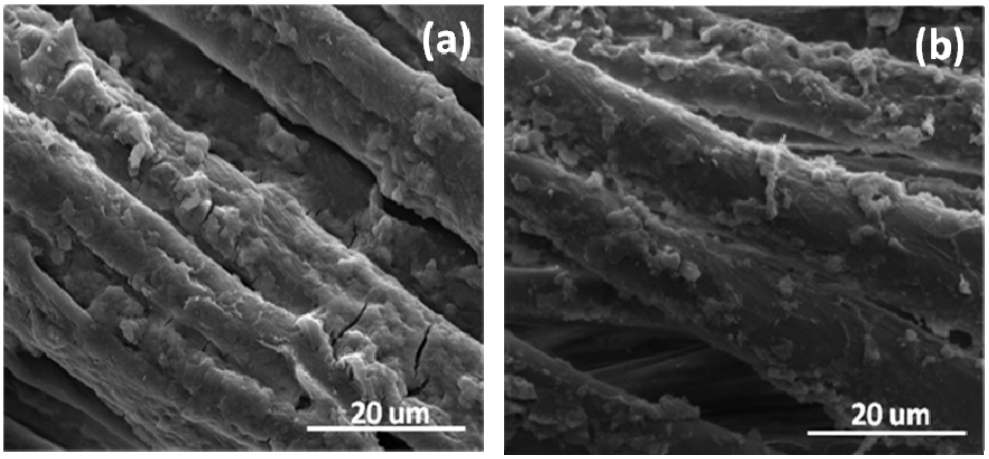

Figure 3.4. SEM of cotton fibers coated with 10 BL PEI-Ludox SM with (a) and without (b) NaOH pretreatment.

3.3.3 Flame Resistance and Thermal Stability of Fabric

Cotton fabric was coated with 10 and 20 bilayers of the four systems described in the previous section. The weight added to fabrics was determined by weighing before and after coating (reported as percent of original mass in Table 3.3). Fabric weight gain does not show the same trend observed with QCM, where films with Ludox TM had a higher weight gain. This observation can be explained by the different chemistries of the deposition substrates. As mentioned earlier, the surface charge of cotton fabric is weak and the coating partially flakes off as it reaches a critical thickness (or mass) that cannot be supported by the weak charge. Films with Ludox TM (27 nm diameter) grow thicker and heavier, so they will experience flaking of the coating earlier than those with Ludox SM (8 nm diameter).

Table 3.3. Coating weight added to fabrics and residue after heat treatment.

	# BL	% gain	% residue (@ 500°C)	% residue (@ 600°C)
Control			5.3	0.2
Ludox CL/Ludox SM	10	3.49	10.7	3.9
	20	5.79	10.7	4.6
Ludox CL/Ludox TM	10	1.98	8.8	2.7
	20	2.01	6.9	1.8
PEI/Ludox SM	10	5.65	13.6	4.7
	10^{NaOH}	6.88	15.7	5.9
	20	8.13	14	6.0
PEI/Ludox TM	10	4.96	11.8	4.3
	20	5.07	11.8	4.5

Figure 3.5 shows TGA results for the four different coating systems at 10 (Fig. 3.5(a)) and 20 BL (Fig. 3.5(b)). Coated fabrics show a slightly slower degradation from 100-300 °C and a significantly higher residue as compared to the control at final stage of the test. As expected, systems containing Ludox SM perform better than systems with Ludox TM. Also worth noting is that samples coated with 10 BL produced the same or greater residue than fabrics coated with 20 BL of the identical composition. The residue amounts for the control fabric and each coated fabric are summarized in Table 3.3. For the most part, the weight retained after heating to 600 °C is proportional to the initial coating weight. The amounts of char obtained after heating correlate well with flame retardance.[218] In all cases, the coated fabric had at least an order of magnitude greater residue than the control.

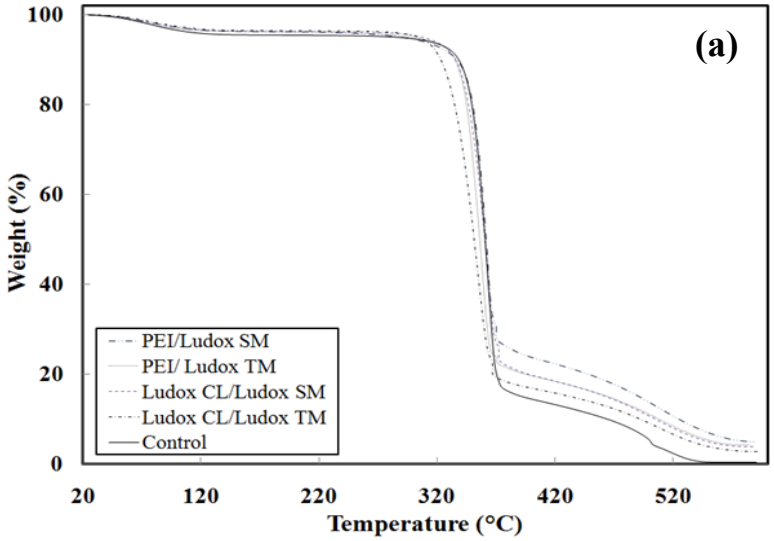

Figure 3.5. Weight loss as a function of temperature for uncoated (control) and 10 BL (a) or 20 BL (b) coated fabrics.

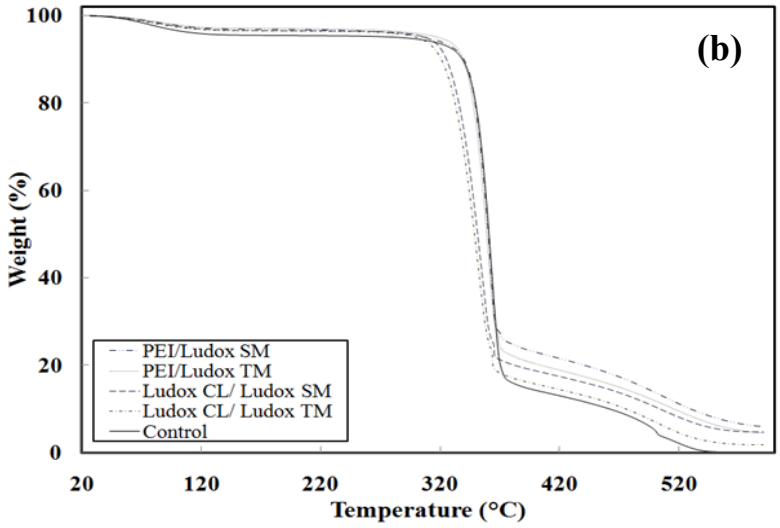

Figure 3.5. Continued.

Vertical flame testing (ASTM D6413) was used to evaluate the coated fabric's flammability. After ignition, flame spreads slower on coated fabrics and, as a result, these fabrics also have twice the afterflame time (fire on the sample after direct flame is removed) compared to the control. Despite the longer afterflame, afterglow was reduced by at least 17 seconds for coated fabrics. Afterglow time is important because it shows how long fabric continues to burn without flame and longer afterglow increases the chances of fire reigniting. Following the test, there was no fabric left on the control sample holder, as shown in Figure 3.6. Coatings with Ludox CL-Ludox SM and PEI-Ludox SM (i.e., smaller silica) left the highest amounts of residue. As discussed earlier, tightly packed silica particles shield cotton fibers from rapid degradation at high temperatures by reducing cotton availability on the surface. Samples coated with Ludox

CL- Ludox TM and PEI- Ludox TM (i.e., larger silica) did not perform as well due to lower packing density, but still retained a significant amount of residue.

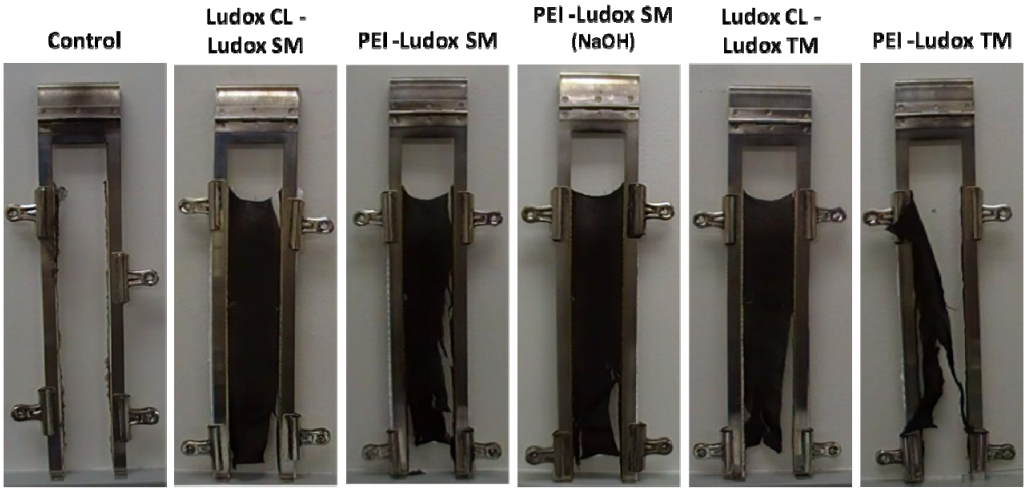

Figure 3.6. Images of control and 10 BL coated fabrics following vertical burn testing.

Following burning, the surfaces of all fabrics were imaged with SEM to evaluate the retention of fabric structure. The after burn image of the uncoated control is omitted because there was no fabric left after the vertical flame test. All four coated samples were able to preserve the fabric weave structure, although significant shrinking of individual fibers is observed in Figure 3.7 (for most systems). Fiber shrinkage is somewhat expected due to poor packing of spherical nanoparticles and non-inform coverage of fibers that cannot provide as effective of a protective shell for cotton, which contributes to the further degradation of fibers, especially for larger silica coatings (Fig.3.7 (d) and (e)). Higher magnification of Figure 3.7(e) confirms cracking of the coating; this cracking is likely due to the high modulus and weaker bonding of this larger

silica system (Ludox CL-Ludox TM). The highest magnification image, with 1μm scale bar, clearly shows the colloidal nature of the coating and its protective shell nature.

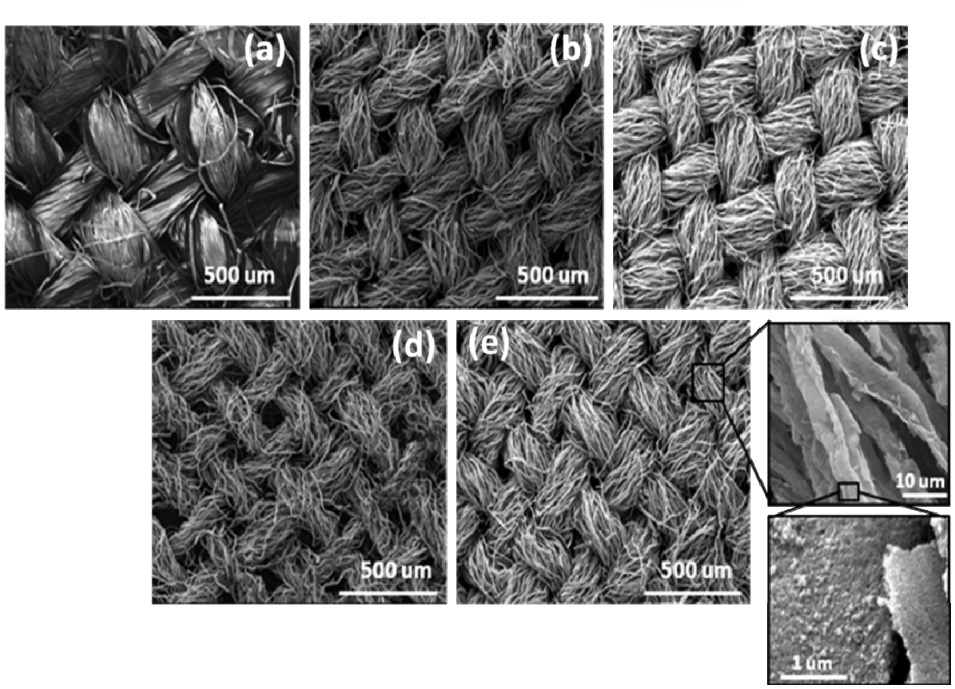

Figure 3.7. SEM mages of control fabric before vertical flame test (a), and 10 BL coated fabrics following the vertical burn test: PEI- Ludox SM (b), Ludox CL-Ludox SM (c), PEI- Ludox TM (d), and Ludox CL-Ludox TM (e).

Micro combustion calorimetry (MCC) was used to evaluate heat release during burning of these cotton fabrics. MCC is a small scale instrument that measures the heat of combustion of the pyrolysis products by oxygen consumption calorimetry. Fabrics were tested under nitrogen up to 600 °C. These heat release measurements are summarized in Table 3.4. Peak heat release rate (pkHRR) is the maximum heat release rate during the experiment. The higher the pkHRR value, the more heat is given off by

the sample. The pkHRR temperatures and the total heat release (HR) are shown in Table 3.4. All coated fabrics show a higher residue mass and a decreased pkHRR, as compared to the control. Comparison of HRR curves between control and fabrics coated with 10 BL PEI/Ludox SM and Ludox CL/Ludox SM is shown in Figure 3.8. The maximum reduction in pkHRR (20 %) and HRR (17 %) was observed in the fabric coated with 10 BL of PEI/Ludox SM, this agrees well with TGA results. This same coating also produced the greatest amount of char (~13 wt%), which is more than double the coating weight (see Table 3.3). Increasing the number of bilayers to 20 does not improve thermal stability of the fabrics based on the MCC data. This was expected based upon the patchy appearance of the coating due to cracking and flaking (see Fig. 3.3).

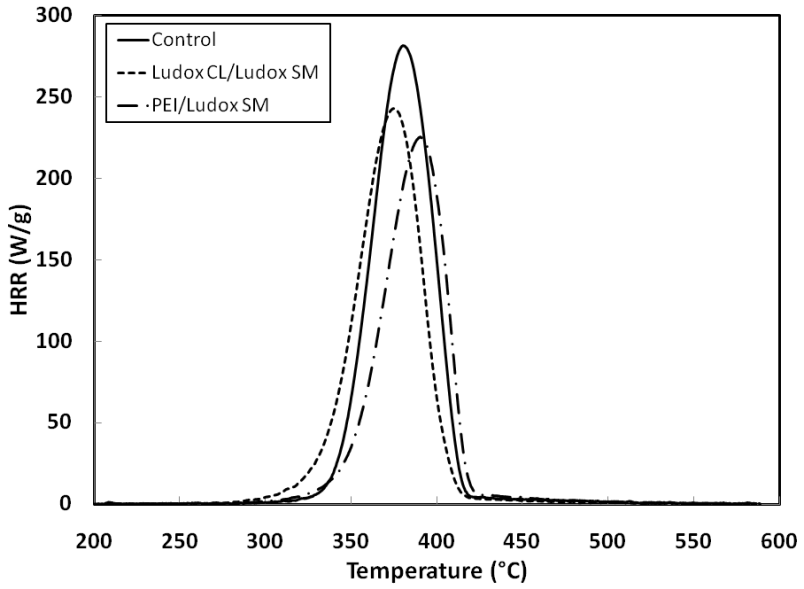

Figure 3.8. Heat release rate curves for uncoated control and 10 BL coated fabrics.

Table 3.4. Micro combustion calorimeter results for various coatings on cotton fabrics

	BL	Char yield (wt%)	pkHRR (W/g)	pkHRR (°C)	Total HR (kJ/g)
Control	-	4.98	285	381	12.8
Ludox CL/ Ludox SM	10	9.53	253	375	11.7
	20	9.58	243	365	11.7
Ludox CL/ Ludox TM	10	6.89	240	361	12.2
	20	6.27	245	361	12.4
PEI/ Ludox SM	10	13.07	227	390	10.5
	20	13.02	234	388	11.2
PEI/ Ludox TM	10	9.59	258	386	11.6
	20	9.04	268	380	11.5

3.4 Conclusions

Silica-based thin film assemblies were deposited on cotton fabric to impart flame-retardant behavior. All assemblies exhibited linear growth as a function of the number of bilayers deposited. The presence of PEI as the cationic component resulted in significantly thicker and heavier coatings. When cotton was used as a deposition substrate, coatings containing larger silica (i.e., Ludox TM with 27 nm particle diameter) appear to flake off at 20 BL due to weak fabric surface charge and high coating mass. Treating cotton fabric with an aqueous NaOH solution prior to LbL assembly increases negative charge of the substrate and results in improved deposition and flame retardant behavior compared to coating on untreated cotton. The flame retardant properties of 10 and 20 BL coated fabric were tested using TGA, vertical flame, and micro combustion

calorimetry. All of the coated fabrics left a significant amount of char following the vertical flame test and retained the fabric weave structure, as observed by SEM. Additionally, micro calorimeter testing revealed a lower peak heat release rate for coated fabrics. With respect to silica particle size, coatings made with small silica particles (~8 nm) resulted in better flame retardant properties relative to those made with large particles (~27 nm). Smaller colloids achieve a higher practical packing density around the cotton fibers. This work demonstrates a simple and convenient method for depositing flame retardant thin films on cotton, a very complex substrate geometry, using relatively benign ingredients (from an environmental standpoint). More work is underway to reduce cotton flammability with other nanoparticles (e.g., layered hydroxides) and surface treatments.

CHAPTER IV

CLAY-CHITOSAN NANOBRICK WALLS: COMPLETELY RENEWABLE FLAME RETARDANT NANOCOATINGS*

4.1 Introduction

Polysaccharides are naturally occurring polymers that are widely available in nature. Of the many kinds of polysaccharides, chitin is the second most abundant after cellulose.[219] Chitin is extracted from the shells of crustaceans (e.g. lobsters and shrimp) and the exoskeletons of arthropods (e.g. insects). Despite its abundance, unmodified chitin's usefulness is very limited due to its poor solubility in most solvents. Chitosan, an amino polysaccharide obtained by alkaline deacetylation of chitin (see structure in Figure 4.1),[220] is soluble in acidic aqueous solutions because of the protonation of its amino groups below a pH of 6.2.[221-222] In addition to its solubility, chitosan is biodegradable, biocompatible, and benign. These traits have led to significant study of chitosan's use in biomedical applications such as drug delivery,[223-226] wound-dressing materials,[227-229] artificial skin,[230-232] and blood anticoagulants.[233-234] Chitosan's positive charge at low pH also allows it to be alternately deposited with negatively charged molecules or nanoparticles to produce multilayer thin films from aqueous solutions.[219, 235]

*Reprinted with permission from Laufer, G.; Kirkland, C.; Cain, A. A.; Grunlan, J. C. Clay-chitosan nanobrick walls: Completely renewable gas barrier and flame-retardant nanocoatings. *ACS Appl Mater Interf* **2012**, 4, 1643-1649. © 2012 American Chemical Society.

In LbL assembly, clay nanoplatelets have often been paired with polymer to improve mechanical,[176, 236] thermal,[237-238] and barrier[131, 239-240] properties of the substrate. Montmorillonite is the most widely used anionic clay and is part of the smectite group. In addition to being exfoliated in water to produce 1 nm thick anionic platelets (l/d~200), montmorillonite is benign, naturally abundant and relatively low cost.

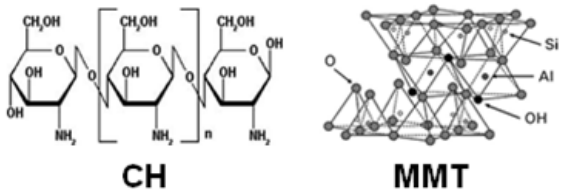

Figure 4.1. Chemical structure of chitosan and montmorillonite.

In this chapter, in an effort to create fully renewable flame retardant assemblies, thin films of chitosan and montmorillonite clay were deposited on polyurethane (PU) foam. These polymer-clay thin films resemble nano brick walls, with CH acting as the mortar holding the MMT bricks together. In terms of fire safety, PU foam (without flame retardant additives) is very flammable, often resulting in dripping of melted material that enhances flame spread through the formation of a pool fire under the burning object. If the pool fire is close enough to another flammable object, the result can be a self-propagating fire.[1] Just ten bilayers of CH pH 6-MMT cuts the peak heat release rate of open-celled, flexible PU foam in half. This same treated foam maintains its shape, with no signs of melting, when exposed to direct flame from a butane torch for 10 s. These results demonstrate the ability to create a fully renewable nanocoating

capable of imparting significant fire resistance to PU foam (e.g. for building insulation or furniture padding).

4.2 Experimental

4.2.1 Materials

Cationic deposition solutions were prepared by adjusting the pH of deionized water (18.2MΩ, pH~5.5) to 2 with hydrochloric acid (HCl) and then adding 0.1 wt% chitosan (MW 50-190 kDa, 75-85% deacetylated) purchased from Aldrich (Milwaukee, WI). This aqueous solution was magnetically stirred for 24 hours until the chitosan was completely dissolved. Solution pH was adjusted to 3 or 6 with 1 M NaOH just prior to deposition. Anionic solutions were prepared by adding 1.0 wt% of sodium montmorillonite, tradename Cloisite® Na^+ provided by Southern Clay Products, Inc. (Gonzales, TX), to deionized water and rolling for 24 h. This MMT has a cationic exchange capacity of 0.926 meq/g and a negative surface charge in deionized water [241]. Individual platelets have a density of 2.86 g/cm^3, with a planar dimension of 10 – 1000 nm (average is around 200 nm) and a thickness of 1 nm [242]. Single-side-polished (1 0 0) silicon wafers (University Wafer, South Boston, MA) were used as the substrate for film thickness characterization and 125 μm polystyrene (PS) film (Goodfellow, Oakdale, PA) was used for TEM images. Polyester-based polyurethane foam (United Foam, Denver, CO), with 100 pores per linear inch (ppi) and without flame retardant additives, was used for flammability experiments.

4.2.2 Layer-by-Layer Deposition

Prior to deposition, the silicon wafers were rinsed with acetone and deionized water, and then dried with filtered air. In the case of PS, methanol was used in place of acetone. This substrate was then corona treated, using a BD-20C Corona Treater (Electro-Technic Products, Inc., Chicago), to create a negative surface charge. Foam samples were dipped into 0.1 M nitric acid for 30 seconds prior to LbL deposition, and then dipped into a 1wt% branched polyethylenimine solution (pH 10, MW 25 kDa) as a primer layer, to improve adhesion. All films were deposited on a given substrate using the procedure described in Section 3.2.2. After the desired number of bilayers was deposited, foam samples were dried at 80 °C in an oven for 2 hours before testing.

4.2.3 Characterization of Film Growth, Structure and Properties

Film thickness was measured with an alpha-SE Ellipsometer (J. A. Woollam Co., Inc., Lincoln, NE). Surface images of control and coated foam samples were acquired with a JEOL JSM-7500F FESEM (JEOL Ltd., Tokyo, Japan). Platinum coating of 8 nm was deposited on all samples prior to the imaging to prevent charging. Surface topography was imaged with a Nanosurf EasyScan 2 Atomic Force Microscope (AFM) (Nanoscience Instruments, Inc., Phoenix, AZ). Foam flammability was evaluated by exposure to direct flame from a ST2200 butane micro torch (Benzomatic, Huntersville, NC) for 10 seconds (approximate flame temperature 2400°F blue flame). Cone calorimetry was performed at the University of Dayton Research Institute using an FTT Dual Cone Calorimeter at one heat flux (35 kW/m^2), with an exhaust flow of 24 L/s, using the standardized cone calorimeter procedure (ASTM E-1354-07).

4.3 Results and Discussion

4.3.1 Film Growth and Microstructure

Growth of chitosan-clay assemblies, as a function of bilayers deposited (Figure 4.2(a)), was monitored using ellipsometry. Both films exhibit linear growth, but film growth at pH 6 is much thicker than the growth at pH 3. It was previously shown that LbL deposition results in the majority of clay platelets being deposited as a single layer,[131] which means that the difference in thickness is primarily influenced by chitosan deposition. Chitosan has primary amine groups that make its conformation and charge density pH dependent, which influences the thickness of adsorbed layers. At pH 3, chitosan is fully ionized and electrostatic repulsions of the free ammonium groups cause polymer chains to become elongated and deposit very thinly onto a substrate.[243] As polymer pH increases, the amines become deprotonated and ionic repulsions are reduced, leading to a more globular conformation of the chains. Lack of self-repulsion leads to thicker films, as shown in Figure 4.2(a). These same trends are observed when growth is measured as a function of weight deposited using a quartz crystal microbalance (QCM).

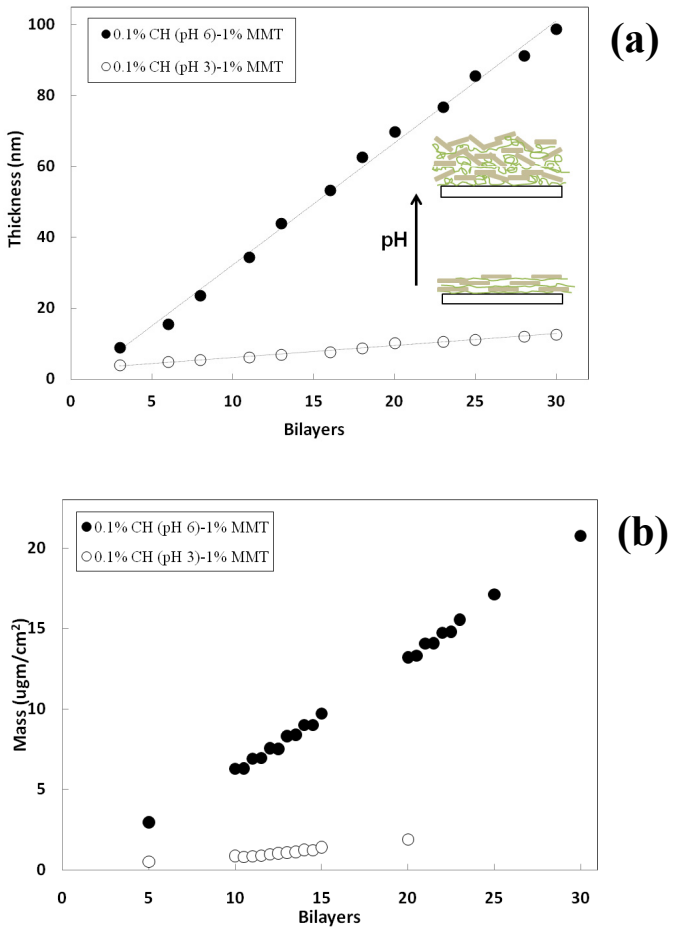

Figure 4.2. Thickness (a) and mass (b) of chitosan-clay assemblies as a function of bilayers deposited.

Figure 4.2(b) shows the weight of each deposited layer for films made with pH 3 or pH 6 chitosan. The growth trend of both systems is similar to the linear trend observed with ellipsometry (Figure 4.2(a)), with higher pH generating heavier layers. It is interesting to note that films at pH 6 also have higher clay loading (expressed as weight percent in Table 4.1), which is somewhat counterintuitive. Previous work with clay-polyethylenimine assemblies showed that thicker polymer deposition resulted in

lower clay concentration due to greater spacing between single clay layers.[131] High pH (low charge density) chitosan deposits less uniformly, creating a rough surface. The coverage of chitosan at different pH levels was revealed by depositing CH onto a Si wafer as a single layer and scanning with AFM. As expected, the surface is very smooth due to strong adsorption of the extended, high charge density polymer at pH 3 (Fig. 4.3(a)). At pH 6, chitosan deposits as clustered globules, as shown in Figure 4.3(b). This nanoscopic roughness provides greater surface area for clay platelets to deposit onto (see proposed schematic of this structure in Figure 4.2(a)). At low pH, the polymer deposits smoothly onto a substrate and clay can only deposit parallel to the substrate. Higher clay concentration at pH 6 results in higher density of the films (Table 4.1).

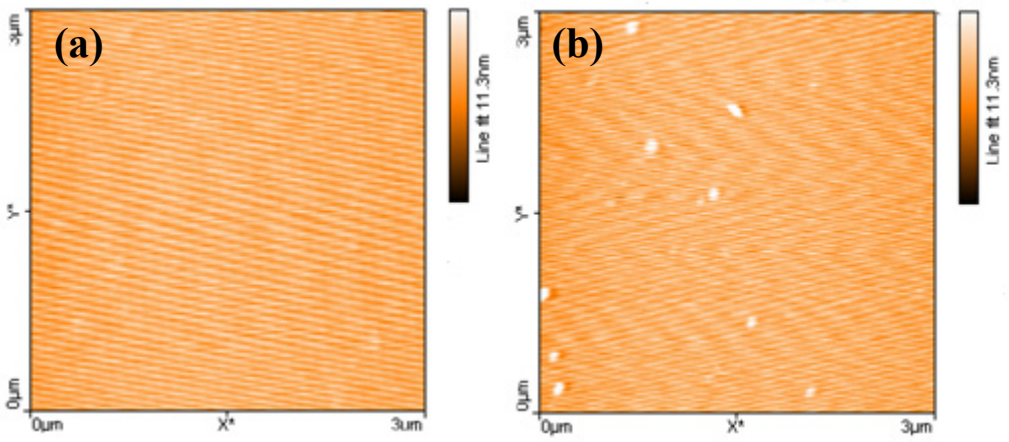

Figure 4.3. AFM height images of a single chitosan layer deposited from pH 3 (a) and pH 6 (b) solutions.

Table 4.1 Composition and density of CH-MMT assemblies.

	CH (wt%)	MMT (wt%)	Density (g/cm^3)
CH pH 3/MMT	33.79	66.21	1.19
CH pH 6/MMT	10.69	89.31	1.89

TEM cross-sections of 100 BL films made with pH 3 and pH 6 chitosan are shown in Figure 4.3. These images clearly show the high level of clay orientation and the structural differences between high and low pH (resembling the schematic images in Figure 4.2(a)) The film deposited with pH 6 (Figure 4.4(a)) is much thicker than that made with pH 3 CH (Figure 4.4(b)) and also shows some misaligned clay platelets. Furthermore, the thickness of these films agrees well with the value extrapolated from the ellipsometric growth curves in Figure 4.2(a). This nano brick wall structure has already been shown to exhibit low oxygen permeability and flame retardant behavior.[17, 38]

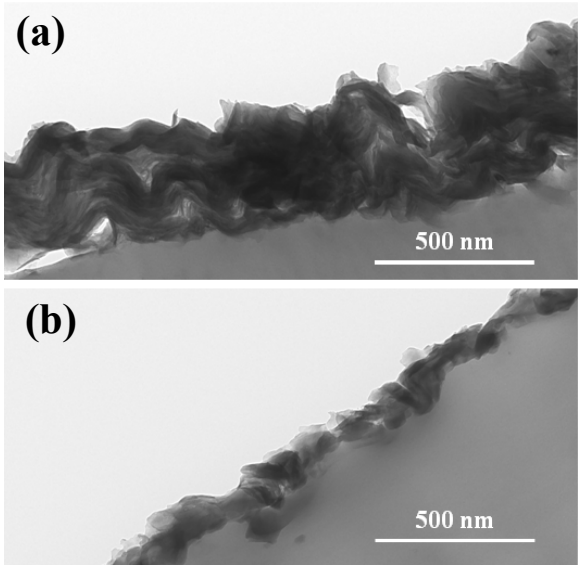

Figure 4.4. TEM cross sections of 100 of BL CH pH 6-MMT (a) and 100 BL of CH pH 3-MMT (b) deposited on polystyrene.

4.3.2 Flame Retardant Behavior on Polyurethane Foam

Ten bilayers of high and low pH chitosan and clay were deposited onto open-celled, flexible polyurethane foam. The weight added to foam was determined by weighing before and after coating (reported as percent of original mass in Table 4.4). Figure 4.5 shows the surfaces of an uncoated control and foam coated with CH ph 3-MMT and CH pH 6-MMT (Figure 4.5(a), (b), and (c) respectively). The control foam is very smooth, while the coated foam has a uniform nanotexture that confirms the conformal nature of layer-by-layer deposition. These are representative images of how the foam looks throughout its entire thickness, revealing excellent coverage of every pore wall without altering the macro-scale porosity of the foam. As expected, the pH 6

coating (Figure 4.5(b)) appears heavier (i.e., has a stronger texture than the thinner (< 10 nm) pH 3 coating (Figure 4.5(c)).

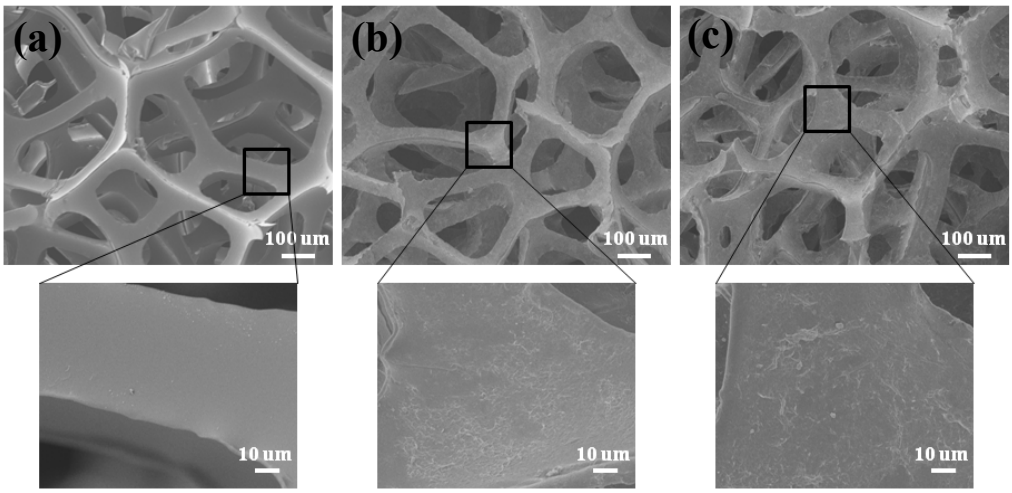

Figure 4.5. SEM images of uncoated polyurethane foam (a) and foam coated with 10 BL of CH pH 3-MMT (b) and CH pH 6-MMT (c).

Foam flammability was initially tested by holding the flame from a butane torch on the foam's surface for 10 seconds. The uncoated foam ignited and started to melt immediately upon exposure to the flame and was ultimately destroyed (i.e., completely consumed). There was no melt dripping exhibited by either of the coated foam samples and the flame was extinguished after it traveled across the foam surface (~30 seconds). Foam coated with 10 BL of CH pH 6-MMT retained its original shape after flame exposure (Figure 4.6(a)), while foam coated with CH pH 3-MMT slightly collapsed (Figure 4.6(b)). When cut through the middle, coated foam samples revealed flexible, undamaged (white) foam underneath the char. Higher magnification images of the

interface between the black char and white foam reveal that foam structure was not damaged and the char consists mostly of aggregated clay platelets. Coating with pH 6 chitosan (Figure 4.6(a)) provides a more protective barrier due to greater thickness and higher clay content than pH 3.

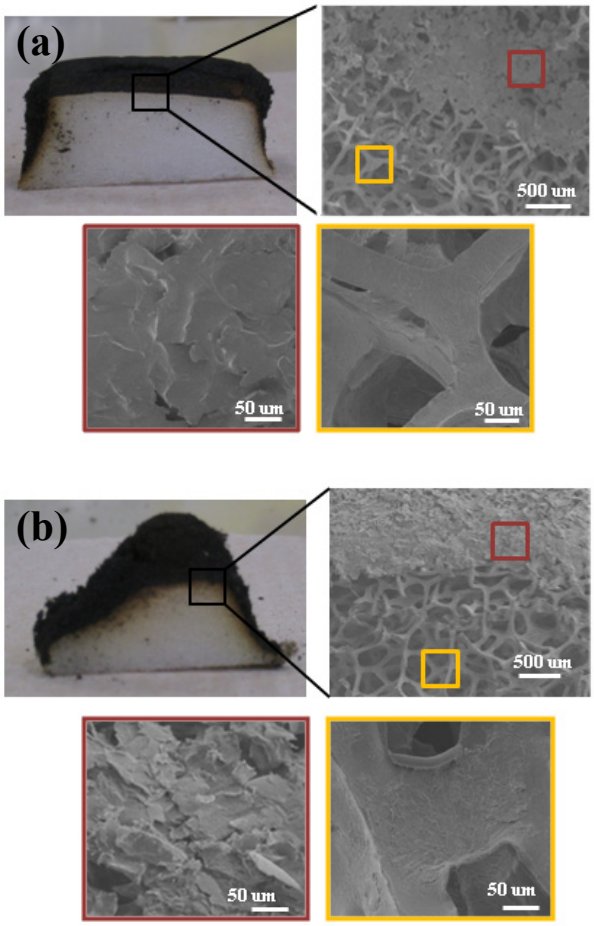

Figure 4.6. SEM images of cross sections of foam coated with 10 BL CH pH 6-MMT (a) and CH pH 3-MMT (b) following the torch burn test. Boxes of the same color correlate to spots that were further magnified in each foam.

In an effort to better understand the effect of the CH-MMT coating on the flammability of PU foam, cone calorimetry was performed on these 10 BL coated samples. A cone calorimeter quantitatively measures the inherent flammability of a material through the use of oxygen consumption calorimetry (ASTM E-1354/ISO 5660). Figure 4.7 shows the heat release rate (HRR) curves for control and coated foam samples. Two different peaks can be seen in the curve for the control foam. There is a rapid rise to the first peak soon after ignition, which is associated with foam collapse. After transforming into a liquid, polyurethane burning tends to accelerate as the decomposing material vaporizes quickly, which quickly leads to a fast progression to a second, larger peak HRR. The decay after the peak is also very rapid, with all material being decomposed.[244] HRR curves for coated foam samples are significantly different from the control, suggesting that the CH-MMT coating fundamentally changes the burning behavior of the foam.

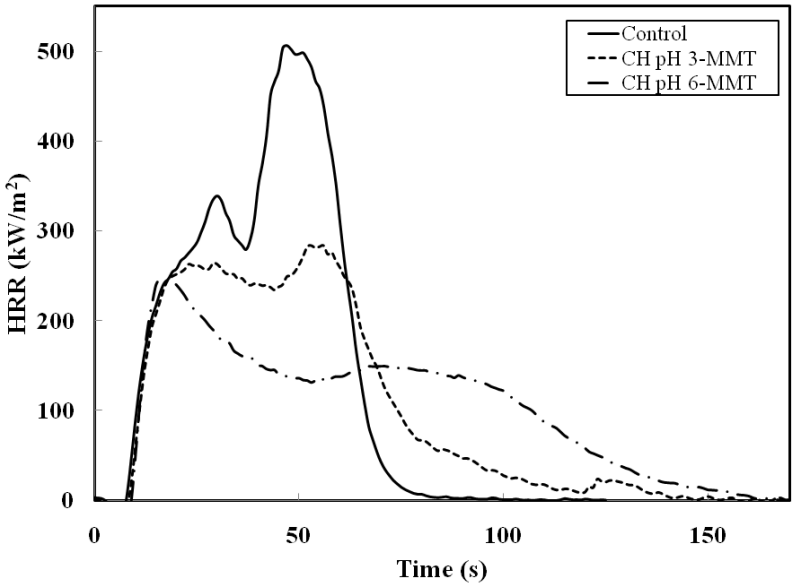

Figure 4.7. Heat release rate as a function of time, during cone calorimeter testing, for uncoated control and 10 BL coated foam.

Ten bilayers of CH pH 6-MMT, which is about 30 nm thick, completely eliminates the second HRR peak. This coating produced the largest reduction (52%) in peak heat release rate (pkHRR), which is the maximum value of the heat release rate during the combustion of the sample. It also lowered the average heat release rate (Avg HRR) by more than 30% and maximum average heat rate emission (MAHRE) by almost 50%. MAHRE is an ignition modified rate of heat emission, that can be used to rank materials in terms of ability to support flame spread to other objects.[245] CH pH 3-MMT also reduced these flammability values, but not as dramatically as pH 6. This was expected due to the higher clay concentration in the pH 6 coating, that formed a thicker, more effective protective layer. Furthermore, pyrolysis of polyurethane decomposition products was delayed because these foams never collapsed into a liquid. Longer burning

times for coated foam ultimately caused the total heat release to be similar to the control, but these CH-MMT coatings make a dramatic difference in the reduction of flammability of foam. The cone calorimeter parameters are summarized in Table 4.4. When comparing pkHRR reduction to clay-filled polymers in the literature, the 10 BL CH-MMT nanocoating achieves similar reduction to the best performing materials, as shown in Table 4.5.

Table 4.2. Cone calorimeter results for control and 10 BL coated foam.

Sample	Weight gain (%)	pkHRR (kW/m2)	Avg HRR (kW/m2)	Total HRR (mJ/m2)	Mass loss (%)	MAHRE (kW/m2)
control	-	517±33.9	178±12.5	18.9±1.6	100	286±22.6
CH pH 3/MMT	1.59	326±60.9	144±18.6	17±0.2	94±1.8	209±46.2
CH pH 6/MMT	4.01	246±5.4	116±7.9	17±0.4	93±1.4	148±7.7

Table 4.3. Cone calorimeter values reported in literature for clay composites.

Sample	pkHRR reduction	Reference
polyethylene/2-15% clay	50-70%	[246]
polystyrene/1-10 % clay	8-23%	[247]
polypropylene/5% clay	33%	[116]
polyamide 6/15% clay	60%	[78]
PU/10 BL CH pH	52%	Table 4.4

4.4 Conclusions

The goal of this work was to develop a truly "green" film with flame-retardant characteristics. Films assembled with high or low pH chitosan and clay showed linear

growth as a function of the number of bilayers deposited. Higher chitosan pH resulted in much thicker assemblies with higher clay loading. When flexible PU foam was coated with 10 BL of CH pH 6-MMT, only the outermost surface was charred after being exposed to the direct flame from a propane torch for 10 seconds. When cut open, undamaged white flexible foam was revealed under a black char layer. Cone calorimetry revealed that this protective nanocoating significantly reduced peak heat release relative to the uncoated control, showing a maximum reduction of 52%. This work demonstrates the first fully renewable flame retardant treatment made via layer-by-layer assembly and provides an environmentally benign alternative to commonly used halogenated materials.

CHAPTER V

HIGH OXYGEN BARRIER, CHITOSAN-BASED THIN FILMS FOR FOOD PACKAGING*, **

5.1 Introduction

The permeation of oxygen through food packaging often leads to spoilage, making oxygen barrier crucial for achieving longer shelf life.[57, 248] Additionally, there is strong interest in developing environmentally-friendly and transparent barrier materials.[249] LbL assembly of multilayered thin films, through electrostatic attraction of oppositely charged polyelectrolytes or particles on a substrate,[250-251] can impart these characteristics to packaging films. LbL assembly has also been used to construct thin transparent films that significantly reduce the oxygen permeability of polyethylene terephthalate (PET) film.[131, 252] The most impressive barrier properties result from the incorporation of clay in these thin films,[131, 239, 252] but little attention has been given to creating these barriers with only food contact approved ingredients. In this chapter, multilayer nanocoatings made with three food contact improved components (chitosan, poly(acrylic acid) [PAA] and montmorillonite (MMT) clay) were deposited onto PET

*Reprinted with permission from Laufer, G.; Kirkland, C.; Cain, A. A.; Grunlan, J. C. Clay-chitosan nanobrick walls: Completely renewable gas barrier and flame-retardant nanocoatings. *ACS Appl Mater Interf* **2012**, 4, 1643-1649. © 2012 American Chemical Society.
** Reprinted with permission from Laufer, G.; Priolo, M. A.; Kirkland, C.; Grunlan, J. C. High oxygen barrier, clay and chitosan-based multilayer thin films: An environmentally-friendly foil replacement. *Green Materials*, ASAP. © 2012 Institution of Civil Engineers.

and polylactic acid (PLA) substrates. Chitosan was approved by the United States Food and Drug Administration (FDA) as a feed additive in 1983 and has recently been designated as GRAS (Generally Recognised As Safe) component.[253] Anionic poly(acrylic acid) and clay have been used previously in food contact materials that have been granted approval by the FDA.[254-255]

5.2 Experimental

5.2.1 Materials

Poly(acrylic acid) (PAA) (Aldrich) (MW 100 kDa) was used as a 0.2 wt % solution in deionized water. The pH of this solution was increased to 4 with NaOH. Polylactic acid with 500 μm thickness (trade name BioWare PLA, produced by Huhtamaki Forchheim), provided by Faerch Plast (Holstebro, Denmarkand), and 179 μm thick poly(ethylene terephthalate) (trade name ST505, produced by Dupont-Teijin), purchased from Tekra (New Berlin, WI), were used for oxygen barrier testing. Other materials used here were already described in Chapter IV (Section 4.2.1).

5.2.2 Layer-by-Layer Deposition

Prior to deposition, plastic substrates were corona treated with a BD-20C Corona Treater (Electro-Technic Products, Inc., Chicago) to create a negative surface charge. CH-MMT assemblies were prepared identical to those described in Chapter IV (Section 4.2.2). Three component films were deposited on a given substrate using the procedure shown schematically in Figure 5.1. Substrates were alternately dipped into chitosan,

polyacrylic acid, chitosan and montmorillonite. One cycle of CH-PAA-CH-MMT is referred to as a quadlayer (QL).

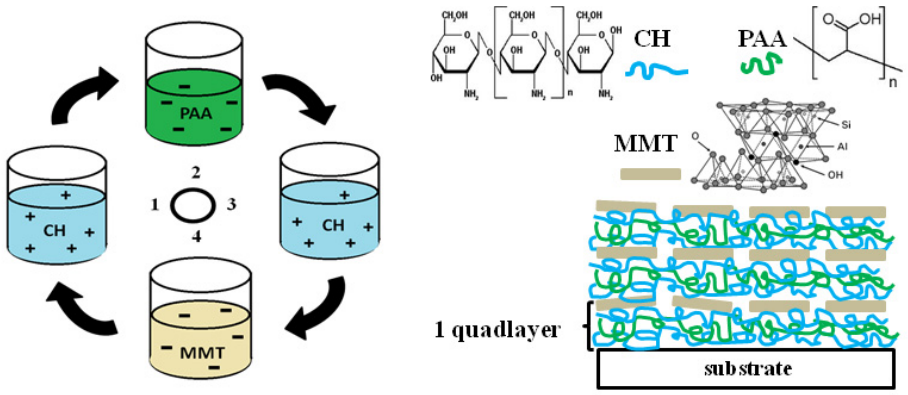

Figure 5.1. Schematic of layer-by-layer deposition of food contact approved ingredients on a substrate (e.g., PLA or PET film).

5.2.3. Characterization of Film Growth, Structure and Properties

Oxygen transmission rates were measured by MOCON (Minneapolis, MN) in accordance with ASTM D-3985, using an Oxtran 2/21 ML instrument. All other characterization is identical to that described in Chapter IV (Section 4.2.3).

5.3 Results and Discussion

5.3.1. Film Growth and Microstructure

Growth and microstructure of films composed of CH at pH 6 and MMT were described in Chapter IV (Section 4.3.1). The CH/PAA/CH/MMT assembly grows linearly as a function of QLs deposited, as shown in Figure 5.2. A similar system, grown with polyethylenimine as the polycation instead of CH, showed exponential growth.[38, 174]

For exponential growth to occur, a given polymer must diffuse in and out of the previously deposited layer.[256] Chitosan's structure consists of a double helix of polysaccharide rings, which makes it much more rigid than PEI.[257] This relatively high stiffness, as evidenced by a large persistence length (>10 nm), prevents chitosan from interdiffusing into underlying layers and the associated exponential growth.[258] Growth of CH-PAA in the absence of MMT is also shown in Figure 5.2 to highlight the linear growth of these two polymers. This polymer-only growth further demonstrates that clay layers are not limiting polymer interdiffusion and therefore preventing the exponential growth of the system. Nevertheless, in a quadlayer system, PAA is replaced by MMT in every other bilayer, which contributes only 1-2 nm of thickness because of complete clay exfoliation. Additionally, clay platelets provide a new, relatively flat deposition surface each time they are deposited. This new surface diminishes growth because less polymer deposits onto flat platelets than it does on top of another polymer layer with more nano-topology. As a result, assemblies with clay are thinner than those grown with polymers only. In comparison to the bilayer system, presence of extra two polymer layers in every deposition cycle, makes these QL assemblies about twice the thickness of CH-MMT films with single layer of polymer between clay platelets (Figure 5.2).

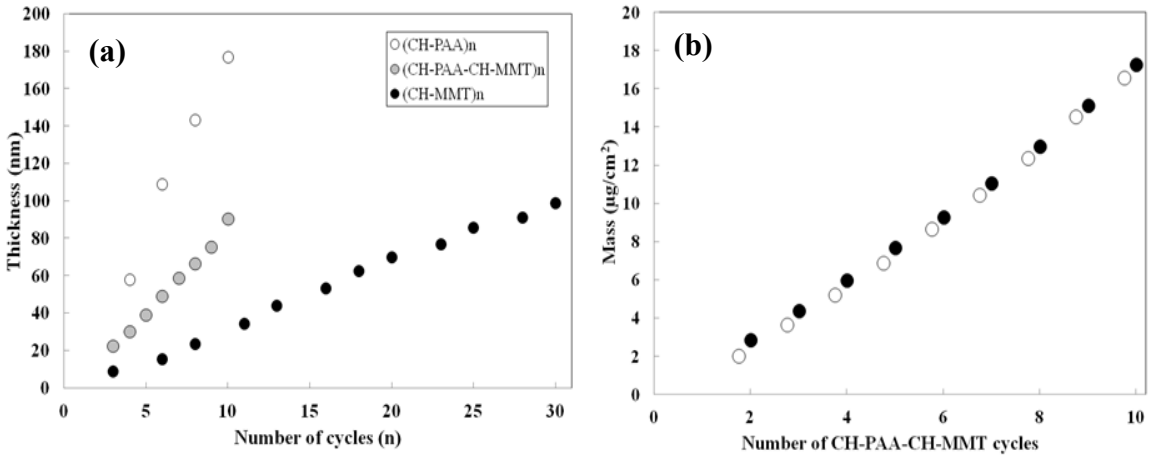

Figure 5.2. Film thickness as a function of cycles deposited of $(CH\text{-}PAA)_n$, $(CH\text{-}PAA\text{-}CH\text{-}MMT)_n$ and (CH-MMT)n(a). Mass as a function of CH-PAA-CH-MMT quadlayers deposited (b), as measured by quartz crystal microbalance, where (CH-PAA-CH) mass deposition is denoted as unfilled points and MMT as filled points.

Linear growth of these CH-based quadlayers is also observed using a quartz crystal microbalance, where every quadlayer contains approximately the same mass (Fig. 5.2(b)). A 10 QL film contains approximately 37 wt% clay, which is very high compared to conventional bulk composites.[259-260] In fact, when the clay concentration exceeds ~10 wt% in bulk materials, their mechanical and optical properties start to degrade due to nanoparticle aggregation.[261-262] UV−vis spectroscopy reveals that this same 10 QL film has an average light transmission of 98% across the visible light spectrum (390−750 nm), as shown in Figure 5.3(a). This transparency is more apparent when examining the inset images of quartz slides with and without the nanocoating. High transparency is attributed to the high level of clay orientation and exfoliation within the deposited film. A TEM image of the cross section of a 10 QL film shows this

high level of clay orientation (Fig. 5.3(b)). Individual clay platelets can be seen as dark lines in this micrograph, which reveals a 'nanobrick wall' structure.[38] This nearly perfect alignment of the platelets is expected to provide excellent gas barrier to the underlying substrate. It has been previously shown that at high clay concentration (i.e., deposition solution concentration > 0.2 wt%) there is a higher degree of lateral packing of clay in each layer, including more overlapping of neighboring platelets.[263]

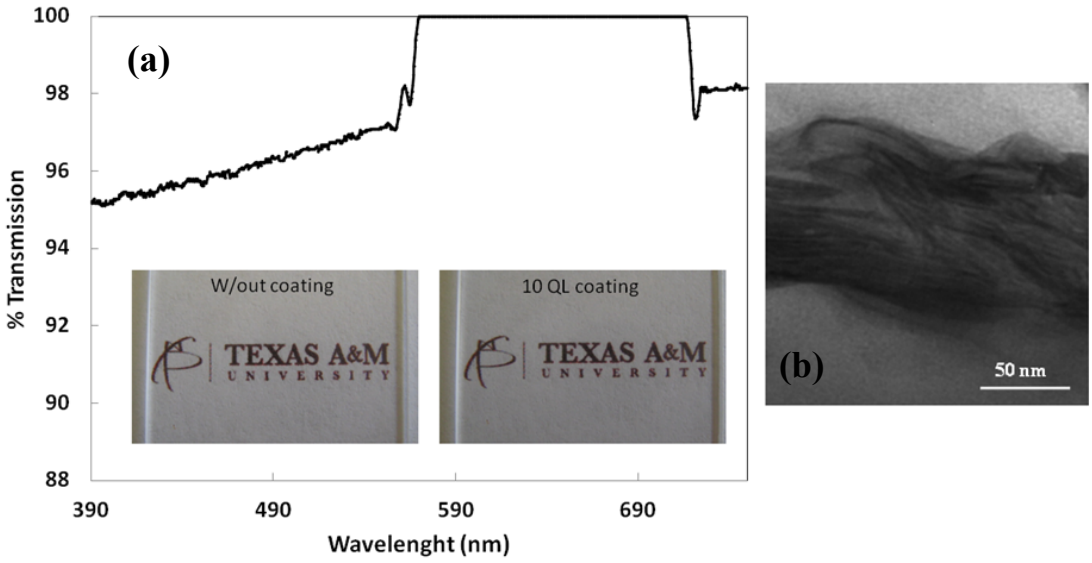

Figure 5.3. Visible light transmission as a function of wavelength for a 10 QL CH/PAA/CH/MMT film deposited on a fused quartz slide (a). The inset images in (a) show quartz slides with (right) and without (left) the 10 QL nanocoating. TEM cross section of 10 QL film deposited on a polystyrene substrate (b).

5.3.2 Oxygen Barrier of Chitosan-based Assemblies

Polylactic acid has received significant attention in recent years due to a desire for biodegradable food packaging.[264] It has already been approved for food contact by

the Food and Drug Administration (FDA) and been primarily used for the packaging of short shelf-life food due to poor oxygen barrier.[265-266] Improving the oxygen barrier of PLA film will allow it to slow down oxidative degradation and increase food shelf-life.[56] It was previously shown that increasing the space between deposited clay layers significantly improves the oxygen barrier of nano brick wall films,[131] so CH pH 6-MMT bilayers were deposited on PLA for this purpose. Table 5.1 shows how the oxygen transmission rate (OTR) of these films decreases with the number of bilayers deposited. With just 10 BL, there is an order of magnitude decrease in OTR relative to the same PLA film with no coating. A 30 BL film, which is only 100 nm thick, exhibits an OTR below the detection limit of commercial instrumentation ($\leq$0.005 $cm^3/(m^2 \cdot day \cdot atm)$). This high barrier behavior is believed to be due to the brick wall nanostructure that produces an extremely tortuous path for oxygen molecules to take as they permeate through the film.[57, 123]

Table 5.1. Oxygen permeability of CH pH 6-MMT assemblies on PLA film at 23 °C.

# of BL	Film thickness (nm)	OTR (cm3/m2 atm·day)	Permeability (x10-16 cm3·cm/cm2·sec·Pa)	
			Film[ab]	Total[b]
0	N/A	30.54	N/A	177.2
10	31.8	2.51	0.0019	14.6
15	48.9	0.68	0.0008	4.0
25	85.6	0.13	0.0002	0.8
30	98.7	<0.005	<0.000008	<0.03

[a] Film permeability was decoupled from the total permeability using a previously described method.[267]
[b] The low end detection limit for an Ox Tran 2/21 L module is 0.005$cm^3/(m^2 \cdot day \cdot atm)$.

CH-PAA-CH-MMT nanocoatings were deposited on PET and polylactic acid film. Figure 5.4(a) shows that OTR significantly decreases, for both PET and PLA, when a 10 QL assembly is deposited. Depositing less than 100 nm of CH-PAA-CH-MMT reduced the OTR of both substrates by two orders of magnitude under dry conditions. These values are well below the required OTR values for packaging processed meat and cheese (3.1-15.5 cc/(m^2•day• atm)) or snack foods (30 cc/(m^2•day•atm)).[268] It is also important to note that PLA coated with 10 QL or 10 BL can achieve a lower OTR than uncoated PET, making it competitive for similar applications (see Table 5.2).

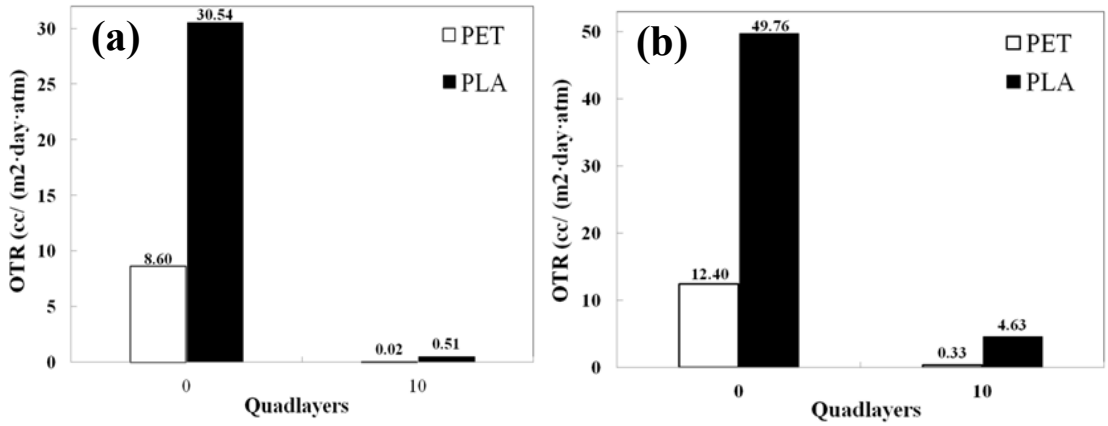

Figure 5.4. Oxygen transmission rate of 175 μm PET and 500 μm PLA with and without a 10 QL CH/PAA/CH/MMT nanocoating. Measurements were made at 23°C and 0% RH (a) or 38°C and 90% RH (b).

It is true that adding clay directly into a polymer matrix improves oxygen barrier of the bulk composite, but these OTR reductions are relatively modest.[52, 269] Permeability of the composite material is predicted to be a function of the aspect ratio of the filler and its orientation.[125] The thickness of a single MMT platelet is roughly 1 nm, while the

length is in the range of 200 – 500 nm.[270] It is very difficult to achieve complete exfoliation of these high aspect ratio nanoplatelets in bulk nanocomposites, which reduces their effectiveness in reducing permeability values.[130] This is emphasized in the literature values presented in Table 5.2, where the addition of clay to PLA and PET provides only a moderate reduction in oxygen permeability. Layer-by-layer assembly provides near perfect control of orientation and exfoliation of clay platelets and this creates an extremely tortuous path for permeating molecules. Highly-oriented layers of tightly-packed, impermeable platelets cause a rerouting of oxygen molecules along the film thickness direction, resulting in a lower transmission rate through the thin film composite.[131]

Another useful tool to evaluate the barrier properties of thin films is the barrier improvement factor (BIF), where BIF equals the permeability of pure polymer divided by the permeability of the composite (or coated substrate). As shown in Table 5.2, a 10 QL coating has a BIF of 263 on PET and 60 on PLA under dry conditions, which is significantly greater than values reported in the literature for bulk composites. Assemblies made with 10 bilayers of CH and MMT, provided smaller BIF values compared to 10 QL film on PLA. This difference is likely due to greater clay spacing in the quadlayer system presented here, where clay layers are separated by three polymer layers (CH-PAA-CH) versus a single CH layer in the bilayer system. Increased clay spacing has been shown to improve oxygen barrier in LbL thin films.[131] Another possible reason for the superior performance of the quadlayer system is the interactions of oppositely charged polyelectrolytes (CH and PAA) which results in more dense

polymer chain packing than CH alone. This effect was observed in assemblies of polyethylenimine and PAA,[17] which also showed good barrier at high humidity. It should be noted tripling the number of clay layers makes oxygen barrier of the CH-MMT below the detection limit of the commercial instrument and provides the highest BIF value.

Table 5.2. Oxygen permeability of chitosan-based assemblies deposited on PET and PLA and of other barrier materials.

Film composition	Oxygen permeability ($x10^{-16}$ cm^3 cm/cm^2 sec Pa)	BIF	Ref.
PET	17.6[a] 25.4[b]		
PLA	177.2[a] 288.7[b]		
10 QL on PET	0.067[a] 0.68[b]	263 37	
10 QL on PLA	2.96[a] 26.87[b]	60 11	
10 BL CH/MMT on PLA	14.6[a]	12	
30 BL CH/MMT on PLA	<0.03[a]	>5906	
PLA/10wt% clay	52.8[a]	2	271
PET/3wt% clay	43.4[a]	2	272
PS/38.8wt% clay	114[a]	20	273

[a] 23 C/0% RH, [b] 38 C/90% RH.

The influence of temperature and relative humidity on oxygen transmission rate is especially important for practical applications. Oxygen barrier is expected to diminish with increasing humidity and temperature due to swelling of the film and an associated

increase in free volume.[274] Despite an increase in OTR, Figure 5.4(b) shows that PLA and PET maintain an oxygen barrier that is an order of magnitude better than uncoated films at 90% RH and 38°C. It is expected that these nanocoatings will be further improved with crosslinking, which has already been shown to reduce moisture sensitivity in LbL nanocoatings.[38, 167, 252]

5.4 Conclusions

Fully transparent nanocoatings with remarkable oxygen barrier properties were deposited on PLA and PET film using biodegradable, food contact approved materials. Layer-by-layer assembled thin films, made with chitosan, polyacrylic acid and natural montmorillonite clay, have near perfect clay platelet orientation and exfoliation that result in exceptional oxygen barrier. Oxygen permeability below 0.03×10^{-16} $cm^3 \cdot cm/cm^2 \cdot sec \cdot Pa$ was achieved with 30 BL of CH pH 6-MMT (< 100 nm thick). Ten CH-PAA-CH-MMT quadlayers reduces oxygen transmission rate of PLA and PET by two orders of magnitude, under dry conditions, and more than one order of magnitude at 38°C and 90 % RH. When comparing these two systems with equal number of clay layers (i.e. 10 BL and 10 QL), the QL system shows greater reduction in oxygen permeability due to increased spacing between clay layers. The combination of all generally recognized as safe materials, high oxygen barrier and transparency exhibited by this film makes it an ideal candidate for food and other types of high performance packaging.

CHAPTER VI

INTUMESCENT MULTILAYER NANOCOATING, MADE WITH RENEWABLE POLYELECTROLYTES, FOR FLAME RETARDANT COTTON*

6.1 Introduction

Intumescent coatings are a subset of flame retardant technology commonly used to protect building materials.[147] The coating does not modify the intrinsic properties (e.g., strength) of the substrate and can be easily applied to a variety of surfaces.[145-146, 275] An intumescent system typically requires three components bound together with a binder: a source of carbon, an acid source and a blowing agent.[148] These components react upon heating to generate a swollen multicellular insulating layer that protects the underlying material from heat and flame.[150] Intumescent nanocoatings were recently applied to cotton fabric using LbL assembly.[276] Layers of polyallylamine (PAAm) and poly(sodium phosphate) (PSP) were conformally deposited on individual fibers, which eliminated the need for a binder. In this case, cotton as well as the PAAm served as the carbon source, creating a complete intumescent system. Twenty bilayers of PAAm-PSP prevented the ignition of cotton fabric, demonstrating the first LbL-based intumescent nanocoating. This effective antiflammable nanocoating, produced with manmade (i.e., synthetic) molecules, can also be prepared with phosphorus and nitrogen-rich renewable

*Reprinted with permission from Laufer, G.; Kirkland, C.; Morgan, A. B.; Grunlan, J. C. Intumescent multilayer nanocoatings, made with renewable polyelectrolytes, for flame retardant cotton, Biomacromolecules, 2012, 13, 2843-2848. © 2012 American Chemical Society.

ingredients.

Interest in green chemistry and concern over toxicity and environmental issues associated with various flame retardant treatments on textiles that come in close contact with skin, have created a desire to use "green" materials. Phytic acid (PA), which is the major storage form of phosphorus in cereal grains, beans, and oil seeds, is one such molecule. [277] Its structure consists of six phosphate groups (Figure 6.1), which is similar to PSP mentioned above. Phytic acid has already been reported as an antioxidant, [278-279] anticancer agent [280-281] and a means of lowering blood glucose level for diabetics.[282-283] Furthermore, it is environmentally-friendly, biocompatible, and nontoxic. PA and its salts are able to interact with positively charged molecules, which makes it a good candidate for layer-by-layer assembly.[284] From a flame retardant perspective, molecules with a higher phosphorus content can deliver more active flame retardant atoms per molecule,[136] and PA has 28wt% P based upon its molecular weight. Chitosan is a nitrogen containing molecule that can be paired with PA to provide a completely renewable intumescent system. Much like phytic acid, CH is biodegradable, biocompatible, and environmentally benign. Chitosan is expected to be an effective intumescent additive, because it will act as a char-forming agent, it is carbon rich, and can be a blowing agent, releasing nitrogen gas as it degrades.[285] Additionally, there is the potential for favorable phosphorus-nitrogen (P-N) condensed phase char formation / flame retardant reactions between chitosan and phytic acid.[286-287]

In this chapter, thin films of chitosan and phytic acid were deposited onto cotton fabric in an effort to create the first bio-based (i.e., renewable) intumescent nanocoating.

Film thickness, as well as phosphorus-to-nitrogen ratio, was tailored by changing the pH of the polyelectrolyte solutions. Three different CH-PA formulations were applied to cotton fabric and their flame retardant properties were studied using vertical flame testing and micro combustion calorimetry (MCC). The thinnest coating (30 BL is ~10 nm thick) was deposited using pH 4 solutions and this multilayer film has the highest PA content (66 wt%) relative to films deposited from pH 5 and 6 solutions. With regard to antiflammability, this pH 4 nanocoating completely stopped flame propagation on cotton fabric, leaving more than 90% residue following the vertical burn test. Calorimetry revealed that all fabrics coated with 30 CH-PA bilayers, exhibited peak heat release rates that were reduced by at least 50% compared to an uncoated control. When CH-PA nanocoatings are normalized by weight deposited on cotton fabric, it appears that greater phosphorus content produces the most effective flame retardant. This work demonstrates the first fully bio-renewable intumescent nanocoating for cotton fabric, whose deposition from aqueous solutions makes this a promising alternative to current antiflammable treatments for fabric.

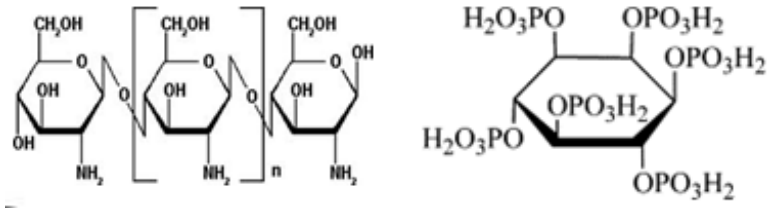

Figure 6.1. Structure of chitosan and phytic acid.

6.2 Experimental

6.2.1 Materials

Cationic deposition solutions were prepared by adjusting the pH of deionized water (18.2MΩ, pH~5.5) to 2 with 1M hydrochloric acid (HCl) and then adding 0.5 wt% chitosan (MW 50-190 kDa, 75-85% deacetylated) purchased from Aldrich (Milwaukee, WI). This solution was magnetically stirred for 24 hours until the chitosan was completely dissolved. Anionic solutions were prepared by adding 2.0 wt% of phytic acid sodium salt hydrate (Aldrich, Milwakee, WI) to deionized water and stirred for 24 hours. The pH of these solutions were adjusted to 4, 5 and 6 with 1 M NaOH or 1 M HCl just prior to deposition. Branched polyethylenimine (1.0 wt% in water) (MW 25,000 g/mol, Aldrich) was used as a primer layer to improve adhesion to cotton. Other materials were described in Chapter III (Section 3.2.1).

6.2.2 Layer-by-Layer Deposition

All films were deposited on a given substrate using the procedure described in Chapter III (Section 3.2.2).

6.2.3 Characterization of Film Growth, Structure and Properties

Film growth characterization is described in Chapter IV (Section 4.2.3). Micro combustion calorimeter, model MCC-1 (Govmark), testing was performed with a 1 °C/sec heating rate under nitrogen, from 200 to 700 °C, using method A of ASTM D7309-07. There was no additional conditioning prior to MCC testing.

6.3 Results and Discussion

6.3.1 Film Growth and Microstructure

Growth of three CH-PA films, assembled from solutions at pH 4, 5 or 6, was monitored using ellipsometry. Figure 6.2(a) shows that all recipes grow linearly, but thickness increases significantly with pH. There are likely two factors causing films to be extremely thin at pH 4. First, chitosan is highly charged at low pH due to the presence of primary amine groups in its structure (Fig. 6.1) and exists in an extended form that deposits very flat (or thin). Thin deposition associated with high charge density polymers has also been observed with polyethylenimine and poly(acrylic acid).[252] Second, there is considerable stiffness in polysaccharides that can hinder the adsorption process and result in island growth.[257] Aggregates observed on the surfaces of 10 BL films are believed to be remnants of these islands. At pH 4 (Fig. 6.2(b)), these raised features are fewer and further between than at pH 6 (Fig. 6.2(c)). Thinner deposition and fewer islands produce the anemic layer thickness growth observed at pH 4. It is also possible that rinsing with unaltered DI water (pH ~5.5) reduces the degree of chitosan ionization and leads to some desorption.

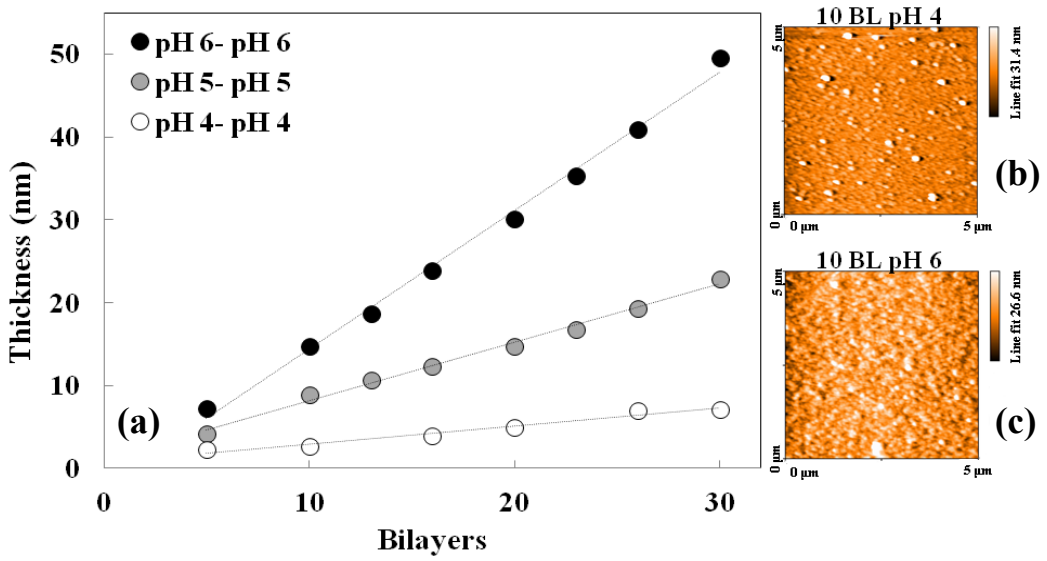

Figure 6.2. Growth of CH-PA assemblies as a function of deposition solution pH, as measured by ellipsometry (a). AFM height images of 10BL assemblies deposited from pH 4 (b) and pH 6 (c) solutions.

As the pH of the chitosan solution increases, chitosan molecules take on a more compact, coiled conformation and deposit in a more globular conformation. This more weakly charged state is also accompanied by reduced self-repulsion that allows more molecules to deposit in a given layer. As a result, thickness of thin film assemblies increases with increasing CH pH. More complete surface coverage can also be observed in the AFM surface scan at pH 6 (Fig. 6.2(c)) relative to pH 4 (Fig. 6.2 (b)). These changes in deposition are also reflected in film composition, as shown in Figure 6.3. Chitosan content decreases with pH due to its thinner deposition. This situation is exacerbated by the fact that higher charge density CH (at pH 4) requires fewer chains to overcompensate the charge of the previously adsorbed PA layer. As the concentration of

phytic acid decreases, from 66 wt% at pH 4 to less than 50 wt% at pH 6, the flammability performance is expected to change due to reduced phosphorus content.[288]

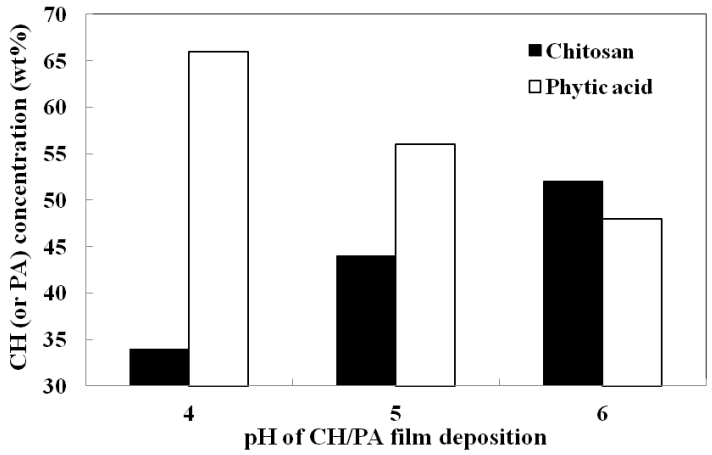

Figure 6.3. Film composition as a function of deposition solution pH for CH-PA assemblies.

6.3.2 Flame Retardant Behavior of Cotton Fabric

Cotton fabric was coated with 30 BL of CH-PA at pH 4, 5 and 6 and subjected to vertical flame testing (ASTM D6413-08). Figure 6.4 shows these fabric samples following a 12 second exposure to direct flame. All coated fabric exhibited a less vigorous flame than the control fabric. Afterflame time was also significantly reduced and afterglow was eliminated. The uncoated control fabric was completely consumed during the test, while fabric coated with 30 BL of pH 5 coating completely stopped the flame from propagating almost immediately after ignition and more than 90 wt% of the fabric was preserved (Fig. 6.4). Fabric coated with pH 4 solutions also showed significant flame retardant capacity, leaving about 80 wt% of the fabric, while adding

only 16 wt% to the fabric weight before burning. Fabric coated with pH 6 solutions was burned much more extensively, but still had some unburned white spots and a significant amount of residue left (42 wt%). Differences in these burn results could be attributed to the difference in the coating weight, as the best flame retardant coating had the highest weight gain added to cotton (~18 wt%).

In an effort to separate the influence of coating weight and composition, fabric coated with 18 wt% at each pH was evaluated. This normalized comparison required 32 and 37 BL coated at pH 4 and 6, respectively. It is interesting to note that there appears to be a substrate influence because pH 6 grows the thickest on Si wafer (Fig. 6.2(a)), which should provide highest weight gain at a given number of bilayers. It is possible that the combination of film rigidity and low charge density at pH 6 contribute to some flaking or peeling of the coating, which would explain this unexpectedly low weight gain on cotton fabric. When comparing the same coating weight, it is clear that higher phytic acid content yields a more effective flame retardant. There was no noticeable change for pH 6 with extra bilayers, but there was a significant improvement for pH 4 with just two additional bilayers. This pH 4 coating has highest concentration of phytic acid among the three recipes tested. In regards to flammability, with phosphorus/phosphate being the active chemistry which induces charring (that in turn lowers heat release and flame propagation), increasing levels of phosphorus should lower flammability in a cellulosic material like cotton.[289-291] With phytic acid containing 28wt% P, higher levels of PA in the pH 4 system yield higher levels of

phosphorus/phosphate available to crosslink the cellulosic fiber and CH to form an intumescent char.

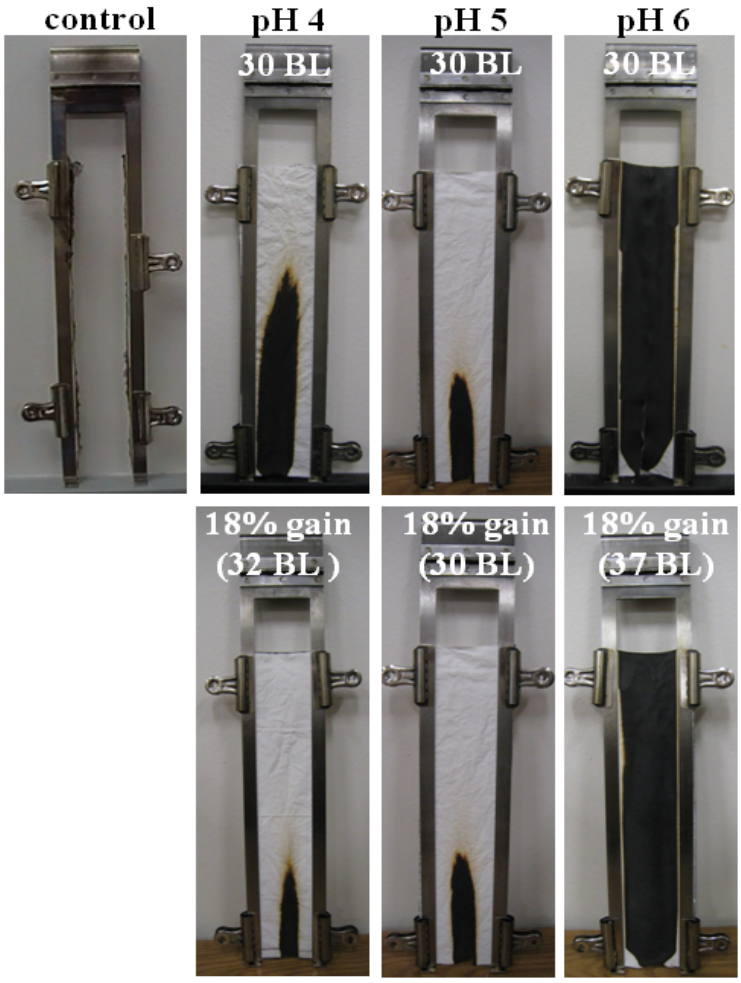

Figure 6.4. Images of uncoated control and fabrics coated with 30 BL of CH-PA (top) and 18 wt% CH-PA (bottom) deposited at varying pH level.

Higher magnification SEM images of burned fabric, as shown in Figure 6.5, provide further insight into the observed antiflammable behavior of these CH-PA

nanocoatings. The coating does not obscure the weave structure of the fabric and, at higher magnification (middle row of images in Fig. 6.5), the conformal coating of individual cotton fibers can be clearly seen. All coated fibers look similar in shape and structure to the uncoated control, but some of the coated fibers are linked together. Fabric coated with pH 6 solutions appears to have the roughest surface with numerous bridges formed between individual fibers. This roughness suggests that this thickly depositing system probably starts to form those bridges early in the deposition process and as more layers get deposited, and the fabric gets twisted during processing steps, the coating connecting the fibers peels off and contributes to a low final weight gain. These gaps in the coating serves as sites where heat will penetrate through the protective coating and thermally damage the underlying cotton, which can lead to pyrolysis of flammable gases and subsequent localized flame propagation. Thin deposition at lower pH delays this inter-fiber linking, which preserves the coating and therefore eliminates the gaps in the protective coating.

Images of the postburn samples (in the bottom row of Fig. 6.5) show that cotton fibers retain their shape and integrity after burning and there is also evidence of intumescent behavior. There are bubbles on top and in the gap between fibers due to expansion of the intumescent carbon layer in the coating as gas evolves during burning. These images clearly demonstrate the protective nature of this coating by forming a swollen, cellular layer. Although this intumescent coating does not expand to 10 times its original size, like most conventional intumescent coatings, it remains able to slow, and in some cases stop, the flame propagation. The pH 6 coating exhibits much less

bubbling (i.e., weaker intumescent effect), which was expected based upon its diminished flame retardant behavior (Fig. 6.4). This coating has the lowest phosphorus content (Fig. 6.3), which is a contributing factor, and the weak points/gaps in this coating likely result in uneven fire protection on the surface of the fibers.

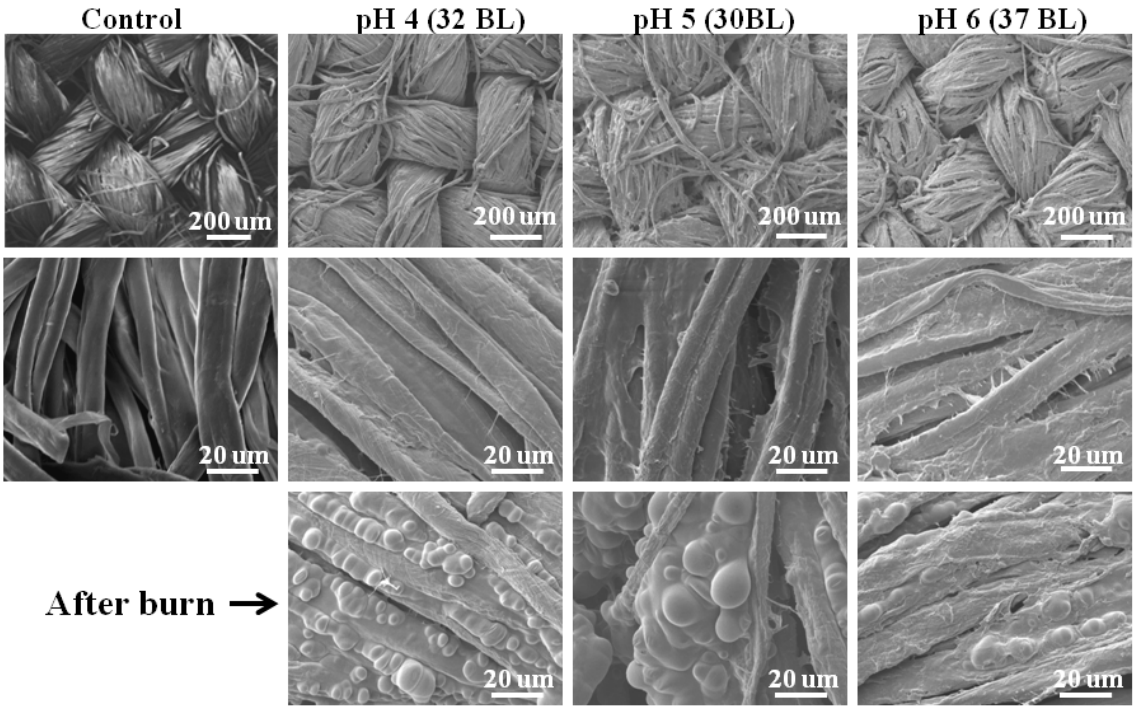

Figure 6.5. SEM images of coated and uncoated cotton fabric before (top two rows) and after (bottom row) vertical burn testing. The uncoated fabric was completely consumed during burning, so no postburn image can be shown.

Micro cone calorimetry (MCC) was used to further investigate the flame retardant properties of coated and uncoated cotton. Figure 6.6 shows heat release rate (HRR) curves generated with fabric containing 18 wt% of CH-PA deposited at pH 4, 5, and 6. It appears that the presence of the intumescent coating decreases the onset

decomposition temperature for coated fabrics and this becomes more pronounced as the phytic acid concentration in the coating increases. This temperature decrease, which has been observed with other phosphorus-containing flame retardants, [140, 276] is due to the catalyzed dehydration of cellulose, which aids in char formation by the decomposition of phosphorus compounds. The best performing pH 4 fabric exhibits the greatest reduction in peak heat release rate (pkHRR) and total heat release (HR) of 60% and 76% respectively, compared to the uncoated control. Although somewhat counterintuitive, it is important for the components of the coating to degrade before the onset of cotton degradation in order to preemptively form the protective layer. This lower temperature of reaction is good because char formation is initiated early in the fire, thus preventing further pyrolysis of the cotton that in turn retards flame spread.

In an effective intumescent system, the acid source must be the first component to decompose to ensure dehydration of the carbon source.[59] Phytic acid begins to decompose around 200 °C, which is below the decomposition temperature of cotton (320 °C) or chitosan (250 °C). [285, 292] Next, the carbon source (chitosan and carbon rich cotton itself) is converted into char by a dehydration reaction with PA. This char is then expanded by gases produced by decomposition of the blowing agent. In this case, chitosan serves as carbon source and blowing agent, so there is a continuous release of foaming gases over the entire char forming area. Eventually, the coating solidifies into a multicellular material that slows the heat flow from the fire to the substrate.[59] To put the HRR reduction into perspective, lowering peak HRR and total HR of a burning material means it is easier for the material to self-extinguish once the flame source is removed.

Lower heat release means that the heat from the burning material is less, so it is harder to propagate flame and for heat to damage unburned portions of the material adjacent to the site of flaming combustion.[291, 293]

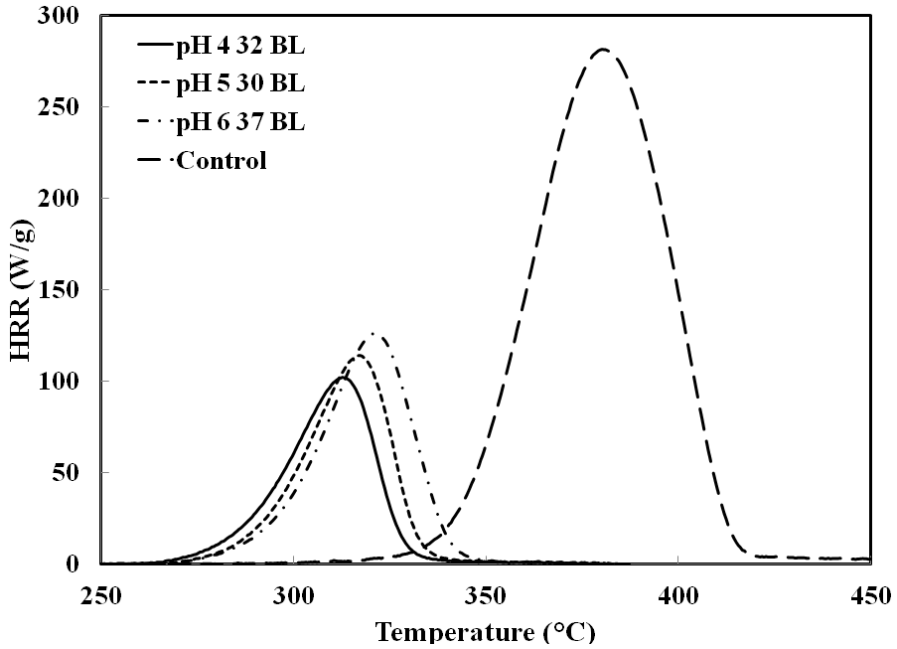

Figure 6.6. Heat release rate as a function of temperature for uncoated control and CH-PA coated cotton fabric. All coated fabrics contained 18 wt% CH-PA.

Table 6.1 summarizes the results of micro cone calorimeter testing. All coated fabric exhibits reduced total HR by at least 70%. Additionally, the amount of char increased by a factor of seven and is significantly greater than the coating weight, confirming that cotton fabric itself was preserved during the burning. It is also clear, from Table 6.1 and Figure 6.4, that burn behavior improves with higher phytic acid concentration. It has been shown previously that flame retardant properties of cellulostic

fabrics improve with increase of phosphorus content due to more effective dehydration of cellulose, prevention of formation of volatile material and accelerating formation of char. [140, 294] Even though these intumescent nanocoatings demonstrate lower flammability of cotton fabric in MCC testing, these results do not directly correlate with postburn residues. The pH 4 coating exhibits the lowest heat release rate even at 30 BL (i.e., lower weight) relative to pH 5 (at the same number of BL), while the latter appears to perform better in the vertical flame test (Fig. 6.4). These seemingly conflicting results could be attributed to uneven surface coverage on the fabric with pH 4 coating, which exhibits the thinnest growth (Fig. 6.2). With just two more BL, the pH 4 coating performs the best in every category and completely prevents flame propagation on cotton. Even with the worst performing pH 6 coating, the heat release was significantly reduced, which is one of the desired characteristics for a flame retardant coating.

Table 6.1. Micro cone calorimeter results for CH-PA coated cotton fabric and an uncoated control.

	# BL (% weight gain)	Char yield (wt%)	pkHRR (W/g)[a]	pkHRR (°C)[a]	Total HR (kJ/g)[b]
Control	-	5.6 ± 0.1	259± 6.7	382 ± 2.1	12.0 ± 0.1
pH 4	30 BL (~16 %)	41.7 ± 1.9	99 ± 3.5	311 ± 0.9	2.8 ± 0.1
	32 BL (~18 %)	42.4 ± 0.3	100 ± 1.8	313 ± 0.8	2.8 ± 0.1
pH 5	30 BL (~18 %)	41.8 ± 0.5	116 ± 3.3	318 ± 0.3	3.2 ± 0.1
pH 6	30 BL (~13 %)	38.7 ± 0.4	134 ± 1.4	318 ± 5.0	3.8 ± 0.1
	37 BL (~18 %)	39.1 ± 0.8	161 ± 12.8	322 ± 1.2	3.8 ± 0.1

[a] pkHRR=peak heat release rate; [b]HR=heat release

6.4 Conclusions

Intumescent nanocoatings were deposited on cotton fabric using environmentally benign components (chitosan and phytic acid) to impart flame retardant behavior. By varying the pH of aqueous depositing solutions, coating thickness and composition were modified. Using solutions at pH 6 resulted in relatively thick coatings with the lowest phytic acid content, while the opposite was achieved at pH 4 (i.e., thin growth and high PA content). The flame retardant properties of 30 BL coated fabric were tested using the vertical flame test, where pH 5 coating (with the heaviest weight gain) was able to extinguish the flame. To eliminate the variable of coating weight, fabrics with equal weight gain (~18 wt%) were subjected to the vertical flame test. There was a clear trend of improvement in burn behavior with higher phytic acid content. Fabric coated with pH 4 (66 wt% PA) left as much as 95% preserved fabric (completely unburned material with a small amount of char) after burning. Small bubbles formed on top of and in the space between the fibers were observed by SEM, which is evidence of the intumescent effect. Additionally, micro calorimeter testing revealed a lower peak heat release rate for all coated fabrics. Coatings made with pH 4 solutions resulted in better flame retardant properties relative to those made at higher pH due to greater phosphorus content (in the form of PA). Higher phosphorus concentration is known prevent formation of volatile material and accelerate formation of char more effectively. This study demonstrates the first completely renewable intumescent LbL nanocoating for cotton fabric, which provides an effective and environmentally-friendly alternative to current flame retardant treatments.

CHAPTER VII

CONCLUSIONS AND FUTURE WORK

The ultimate goal of this dissertation was to create a nanocoating system that would be compatible with any substrate (with proper surface pre-treatment) and extinguish flame on the coated substrate. By incorporating flame retardant materials into layer-by-layer assemblies, anti-flammable nanocoatings were deposited onto complex substrates, such as cotton fabric and open-celled polyurethane foam, to impart anti-flammability. In addition to reducing flammability, this dissertation explored the use of food contact approved materials to create transparent nanocoatings with high oxygen barrier that could serve as an for environmentally-friendly foil replacement.

7.1 Colloidal Silica-based Thin Film Assemblies

Thin films of colloidal silica were deposited on cotton fibers via layer-by-layer assembly in an effort to reduce the flammability of cotton fabric. Negatively charged silica nanoparticles of two different sizes (8 and 27 nm) were paired with either positively charged silica (12 nm) or cationic polyethylenimine (PEI). PEI/silica films were thicker due to better (more uniform) deposition of silica particles that contributed to more than 90% of the film weight. Each coating was evaluated at 10 and 20 bilayers (BL). All coated fabrics retained their weave structure after being exposed to a vertical flame test, while uncoated cotton was completely destroyed. Micro combustion calorimetry confirmed that coated fabrics exhibited a reduced peak heat release rate, by

as much as 20% relative to the uncoated control. The 10 BL PEI- 8 nm silica recipe was the most effective because the coating is relatively thick and uniform relative to the other systems. Soaking cotton in basic water (pH 10) prior to deposition resulted in better assembly adhesion and flame retardant behavior. These results demonstrate that LbL assembly is a useful technique for imparting flame retardant properties through conformal coating of complex substrates like cotton fabric.

7.2 Clay-Chitosan Nanobrick Walls for Flame Retardant Foam

Thin films prepared via LbL assembly of renewable materials exhibit exceptional flame retardant properties. Positively-charged chitosan, at two different pH levels (3 and 6), was paired with anionic montmorillonite clay nanoplatelets. Thin film assemblies prepared with CH at high pH are thicker due to low polymer charge density. A 10 bilayer (CH pH 6-MMT) nanocoating (~30 nm thick) completely stops the melting of a flexible polyurethane foam, when exposed to direct flame from a butane torch. Cone calorimetry confirms that this coated foam exhibited a reduced peak heat release rate, by as much as 52%, relative to the uncoated control. These environmentally benign nanocoatings could prove beneficial as a replacement for environmentally persistent antiflammable compounds.

7.3 Oxygen Barrier of Chitosan-Based Nanobrick Wall Thin Films

Multilayered thin films assembled with “green” food contact approved materials (i.e., chitosan, polyacrylic acid and montmorillonite clay). Thin coatings of CH-MMT

bilayers, and CH-PAA-CH-MMT quadlayers, were deposited on PLA and PET films. PLA has poor oxygen barrier properties relative to petroleum-based polymers that are widely used as food packaging (e.g. PET). Only ten CH/PAA/CH/MMT quadlayers (~90 nm thick), can cause PLA film to behave like PET in terms of oxygen barrier. A thirty bilayer CH-MMT assembly (~100 nm thick) on PLA exhibits an oxygen transmission rate (OTR) below the detection limit of commercial instrumentation (≤0.005 $cm^3/(m^2 \cdot day \cdot atm)$). This high barrier behavior is believed to be due to the brick wall nanostructure that produces an extremely tortuous path for oxygen molecules to take as they permeate through the film. The combination of all generally recognized as safe (GRAS) materials, high oxygen barrier and transparency exhibited by this film makes it an ideal candidate for food and other types of high performance packaging.

7.4 Intumescent Nanocoating

Thin films of fully renewable and environmentally benign electrolytes, cationic chitosan and anionic phytic acid, were deposited on cotton fabric via layer-by-layer assembly in an effort to reduce flammability. Altering the pH of aqueous deposition solutions modifies the composition of the final nanocoating. CH-PA films created at pH 6 were thicker and had 48wt% PA in the coating, while the thinnest films (with a PA content of 66 wt%) were created at pH 4. Each coating was evaluated at both 30 BL and at the same coating weight added to the fabric. In a vertical flame test, fabrics coated with high PA content multilayers completely extinguished the flame, while uncoated cotton was completely consumed. Micro combustion calorimetry confirmed that all

coated fabric reduces peak heat release rate (pkHRR) by at least 50% relative to the uncoated control. Fabric coated with pH 4 solutions shows the greatest reduction in pkHRR and total heat release of 60% and 76%, respectively. This superior performance is believed to be due to high phosphorus content that enhances the intumescent behavior of these nanocoatings. These results demonstrate the first completely renewable intumescent LbL assembly, which conformally coats every fiber in cotton fabric and provides an effective alternative to current flame retardant treatments.

7.5 Future Research Direction

From the results in Chapter VI, it is known that intumescent components chemically react with each other, which results in a self-extinguishing treatment. There is still room to improve LbL-based current intumescent systems by exploring the effect of synergistic components. Durability of these flame retardant coatings on fabric is another issue to be investigated. In most cases, fabric needs to be washed and still retain the FR nanocoating. It is also important to explore other renewable food contact approved ingredients that can result in nanocoatings with higher oxygen barrier and/or fewer layers to achieve a given barrier level. These three areas of future work are described in more detail below.

7.5.1 Synergistic Influence of Colloidal Silica in Intumescent Coating Assemblies

Chapter VI showed that an intumescent nanocoating is very effective in preventing the ignition of cotton fabric. It has been also shown that the incorporation of nanoparticles into intumescent systems leads to a synergistic effect between the

components that improves the fire retarding properties.[295-296] It is believed that these particles act as char stabilizers and reinforcers.[297] Colloidal silica is a known FR addititive, as shown in Chapter III, that can be incorporated into the chitosan-phytic acid intumescent coating described in Chapter VI. The silica is expected to improve the nanocoating's FR performance or to achieve the same FR with fewer layers. Two different methods of incorporating silica should be investigated. In one case, several silica layers could be strategically incorporated into the nanocoating, as shown in Figure 7.1 (a). The effect of the number of these layers, as well as their placement (i.e. top, middle or bottom of the film) and spacing should be studied. Another approach involves mixing small amounts of silica nanoparticles (0.1-1 wt%) with one of the LbL film components, which should result in particles randomly attaching themselves throughout the film structure, as shown in Figure 7.1 (b). For this approach, the relation between silica concentration and FR performance would be investigated. The ultimate goal of this study is to achieve FR performance of cotton fabric similar to the one described in Chapter V, but with no more than 20 bilayers. If successful, this same approach could be used to reduce the number of layers in any FR nanocoating, which would improve the commercial viability of this technology.

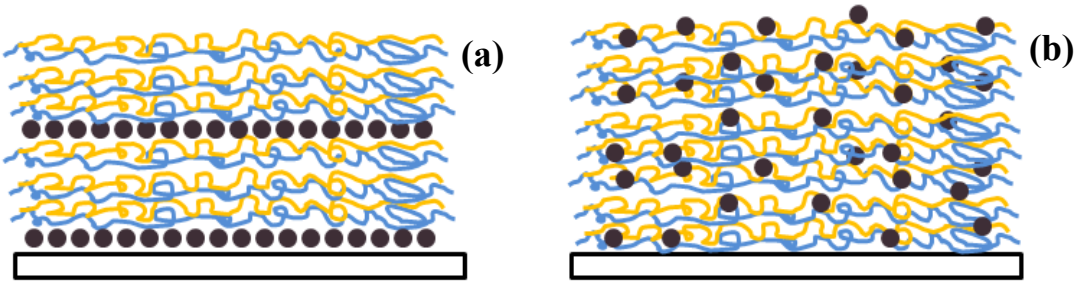

Figure 7.1. Proposed film structures with varying synergist placement inside the intumescent film: silica as individual layers (a) and silica mixed with one of the two film components (b).

7.5.2 Wash Durability of Nanocoating on Cotton Fabric

As most textile fabrics would undergo repeated laundering during their lifetime, the washing durability of cotton fabric is of significant importance. It has been suggested that during laundering the interactions between nanocoating layers could be destroyed, and the LbL films could be removed from the substrate (e.g. textile fibers), resulting in loss of functionality. To strengthen and stabilize the nanocoatings, crosslinking can be introduced between functional groups. It has been reported that the mechanical properties of crosslinked thin films improved up to three orders of magnitude relative to neat polymer,[176] with chemical and thermal stability greatly improved. Coatings already developed by our group, with known flame retardant characteristics, could be used as model systems in this study.[276] Gluteraldehyde (GA) can be used for crosslinking poly(sodium phosphate) (PSP) and polyallylamine (PAAm), as it capable of reacting with amine groups of PAAm. Crosslinking can be acomplished by soaking coated fabric in a water-based solution containing GA. Preliminary results have shown that soaking

fabric in 0.05 M GA solution for 30 minutes preserved the coating and its flame retardant properties after one wash, as shown in Figure 7.2. The effect of crosslinking agent concentration and exposure time still needs to be evaluated. Wash durability of coated fabrics can be tested by laundering them for 5, 10, 15, and 20 cycles in a washing machine according to AATCC Test Method 124-2006. After each set of washes, flammability of fabrics can be evaluated.

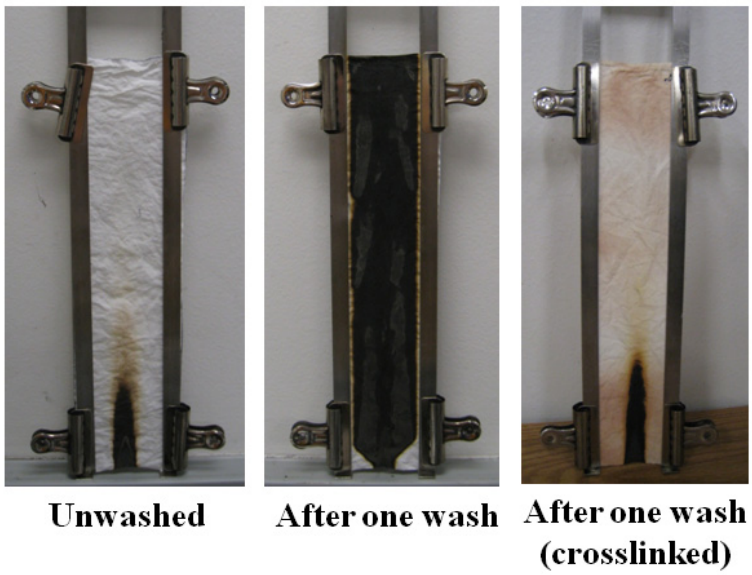

Figure 7.2. Cotton fabric coated with 20 BL of PAAm-PSP after vertical flame testing.

7.5.3 High Oxygen Barrier with Renewable, Food Contact Safe Polyelectrolytes

Chapter IV revealed the ability to improve gas barrier performance of PLA and PET films by applying a thin coating of polymer and clay. It has also been shown that all-polymer LbL assemblies, created with PEI and PAA, can effectively reduce oxygen permeability.[252] These films can be re-created with renewable food contact approved

materials. Carrageenan (CR) is a sulfated polysaccharide extracted from certain red seaweeds. It is extensively used in the food industry as gelling and stabilizing agent.[298] Pairing CR with cationic chitosan, used for oxygen barrier in Chapter IV, will result in fully renewable polysaccharide-based films. Preliminary growth results for these assemblies are shown in Figure 7.3. These films can be deposited on PET and PLA substrates to examine their oxygen permeability as a function of bilayers deposited. Additionally, chitosan and carrageenan both exhibit antimicrobial properties, so this same coating can be evaluated for its antimicrobial efficacy. [299-300]

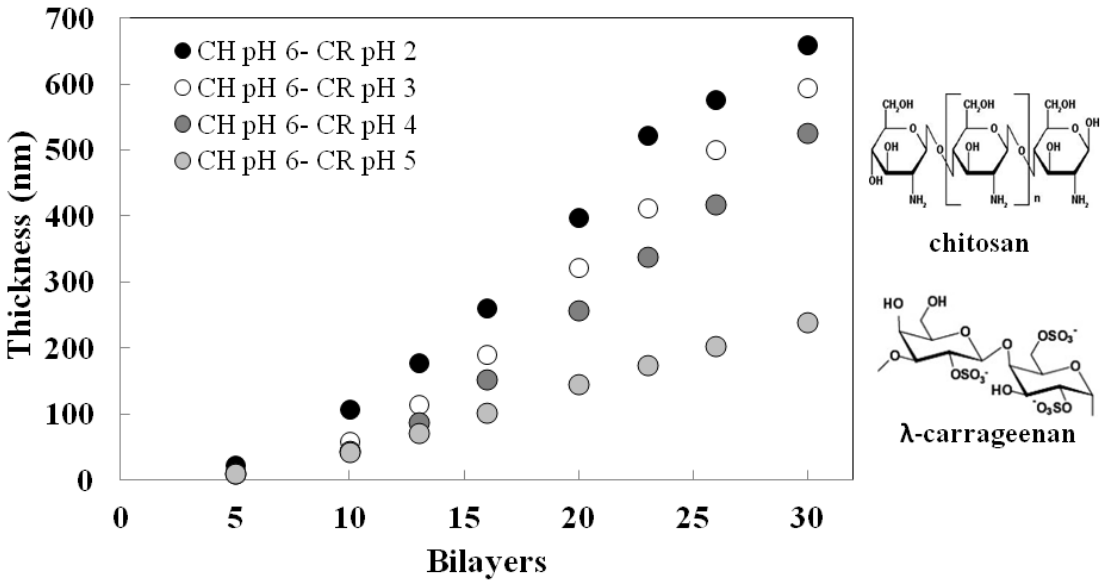

Figure 7.3. Growth of chitosan/carrageenan thin film assemblies as a function of bilayers deposited under varying pH conditions.

REFERENCES

(1) Hirschler, M. M. *Polym. Adv. Technol.* **2008,** *19,* 521-529.

(2) Kamath, M. G.; Bhat, G. S.; Parikh, D. V.; Condon, B. D. *J. Ind. Text.* **2009,** *38,* 251-262.

(3) de Wit, C. A. *Chemosphere* **2002,** *46,* 583-624.

(4) Watanabe, I.; Sakai, S. *Environ. Int.* **2003,** *29,* 665-682.

(5) Guo, J. W.; Park, C. B.; Lee, Y. H.; Kim, Y. S.; Sain, M. *Polym. Eng. Sci.* **2007,** *47,* 330-336.

(6) Gilman, J. W.; Harris, R. H.; Shields, J. R.; Kashiwagi, T.; Morgan, A. B. *Polym. Adv. Technol.* **2006,** *17,* 263-271.

(7) Si, M.; Goldman, M.; Rudomen, G.; Gelfer, M. Y.; Sokolov, J. C.; Rafailovich, M. H. *Macromol. Mater. Eng* **2006,** *291,* 602-611.

(8) Song, L.; Hu, Y.; Tang, Y.; Zhang, R.; Chen, Z.; Fan, W. *Polym. Degrad. Stab.* **2005,** *87,* 111-116.

(9) Bartholmai, M.; Schartel, B. *Polym. Adv. Technol.* **2004,** *15,* 355-364.

(10) Zhu, J.; Start, P.; Mauritz, K. A.; Wilkie, C. A. *Polym. Degrad. Stab.* **2002,** *77,* 253-258.

(11) Brown, J. M.; Curliss, D.; Vaia, R. A. *Chem. Mater.* **2000,** *12,* 3376-3384.

(12) Kashiwagi, T.; Grulke, E.; Hilding, J.; Harris, R. H.; Awad, W.; Douglas, J. *Macromol. Rapid Commun.* **2002,** *23,* 761-765.

(13) Schartel, B.; Potschke, P.; Knoll, U.; Abdel-Goad, M. *Eur. Polym. J.* **2005,** *41,* 1061-1070.

(14) Peeterbroeck, S.; Laoutid, F.; Swoboda, B.; Lopez-Cuesta, J. M.; Moreau, N.; Nagy, J. B.; Alexandre, M.; Dubois, P. *Macromol. Rapid Commun.* **2007,** *28,* 260-264.

(15) Ray, S. S.; Okamoto, M. *Prog. Polym. Sci.* **2003,** *28,* 1539-1641.

(16) Laufer, G.; Carosio, F.; Martinez, R.; Camino, J.; Grunlan, J. C. *J. Colloid Interface Sci.* **2011,** *356,* 69-77.

(17) Li, Y. C.; Schulz, J.; Mannen, S.; Delhom, C.; Condon, B.; Chang, S.; Zammarano, M.; Grunlan, J. C. *ACS Nano* **2010,** *4,* 3325-3337.

(18) Zanetti, M.; Kashiwagi, T.; Falqui, L.; Camino, G. *Chem. Mater.* **2002,** *14,* 881-887.

(19) Hao, J.; Lewin, M.; Wilkie, C. A.; Wang, J. *Polym. Degrad. Stab.* **2006,** *91,* 2482-2485.

(20) Tang, Y.; Lewin, M.; Pearce, E. *Macromol. Rapid Commun.* **2006,** *27,* 1545-1549.

(21) Hribernik, S.; Smole, M. S.; Kleinschek, K. S.; Bele, M.; Jamnik, J.; Gaberscek, M. *Polym. Degrad. Stab.* **2007,** *92,* 1957-1965.

(22) Kashiwagi, T.; Gilman, J. W.; Butler, K. M.; Harris, R. H.; Shields, J. R. *Fire Mater.* **2000,** *24,* 277-289.

(23) Yang, F.; Nelson, G. L. *J. Appl. Polym. Sci.* **2004,** *91,* 3844-3850.

(24) Lu, Z.; Eadula, S.; Zheng, Z.; Xu, K.; Grozdits, G.; Lvov, Y. *Colloids Surf. Physicochem. Eng. Aspects* **2007,** 56-62.

(25) Lvov, Y.; Ariga, K.; Onda, M.; Mitsuhiko, O.; Ichinose, I.; Kunitake, T. *Langmuir* **1997,** *13,* 6195-6203.

(26) Lee, D.; Gemici, Z.; Rubner, M. F.; Cohen, R. E. *Langmuir* **2007,** *23,* 8833-8837.

(27) Decher, G.; Eckle, M.; Schmitt, J.; Struth, B. *Curr. Opin. Colloid Interface Sci.* **1998,** *3,* 32-39.

(28) Decher, G.; Essler, F.; Hong, J. D.; Lowack, K.; Schmitt, J.; Lvov, Y. *Abstr. Paper Am. Chem. Soc.* **1993,** *205,* 334-POLY.

(29) Hammond, P. *Adv. Mater.* **2004,** *16,* 1271-1293.

(30) Shiratori, S. S.; Rubner, M. F. *Macromolecules* **2000,** *33,* 4213-4219.

(31) Chang, L.; Kong, X.; Wang, F.; Wang, L.; Shen, J. *Thin Solid Films* **2008,** *516,* 2125-2129.

(32) Sui, Z.; Salloum, D.; Schlenoff, J. B. *Langmuir* **2003,** *19,* 2491-2495.

(33) McAloney, R. A.; Sinyor, M.; Dudnik, V.; Goh, M. C. *Langmuir* **2001,** *17,* 6655-6663.

(34) Tan, H. L.; McMurdo, M. J.; Pan, G. Q.; Van Patten, P. G. *Langmuir* **2003,** *19,* 9311-9314.

(35) Hiller, J.; Mendelsohn, J. D.; Rubner, M. F. *Nature Materials* **2002,** *1,* 59-63.

(36) Cho, J.; Hong, J.; Char, K.; Caruso, F. *J. Am. Chem. Soc.* **2006,** *128,* 9935-9942.

(37) Zhang, X.; Fujishima, A.; Jin, M.; Emeline, A. V.; Murakami, T. *J. Phys. Chem. B* **2006,** *110,* 25142-25148.

(38) Priolo, M.; Gamboa, D.; Holder, K.; Grunlan, J. C. *Nano Lett.* **2010,** *10,* 4970-4974.

(39) Shen, L.; Hu, N. *Biomacromolecules* **2005,** *6,* 1475-1483.

(40) Yan, X. B.; Chen, X. J.; Tay, B. K.; Khor, K. A. *Electrochem. Commun.* **2007,** *9,* 1269-1275.

(41) Aoki, P. H.; Volpati, D.; Riul, A.; Caetano, W.; Constantino, C. J. L. *Langmuir* **2009,** *25,* 2331-2338.

(42) Park, Y. T.; Grunlan, J. C. *Electrochim. Acta* **2010,** *55,* 3257-3267.

(43) DeLongchamp, D. M.; Kastantin, M.; Hammond, P. T. *Chem. Mater.* **2003,** *15,* 1575-1586.

(44) Liu, S.; Kurth, D. G.; Mohwald, H.; Volkmer, D. *Adv. Mater.* **2002,** *14,* 225-228.

(45) Dvoracek, C. M.; Sukhonosova, G.; Benedik, M. J.; Grunlan, J. C. *Langmuir* **2009,** *25,* 10322-10328.

(46) Podsiadlo, P.; Paternel, S.; Rouillard, J. M.; Zhang, Z. F.; Lee, J.; Lee, J. W.; Gulari, L.; Kotov, N. A. *Langmuir* **2005,** *21,* 11915-11921.

(47) Li, Z.; Lee, D.; Sheng, X.; Cohen, R. E.; Rubner, M. F. *Langmuir* **2006,** *22,* 9820-9823.

(48) Macdonald, M.; Rodriguez, N. M.; Smith, R.; Hammond, P. T. *J. Controlled Release* **2008,** *131,* 228-234.

(49) Caruso, F.; Trau, D.; Mohwald, H.; Renneberg, R. *Langmuir* **2000,** *16,* 1485-1488.

(50) Lefebvre, J.; Bras, M.; Bastin, B.; Paleja, R.; Delobel, R. *J. Fire Sci.* **2003,** *21,* 343-367.

(51) Wakelyn, P. J.; Bertoniere, N. R.; French, A. D.; Thibodeaux, D., Chemical Properties of Cotton. In *Cotton Fiber Chemistry and Technology*, CRP Press: Boca Raton, FL, 2007.

(52) Zhong, Y.; Janes, D.; Zheng, Y.; Hetzer, M.; De, K. D. *Polym. Eng. Sci.* **2007,** *47,* 1101-1107.

(53) Bieder, A.; Gruniger, A.; von Rohr, P. R. *Surf. Coat. Technol.* **2005,** *200,* 928-931.

(54) Garlotta, D. *J. Polym. Environ.* **2001,** *9,* 63-84.

(55) Jarerat, A.; Tokiwa, Y. *Macromol. Biosci.* **2001,** *1,* 136-140.

(56) Auras, R.; Singh, S. P.; Singh, J. J. *Packag. Technol. Sci.* **2005,** *18,* 207-216.

(57) Duncan, T. V. *J. Colloid Interface Sci.* **2011,** *363,* 1-24.

(58) Beyler, C. L.; Hirschler, M. M., Thermal Decomposition of Polymers. In *SFPE Handbook of Fire Protection Engineering*, 3rd ed.; DiNenno, P. J., Ed. National Fire Protection Association: 2002; pp 110-131.

(59) Mouritz, A.; Gibson, A., Fire Properties of Polymer Composite Materials. In *Fire Properties of Polymer Composite Materials*, Mouritz, A.; Gibson, A., Eds. Springer: 2006; pp 237-286.

(60) Sergio, B.; Giovanni, C., Halogen-Containing Flame Retardants. In *Fire Retardancy of Polymeric Materials, Second Edition*, CRC Press: 2009; pp 75-105.

(61) Wilkie, C.; McKinney, M., Thermal Properties of Thermoplastics. In *Plastics Flammability Handbook: Principles, Regulations, Testing, and Approval*, Troitzsch, J., Ed. Hanser Publications: Munich, 2004; pp 58-76.

(62) Hull, T. R.; Kandola, B. K., *Fire Retardancy of Polymers: New Strategies and Mechanisms*. The Royal Society of Chemistry: Cambridge, UK, 2009.

(63) Staggs, J. E. J., Modeling Thermal Degradation of Polymers by Population Balance Methods. In *Fire Retardancy of Polymeric Materials*, Wilkie, C.; Morgan, A. B., Eds. CRC Press: Boca Raton, Fl, 2009; pp 479-508.

(64) Ketata, N.; Sanglar, C.; Waton, H.; Alemercery, S.; Delolme, F.; Raffin, G.; Grenier-Loustalot, M. E. *Polym. Polym. Compos.* **2005,** *13,* 1-26.

(65) Yang, W. P.; Macosko, C. W.; Wellinghoff, S. T. *Polymer* **1986,** *27,* 1235-1240.

(66) Voorhees, K.; Hileman, F.; Einhorn, I.; Futrell, J. *J. Polym. Sci.* **1978,** *16,* 213-228.

(67) Rogers, F.; Ohlemiller, T. *J. Macromol. Sci., Pure Appl. Chem.* **1981,** *15,* 169-185.

(68) Shen, D. K.; Gu, S. *Bioresour. Technol.* **2009,** *100,* 6496-6504.

(69) Factor, A. *J. Chem. Educ.* **1974,** *51,* 453-456.

(70) van Krevelen, D. W. *Polymer* **1975,** *16,* 615-620.

(71) Weil, E.; Lewin, M., Mechanisms and Modes of Action in Flame Retardancy of Polymers. In *Fire Retardant Materials*, Horrocks, A. R.; Price, D., Eds. Woodhead Publishing: Cambridge, 2001; pp 31-68.

(72) Alexandre, M.; Dubois, P. *Mat. Sci. Eng. R.* **2000,** *28,* 1-63.

(73) Zammarano, M.; Franceschi, M.; Bellayer, S.; Gilman, J. W.; Meriani, S. *Polymer* **2005,** *46,* 9314-9328.

(74) Alongi, J.; Franche, A. *Polym. Degrad. Stab.* **2010,** *95,* 1928-1933.

(75) Moniruzzaman, M.; Winey, K. I. *Macromolecules* **2006,** *39,* 5194-5205.

(76) Kashiwagi, T.; Fangming, D.; Douglas, J. F.; Winey, K. I.; Harris, R. H.; Shields, J. R. *Nature Materials* **2005,** *4,* 928-933.

(77) Fina, A.; Abbenhuis, H. C. L.; Tabuani, D.; Camino, G. *Polym. Degrad. Stab.* **2006,** *91,* 2275-2281.

(78) Dasari, A.; Yu, Z.-Z.; Mai, Y.-W.; Cai, G.; Song, H. *Polymer* **2009,** *50,* 1577-1587.

(79) Yang, F.; Nelson, G. L. *Polym. Adv. Technol.* **2006,** *17,* 320-326.

(80) Vaia, R. A.; Giannelis, E. P. *MRS Bull.* **2001,** *26,* 394-401.

(81) Schadler, L. S.; Kumar, S. K.; Benicewicz, B. C.; Lewis, S. L.; Harton, S. E. *MRS Bull.* **2007,** *32,* 335-340.

(82) Roy, M.; Nelson, J. K.; MacCrone, R. K.; Schadler, L. S.; Reed, C. W.; Keefe, R. *IEEE Trans. Dielectr. Electr. Insul.* **2005,** *12,* 629-643.

(83) Winey, K. I.; Vaia, R. A. *MRS Bull.* **2007,** *32,* 314-319.

(84) Chen, B.; Evans, J. R. G.; Greenwell, H. C.; Boulet, P.; Coveney, P. V.; Bowden, A. A.; Whiting, A. *Chem. Soc. Rev.* **2008,** *37,* 568-594.

(85) Aranda, P.; Ruiz-Hitzky, E. *Chem. Mater.* **1992,** *4,* 1395-1403.

(86) Wu, J.; Lerner, M. M. *Chem. Mater.* **1993,** *5,* 835-838.

(87) Reichert, P.; Kressler, J.; Thomann, R.; Mullhaupt, R.; Stoppelmann, G. *Acta Polym.* **1998,** *49,* 116-123.

(88) Zeng, Q. H.; Wang, D. Z.; Yu, A. B.; Lu, G. Q. *Nanotechnology* **2002,** *13,* 549-553.

(89) Vaia, R. A.; Ishii, H.; Giannelis, E. P. *Chem. Mater.* **1993,** *5,* 1694-1696.

(90) Fornes, T. D.; Yoon, P. J.; Keskkula, H.; Paul, D. R. *Polymer* **2001,** *42,* 9929-9940.

(91) Biswas, M.; Ray, S. S. *Adv. Polym. Sci.* **2001,** *155,* 167-221.

(92) Theng, B. K. G. *Clays Clay Miner.* **1970,** *18,* 357-362.

(93) Gilman, J. W.; Kashiwagi, T.; Lichtenhan, J. *SAMPE J.* **1997,** *33,* 40-46.

(94) Tyan, H. L.; Leu, C. M.; Wei, K. H. *Chem. Mater.* **2001,** *13*.

(95) Zhang, X.; Yang, M.; Zhao, Y.; Zhang, S.; Dong, X.; Liu, X.; Wang, D.; Xu, D. *J. Appl. Polym. Sci.* **2004,** *92,* 552-558.

(96) Page, D. J. Y. S.; Cunningham, N.; Chan, N.; Carran, G.; Kim, J. *J. Vinyl Addit. Techn.* **2007,** *13,* 91-97.

(97) Yang, L.; Hu, Y.; Lu, H.; Song, L. *J. Appl. Polym. Sci.* **2006,** *99,* 3275-3280.

(98) Ranade, A.; D'Souza, N. A.; Gnade, B.; Dharia, A. *J. Plast. Film Sheet.* **2003,** *19,* 271-285.

(99) Ras, R. H. A.; Umemura, Y.; Johnston, C. T.; Yamagishi, A. S., R. A. *PCCP* **2007,** *9,* 918-932.

(100) Almasri, A.; Ounaies, Z.; Kim, Y. S.; Grunlan, J. *Macromol. Mater. Eng* **2008,** *293,* 123-131.

(101) Jiang, X.; Bin, Y.; Matsuo, M. *Polymer* **2005,** *46,* 7418-7424.

(102) Ruoff, R.; Lorents, D. C. *Carbon* **1995,** *33,* 925-930.

(103) Wang, S.-F.; Shen, L.; Zhang, W.-D.; Tong, Y.-J. *Biomacromolecules* **2005,** *6,* 3067-3072.

(104) Chen, H.; Muthuraman, H.; Stokes, P.; Zou, J.; Liu, X.; Wang, J.; Hou, Q.; Khondaker, S. I.; Zhai, L. *Nanotechnology* **2007,** *18,* 1-9.

(105) Laoutid, F.; Bonnaud, L.; Alexandre, M.; Lopez-Cuesta, J.-M.; Dubois, P. *Mat. Sci. Eng. R.* **2009,** *63,* 100-125.

(106) Leroux, F.; Besse, J.-P. *Chem. Mater.* **2001,** *13,* 3507-3515.

(107) Costa, F. R.; Wagenknecht, U.; Heinruch, G. *Polym. Degrad. Stab.* **2007,** *92,* 1813-1823.

(108) Taviot-Gueho, C.; Leroux, F. *Struct. Bond.* **2006,** *119,* 121-159.

(109) Glodek, T. E.; Boyd, S. E.; McAnich, I. M.; LaScala, J. J. *Compos. Sci. Technol.* **2008,** *68,* 2994-3001.

(110) Kuo, S. W.; Lin, H. C.; Huang, W. J.; Huang, C. F.; Chang, F. C. *J. Polym. Sci., Part B: Polym. Phys.* **2006,** *44,* 673-686.

(111) Misra, M.; Fu, B., X.; Morgan, S. E. *J. Polym. Sci., Part B: Polym. Phys.* **2007,** *45,* 2441-2455.

(112) Kashiwagi, T.; Morgan, A. B.; Antonucci, J. M.; VanLandingham, M.; Harris, R.; Awad, W. H.; Shields, J. *J. Appl. Polym. Sci.* **2003,** *89,* 2072-2078.

(113) Hornsby, P. R. *Macromol. Sy.* **1996,** *108,* 203-219.

(114) Wang, L.; He, X.; Wilkie, C. *Materials* **2010,** *3,* 4580-4606.

(115) Kashiwagi, T.; Harris, J., R. H.; Zhang, X.; Briber, R. M.; Cipriano, B. H.; Raghavan, S. R.; Awad, W. H.; Shields, J. R. *Polymer* **2004,** *45,* 881-891.

(116) Qin, H.; Zhang, S.; Zhao, C.; Hu, G.; Yang, M. *Polymer* **2005,** *46,* 8386-8395.

(117) Kashiwagi, T.; Du, F.; Winey, K. I.; Groth, K. M.; Shields, J. R.; Bellayer, S. P.; Kim, H.; Douglas, J. F. *Polymer* **2005,** *46,* 471-481.

(118) Svagan, A. J.; Akesson, A.; Cardenas, M.; Bulut, S.; Knudsen, J. C.; Risbo, J.; Plackett, D. *Biomacromolecules* **2012,** *13,* 397-405.

(119) Shields, R. J.; Bhattacharyya, D.; Fakirov, S. *Composites Part A* **2008,** *39,* 940-949.

(120) Choudalakis, G.; Gotsis, A. D. *Eur. Polym. J.* **2009,** *45,* 967-984.

(121) Fredrickson, G. H.; Bicerano, J. *J. Chem. Phys.* **1999,** *110,* 2181-2188.

(122) Nielsen, L. E. *J. Macromol. Sci., Pure Appl. Chem.* **1967,** *1,* 929-942.

(123) Cussler, E. L.; Hughes, S. E.; Ward, W. J., III; Arias, R. *J. Membr. Sci.* **1988,** *38,* 161-174.

(124) Lape, N. K.; Nuxoll, E. E.; Cussler, E. l. *J. Membr. Sci.* **2004,** *236,* 29-37.

(125) Gusev, A.; Lusti, H. R. *Adv. Mater.* **2001,** *13,* 1641-1643.

(126) DeRocher, J. P.; Gettelfinger, B. T.; Wang, J.; Nuxoll, E. E.; Cussler, E. L. *J. Membr. Sci.* **2005,** *254,* 21-30.

(127) Bharadwaj, R. k. *Macromolecules* **2001,** *34,* 9189-9192.

(128) Ebina, T.; Mizukami, F. *Adv. Mater.* **2007,** *19,* 2450-2453.

(129) Triantafyllidis, K. S.; LeBaron, P. C.; Park, I.; Pinnavaia, T. J. *Chem. Mater.* **2006,** *18,* 4393-4398.

(130) Osman, M. A.; Mittal, V.; Lusti, H. R. *Macromol. Rapid Commun.* **2004,** *25,* 1145-1149.

(131) Priolo, M.; Gamboa, D.; Grunlan, J. C. *ACS Appl. Mater. Interfaces* **2010,** *2,* 312.

(132) Green, J. *J. Fire Sci.* **1996,** *14,* 426-442.

(133) Larsen, E. R. *J Fire Flammability Fire Retard Chem Suppl* **1974,** *1,* 4-12.

(134) Larsen, E. R., Fire Retardants (Halogenated). In *Kirk-Othmer Encyclopedia of Chemical Technology*, Wiley-Interscience: 1980; Vol. 3rd edition, pp 373-395.

(135) Larsen, E. R. *J Fire Flammability Fire Retard Chem Suppl* **1979,** *10,* 69-77.

(136) Levchik, S. V.; Weil, E. D. *J. Fire Sci.* **2006,** *24,* 345-364.

(137) Schartel, B.; R., K.; Neubert, D. *J. Appl. Polym. Sci.* **2001,** *83,* 2060-2071.

(138) Levchik, S. V.; Levchik, G. F.; Balabanovich, A. I.; Weil, E. D.; Klatt, M. *Die Angewandte Makromolekulare Chemie* **1999,** *264,* 48-55.

(139) Price, D.; Horrocks, A. R.; Akalin, M.; Faroq, A. A. *J. Anal. Appl. Pyrolysis* **1997,** *40-41,* 511-524.

(140) Gaan, S.; Sun, G. *Polym. Degrad. Stab.* **2007,** *92,* 968-974.

(141) Kandola, B. K.; Horrocks, A. R.; Price, D.; Coleman, G. *J. Macromol. Sci., Polym. Rev.* **1996,** *36,* 721-794.

(142) Schartel, B. *Materials* **2010,** *3,* 4710-4745.

(143) Hörold, S. *Polym. Degrad. Stab.* **1999,** *64,* 427-431.

(144) Babushok, V.; Tsang, W. *Combust. Flame* **2000,** *123,* 488-506.

(145) Duquesne, S.; Magnet, S.; Jama, C.; Delobel, R. *Surf. Coat. Technol.* **2003,** *180-181,* 302-307.

(146) Chen-Yang, Y. W.; Chuang, J. R.; Yang, Y. C.; Li, C. Y.; Chiu, Y. S. *J. Appl. Polym. Sci.* **1998,** *69,* 115-122.

(147) Weil, E. D. *J. Fire Sci.* **2011,** *29,* 259-296.

(148) Duquesne, S.; Magnet, S.; Jama, C.; Delobel, R. *Polym. Degrad. Stab.* **2005,** *88,* 63-69.

(149) Bourbigot, S.; Duquesne, S., Intumescence-Based Fire Retardants. In *Fire Retardancy of Polymeric Materials*, Wilkie, C.; Morgan, A. B., Eds. CRC Press: 2009.

(150) Leca, M.; Cioroianu, L.; Cioroianu, G.; Damian, G.; Costea, C.; Matei, A. M. *Rev. Roum. Chim.* **2007,** *52,* 745-752.

(151) Armitage, P.; Ebdon, J. R.; Hunt, B. J.; Jones, M. S.; Thorpe, F. G. *Polym. Degrad. Stab.* **1996,** *54,* 387-393.

(152) Dogan, M.; Bayramli, E. *J. Appl. Polym. Sci.* **2010,** *118,* 2722-2727.

(153) Morgan, A. B.; Jurs, J. L.; Tour, J. M. *J. Appl. Polym. Sci.* **2000,** *76,* 1257-1268.

(154) Todd, M. H.; Balasubramania, S.; Abell, C. *Tetrahedron Lett.* **1997,** *38,* 6781-6784.

(155) Horacek, H.; Grabner, R. *Polym. Degrad. Stab.* **1996,** *54,* 205-215.

(156) Konig, A.; Fehrenbacher, U.; T., H.; Kroke, E. *J Cell Plast* **2008,** *44,* 469-480.

(157) Casu, A.; Camino, G.; De Giogi, M.; Morone, V.; Zenoni, R. *Polym. Degrad. Stab.* **1997,** *58,* 297-302.

(158) Chen, Y.; Wang, Q.; Yan, W.; Tang, H. *Polym. Degrad. Stab.* **2006,** *91,* 2632-2643.

(159) Chen, Y.; Wang, Q. *Polym. Adv. Technol.* **2007,** *18,* 587-600.

(160) Zhou, S.; Song, L.; Wang, Z.; Hu, Y.; Xing, W. *Polym. Degrad. Stab.* **2008,** *93,* 1799-1806.

(161) Sawada, Y.; Yamaguchi, J.; Sakurai, O.; Uematsu, K.; Mizutani, N.; Kato, M. *Thermochim. Acta* **1979,** *33,* 127-140.

(162) Haurie, L.; Fernandez, A. I.; Velasco, J. I.; Chimenos, J. M.; Tico-Grau, J. R.; Espiell, F. *Macromol. Sy.* **2005,** *221,* 165-174.

(163) Iler, R. K. *J. Colloid Interface Sci.* **1966,** *21,* 569-594.

(164) Decher, G.; Hong, J. D. *Makromolekulare Chemie-Macromolecular Symposia* **1991,** *46,* 321-327.

(165) Decher, G.; Hong, J. D.; Schmitt, J. *Thin Solid Films* **1992,** *210,* 831-835.

(166) Decher, G.; Lehr, B.; Lowack, K.; Lvov, Y.; Schmitt, J. *Biosens. Bioelectron.* **1994,** *9,* 677-684.

(167) Lutkenhaus, J. L.; McEnnis, K.; Hammond, P. T. *Macromolecules* **2008,** *41,* 6047-6054.

(168) Decher, G. *Abstr. Paper Am. Chem. Soc.* **2003,** *225,* U615-U615.

(169) Wood, K. C.; Little, S. R.; Langer, R.; Hammond, P. T. *Angewandte Chemie-International Edition* **2005,** *44,* 6704-6708.

(170) Kim, B.-S.; V., L. O.; Koynov, K.; Gong, H.; Caminade, A.-M.; Majoral, J. P.; Vinogradova, O. I. *Macromolecules* **2006,** *39,* 5479-5483.

(171) Angelatos, A. S.; Katagiri, K.; Caruso, F. *Soft Matter* **2006,** *2,* 18-23.

(172) Smith, A. R.; Ruggles, J. L.; Yu, A.; Gentle, I. R. **2009,** *25,* 9873-9878.

(173) Araki, K.; Wagner, M. J.; Wrighton, M. S. *Langmuir* **1996,** *12,* 5393-5398.

(174) Podsiadlo, P.; Michel, M.; Lee, J.; Verploegen, E.; Kam, N. W. S.; Ball, V.; Lee, J.; Qi, Y.; Hart, A. J.; Hammond, P. T.; Kotov, N. A. *Nano Lett.* **2008,** *8,* 1762-1770.

(175) Lutkenhaus, J. L.; Olivetti, E. A.; Verploegen, E. A.; Cord, B. M.; Sadoway, D. R.; Hammond, P. T. *Langmuir* **2007,** *23,* 8515-8521.

(176) Podsiadlo, P.; Kaushik, A. K.; Arruda, E. M.; Waas, A. M.; Shim, B. S.; Xu, J.; Nandivada, H.; Pumplin, B. G.; Lahann, J.; Ramamoorthy, A.; Kotov, N. A. *Science* **2007,** *318,* 80-83.

(177) Zucolotto, V.; Gattas-Asfura, K. M.; Tumolo, T.; Perinotto, A. C.; Antunes, P. A.; Constantino, C. J. L.; Baptista, M. S.; Leblanc, R. M.; Jr., O. N. O. *Appl. Surf. Sci.* **2005,** *246,* 397-402.

(178) Zhang, J.; Li, Q.; Di, X.; Liu, Z.; Xu, G. *Nanotechnology* **2008,** *19,* 435606.

(179) Srivastava, S.; Kotov, N. A. *Acc. Chem. Res.* **2008,** *41,* 1831-1841.

(180) Park, Y. T.; Ham, A.; Grunlan, J. C. *J. Phys. Chem. C* **2010,** *114*.

(181) Shim, B. S.; Tang, Z. Y.; Morabito, M. P.; Agarwal, A.; Hong, H. P.; Kotov, N. A. *Chem. Mater.* **2007,** *19,* 5467-5474.

(182) Liu, X.; Zhou, L.; Geng, W.; Sun, J. *Langmuir* **2008**.

(183) Tokuhisa, H.; Hammond, P. *Adv. Funct. Mater.* **2003,** *13,* 831-839.

(184) Serizawa, T.; Yamaguchi, M.; Akashi, M. *Biomacromolecules* **2002,** *3,* 724-731.

(185) Chen, Y.; Lin, X.; Park, H.; Greever, R. *Nanomed. Nanotechnol. Biol. Med.* **2009,** *5,* 316-322.

(186) Ariga, K.; Hill, J. P.; Ji, Q. *PCCP* **2007,** *9,* 2319-2340.

(187) Lvov, Y.; Ariga, K.; Kunitake, T. *Chem. Lett.* **1994,** *23,* 2323-2326.

(188) He, P.; Hu, N.; Rusling, J. F. *Langmuir* **2004,** *20,* 722-729.

(189) Shchukin, D. G.; Patel, A. A.; Sukhorukov, G. B.; Lvov, Y. M. *J. Am. Chem. Soc.* **2004,** *126,* 3374-3375.

(190) Jiang, B.; Li, B. *Int. J. Nanomedicine* **2009,** *4,* 37-53.

(191) Haynie, D. T.; Balkundi, S.; Palath, N.; Chakravarthula, K.; Dave, K. *Langmuir* **2004,** *20,* 4540-4547.

(192) Toellner, L.; Fischlechner, M.; Ferko, B.; Grabherr, R. M.; Donath, E. *Clin. Chem.* **2006,** *52,* 1575-1583.

(193) Steinmetz, N. F.; Findlay, K. C.; Noel, T. R.; Parker, R.; Lomonossoff, G. R.; Evans, D. J. *ChemBioChem* **2008,** *9,* 1662-1670.

(194) Caruso, F.; Schuler, C. *Langmuir* **2000,** *16,* 9595-9603.

(195) Anzai, J.; Kobayashi, Y.; Suzuki, Y.; Takeshita, H.; Chen, Q.; Osa, T.; Hoshi, T.; Du, X.-Y. *Sensors Actuators B: Chem.* **1998,** *53,* 3-9.

(196) Lvov, Y.; Onda, M.; Ariga, K.; Kunitake, T. *J. Biomater. Sci., Polym. Ed.* **1998,** *9,* 345-355.

(197) Dubas, S. T.; Iamsamai, C.; Potiyaraj, P. *Sensors Actuators B: Chem.* **2006,** *113,* 370-375.

(198) Wang, Y.; Wei, W.; Liu, X.; Zeng, X. *Mater. Sci. Eng. C- Bio. S.* **2009,** *29,* 50-54.

(199) Grech, J. M.; Mano, J. F.; Reis, R. L. *J. Bioact. Compat. Polym.* **2008,** *23,* 367-380.

(200) Li, Q.-L.; Huang, N.; Chen, J.; Wan, G.; Zhao, A.; Chen, J.; Wang, J.; Yang, P.; Leng, Y. *J. Biomed. Mater. Res.* **2009,** *89A,* 575-584.

(201) Fu, J.; Ji, J.; Fan, D.; Shen, J. *J. Biomed. Mater. Res.* **2006,** *79A,* 665-674.

(202) Cecius, M.; Jerome, C. *Prog. Org. Coat.* **2011,** *70,* 220-223.

(203) Caseli, L.; dos Santos, D. S.; Aroca, R. F.; Oliveira, O. N. *Mater. Sci. Eng., C* **2009,** *29,* 1687-1690.

(204) Schmidt, T. F.; Caseli, L.; dos Santos, D. S.; Oliveira, O. N. *Mater. Sci. Eng., C* **2009,** *29,* 1889-1892.

(205) Yin, B.; Yuan, R.; Chai, Y.; Chen, S.; Cao, S.; Xu, Y.; Fu, P. *Biotechnol. Lett* **2008,** *30,* 317-322.

(206) Lu, C.; Mu, B.; Liu, P. *Colloids Surf. B. Biointerfaces* **2011,** *83,* 254-259.

(207) Chen, M.-C.; Liang, H.-F.; Chiu, Y.-L.; Chang, Y.; Wei, H.-J.; Sung, H.-W. *J. Controlled Release* **2005,** *108,* 178-189.

(208) Miao, X.; Liu, Y.; Gao, W.; Hu, N. *Bioelectrochemistry* **2010,** *79,* 187-192.

(209) Zhang, J.; Senger, B.; Vautier, D.; Picart, C.; Schaaf, p.; Voegel, J.-C.; Lavalle, P. *Biomaterials* **2005,** *26,* 3353-3361.

(210) de Mesquita, J. P.; Patrício, P. S.; Donnici, C. L.; Petri, D. F.; de Oliveira, L. C.; Pereira, F. V. *Soft Matter* **2011,** *7,* 4405-4413.

(211) Gilman, J. W.; Kashiwagi, T.; Morgan, A. B.; Harris, R. H.; Brassell, L.; VanLandingham, M.; Jackson, C. L., 6513, N., Ed. 2000.

(212) Ribitsch, V.; Stana-Kleinschek, K.; Jeler, S. *Colloid. Polym. Sci.* **1996,** *274,* 388-394.

(213) Ma, R.; Sasaki, T.; Bando, Y. *J. Am. Chem. Soc.* **2004,** *126,* 10382-10388.

(214) Reisch, A.; Voegel, J.-C.; Gonthier, E.; Decher, G.; Senger, B.; Schaaf, P.; Mesini, P. J. *Langmuir* **2009,** *25,* 3610-3617.

(215) Pei, R.; Cui, X.; Yang, X.; Wang, E. *Biomacromolecules* **2001,** *2*.

(216) Ostrander, J. W.; Mamedov, A. A.; Kotov, N. A. *J. Am. Chem. Soc.* **2001,** *123,* 1101-1110.

(217) Buchert, J.; Pere, J.; Johansson, L. S.; Campbell, J. M. *Text Res J* **2001,** *71,* 626-629.

(218) Nakanishi, S.; Hashimoto, T. *Text Res J* **1998,** *68,* 807-813.

(219) Lee, D. W.; Lim, H.; Chong, H. N.; Shim, W. S. *Open Biomed. J.* **2009,** *1,* 10-20.

(220) El-Tahlawy, K.; Hudson, S. M. *J. Appl. Polym. Sci.* **2006,** *100,* 1162-1168.

(221) Kurita, K. *Prog. Polym. Sci.* **2001,** *26,* 1921-1971.

(222) Desbrieres, J. *Polymer* **2004,** *45,* 3285-3295.

(223) Prabaharan, M. *J. Biomater. Appl.* **2008,** *23,* 5-36.

(224) Shu, X. Z.; Zhu, K. J. *Int. J. Pharm.* **2002,** *233,* 217-225.

(225) Felt, O.; Buri, P.; Gurny, R. *Drug Dev. Ind. Pharm.* **1998,** *24,* 979-993.

(226) Lee, K. Y.; Kwon, I. C.; Kim, Y.-H.; Jo, W. H.; Jeong, S. Y. *J. Controlled Release* **1998,** *51,* 213-220.

(227) Mi, F.-L.; Shyu, S.-S.; Wu, Y.-B.; Lee, S.-T.; Shyong, J.-Y.; Huang, R.-N. *Biomaterials* **2001,** *22,* 165-173.

(228) Kim, H. J.; Lee, H. C.; J.S., O.; Shin, B. A.; Oh, C. S.; Park, R. D.; Yang, K. S.; Cho, C. S. *J. Biomater. Sci., Polym. Ed.* **1999,** *10,* 543-556.

(229) Mi, F.-L.; Wu, Y.-B.; Shyu, S.-S.; Schoung, J.-Y.; Huang, Y.-B.; Hao, J.-Y. *J. Biomed. Mater. Res. B Appl. Biomater.* **2002,** *59,* 438-449.

(230) Mao, J.; Zhao, L.; Yao, K.; Shang, Q.; Yang, G.; Cao, Y. *J. Biomed. Mater. Res. A* **2003,** *64A,* 301-308.

(231) Gingras, M.; Paradis, I.; Berthod, F. *Biomaterials* **2003,** *24,* 1653-1661.

(232) Ma, L.; Shi, Y.; Chen, Y.; Zhao, H.; Gao, C.; Han, C. *J. Mater. Sci. Mater. Med.* **2007,** *18,* 2185-2191.

(233) Suwan, J.; Zhang, Z.; Li, B.; Vongchan, P.; Meepowpan, P.; Zhang, F.; Mousa, S.; Premanode, B.; Kongtawelert, P.; Linhardt, R. *Carbohydr. Res.* **2009,** *344,* 1190-1196.

(234) Lin, W.-C.; Liu, T.-Y.; Yang, M.-C. *Biomaterials* **2004,** *25,* 1947-1957.

(235) Richert, L.; Lavalle, P.; Payan, E.; Shu, X. Z.; Prestwich, G. D.; Stoltz, J. F.; Schaaf, P.; Voegel, J. C.; Picart, C. *Langmuir* **2004,** *20,* 448-458.

(236) Podsiadlo, P.; Tang, Z.; Shim, B. S.; Kotov, N. A. *Nano Lett.* **2007,** *7,* 1224-1231.

(237) Kim, D. W.; Kumar, J.; Blumstein, A. *Appl. Clay Sci.* **2005,** *30,* 134-140.

(238) Li, Y.-C.; Schulz, J.; Grunlan, J. C. *ACS Appl. Mater. Interfaces* **2009,** *1,* 2338-2347.

(239) Hickey, J.; Burke, N. A. D.; Stöver, H. D. H. *J. Membr. Sci.* **2011,** *369,* 68-76.

(240) Yang, Y.-H.; Malek, F. A.; Grunlan, J. C. *Ind. Eng. Chem. Res.* **2010,** *49,* 8501-8509.

(241) Annabi-Bergaya, F. *Microporous Mesoporous Mater.* **2008,** *107,* 141-148.

(242) Ploehn, H. J.; Liu, C. Y. *Ind. Eng. Chem. Res.* **2006,** *45,* 7025-7034.

(243) Simchi, A.; Pishbin, F.; Boccaccini, A. R. *Mater. Lett.* **2009,** *63,* 2253-2256.

(244) Kramer, R. H.; Zammarano, M.; Linteris, G. T.; Gedde, U. W.; Gilman, J. W. *Polym. Degrad. Stab.* **2010,** *95,* 1115-1122.

(245) Schartel, B.; Hull, T. R. *Fire Mater.* **2007,** *31,* 327-354.

(246) Zhao, C.; Qin, H.; Gong, F.; Feng, M.; Zhang, S.; Yang, M. *Polym. Degrad. Stab.* **2005,** *87,* 183-189.

(247) Morgan, A. B.; Chu, L.-L.; Harris, J. D. *Fire Mater.* **2005,** *29,* 213-229.

(248) Aider, M. *LWT- Food Science and Technology* **2010,** *43,* 837-842.

(249) Jahromi, S. *Macromolecules* **2000,** *33,* 7582-7587.

(250) Decher, G.; Schlenoff, J. B., *Multilayer Thin Films – Sequential Assembly of Nanocomposite Materials*. Wiley-VCH: Weinheim, Germany, 2003.

(251) De Villiers, M. M.; Otto, D. P.; Strydom, S. J.; Lvov, Y. M. *Adv. Drug Del. Rev.* **2011,** *63,* 701-715.

(252) Yang, Y.-H.; Haile, M.; Park, Y. T.; Malek, F. A.; Grunlan, J. C. *Macromolecules* **2011,** *44,* 1450-1459.

(253) *GRN No. 170* US Food and Drug Administration.

(254) *Doc No. 6198* U.S. Food and Drug Administration.

(255) *21CFR184.1155* U.S. Food and Drug Administration.

(256) Picart, C.; Mutterer, J.; Richert, L.; Luo, Y.; Prestwich, G. D.; Schaaf, P.; Voegel, J. C.; Lavalle, P. *Proceedings of the National Academy of Sciences of the United States of America* **2002,** *99,* 12531-12535.

(257) Skovstrup, S.; Hansen, S. G.; Skrydstrup, T.; Schiott, B. *Biomacromolecules* **2010,** *11,* 3196-3207.

(258) Morris, G. A.; Castile, J.; Smith, A.; Adams, G. G.; Harding, S. E. *Carbohydr. Polym.* **2009,** *76,* 616-621.

(259) Kumar, S. A.; Yuelong, H.; Yumei, D.; Le, Y.; Kumaran, M. G.; Thomas, S. *Ind. Eng. Chem. Res.* **2008,** *47,* 4898-4904.

(260) Choi, R.-N.; Cheigh, C.-I.; Lee, S.-Y.; Chung, M.-S. *Food Science* **2011,** *76,* N62-N67.

(261) Gao, F. *Mater. Today* **2004,** *7,* 50-55.

(262) Grunlan, J. C.; Grigorian, A.; Hamilton, C. B.; Mehrabi, A. R. *J. Appl. Polym. Sci.* **2004,** *93,* 1102-1109.

(263) Priolo, M. A.; Holder, K. H.; Gamboa, D.; Grunlan, J. C. *Langmuir* **2011,** *27,* 12016-12114.

(264) Drumright, R. E.; Gruber, P. R.; Henton, D. E. *Adv. Mater.* **2000,** *12,* 1841-1846.

(265) Plackett, D. V.; Holm, V. K.; Johansen, P.; Ndoni, S.; Nielsen, P. V.; Sipilainen-Malm, T.; Sodergard, A.; Verstichel, S. *Packag. Technol. Sci.* **2006,** *19,* 1-24.

(266) Jin, T.; Zhang, H. *J. Food Sci.* **2008,** *73,* M127-M134.

(267) Roberts, A. P.; Henry, B. M.; Sutton, A. P.; Grovenor, C. R. M.; Briggs, G. A. D.; Miyamoto, T.; Kano, A.; Tsukahara, Y.; Yanaka, M. *J. Membr. Sci.* **2002,** *208,* 75-88.

(268) Wagner, J. R., *Multilayer Flexible Packaging*. 1 ed.; Elsevier: Oxford, 2009; p 258.

(269) Krook, M.; Albertsson, A.-C.; Gedde, U. W.; Hedenqvist, M. S. *Polym. Eng. Sci.* **2002,** *42,* 1238-1246.

(270) Ploehn, H. J.; Liu, C. *Ind. Eng. Chem. Res.* **2006,** *45,* 7025-7034.

(271) Chang, J.-H.; An, Y. U.; Sur, G. S. *J. Polym. Sci., Part B: Polym. Phys.* **2003,** *41,* 94-103.

(272) Ke, Z.; Yongping, B. *Mater. Lett.* **2005,** *59,* 3348-3351.

(273) Dunkerley, E.; Schmidt, D. *Macromolecules* **2010,** *43,* 10536-10544.

(274) Nolte, A. J.; Treat, N. D.; Cohen, R. E.; Rubner, M. F. *Macromolecules* **2008,** *41,* 5793-5798.

(275) Horrocks, A. R.; Wang, M. Y.; Hall, M. E.; Sunmonu, F.; Pearson, J. S. *Polym Int* **2000,** *49,* 1079-1091.

(276) Li, Y.-C.; Mannen, S.; Morgan, A. B.; Chang, S.; Yang, Y.-H.; Condon, B.; Grunlan, J. C. *Adv. Mater.* **2011,** *23,* 3926-3931.

(277) Duskova, D.; Marounek, M.; Brezina, P. *J. Sci. Food Agric.* **2000,** *81,* 36-41.

(278) Graf, E.; Eaton, J. W. *Free Radical Biol. Med.* **1990,** *8,* 61-69.

(279) Stodolak, B.; Starzynska, A.; Czyszczon, M.; Zyla, K. *Food Chem.* **2007,** *101,* 1041-1045.

(280) Shamsuddin, A. M.; Vucenik, I.; Cole, K. E. *Life Sci.* **1997,** *61,* 343-354.

(281) Fox, C. H.; Eberl, M. *Complement Ther Med* **2002,** *10,* 229-234.

(282) Kunyanga, C. N.; Imungi, J. K.; Okoth, M. W.; Biesalski, H. K.; V., V. *Ecol. Food Nutr.* **2011,** *50,* 452-471.

(283) Lee, S.-H.; Park, H.-J.; Chun, H.-K.; Cho, S.-Y.; Cho, S.-M.; Lillehoj, H. S. *Nutr Res* **2006,** *26,* 474-479.

(284) Tang, F.; Wang, X.; Xu, X.; Li, L. *Colloids Surf. Physicochem. Eng. Aspects* **2010,** *369,* 101-105.

(285) Zeng, L.; Qin, C.; Wang, L.; Li, W. *Carbohydr. Polym.* **2011,** *83,* 1553-1557.

(286) Leu, T.-S.; Wang, C.-S. *J. Appl. Polym. Sci.* **2004,** *92,* 410-417.

(287) Toldy, A.; Toth, N.; Anna, P.; Marosi, G. *Polym. Degrad. Stab.* **2006,** *91*.

(288) Fontaine, G.; Bourbigot, S. *J. Appl. Polym. Sci.* **2009,** *113,* 3860-3865.

(289) Weil, E. D.; Levchik, S. V., *Flame Retardants for Plastics and Textiles: Practical Applications*. Hanser Publishers: Cincinnati, OH 2009.

(290) Lecoeur, E.; Vroman, I.; Bourbigot, S.; Lam, T. M.; Delobel, R. *Polym. Degrad. Stab.* **2001,** *74,* 487-492.

(291) Yang, C. Q.; He, Q.; Lyon, R. E.; Hu, Y. *Polym. Degrad. Stab.* **2010,** *95,* 108-115.

(292) Reda, S. Y. *Cien Tecnol Aliment* **2011,** *31,* 475-190.

(293) Lyon, R. E.; Crowley, S.; Walters, R. N. *Fire Mater.* **2008,** *32,* 199-212.

(294) Gaan, S.; Sun, G. *J. Anal. Appl. Pyrolysis* **2007,** *78,* 371-377.

(295) Wei, P.; Hao, J.; Du, J.; Han, Z.; Wang, J. *J. Fire Sci.* **2003,** *21,* 17-28.

(296) Ma, Z.-L.; Fan, C.-R.; Lu, G.-Y.; Liu, X.-Y.; Zhang, H. *J. Appl. Polym. Sci.* **2012,** *125,* 3567-3574.

(297) Bourbigot, S.; Le Bras, M.; Delobel, R.; Decressain, R.; Amoureux, J.-P. *J. Chem. Soc., Faraday Trans.* **1996,** *92,* 149-158.

(298) Cerna, M.; Barros, A. S.; Nunes, A.; Rocha, S. M.; Delgadillo, I.; Copikova, J.; Coimbra, M. A. *Carbohydr. Polym.* **2003,** *51,* 383-389.

(299) Choi, J. H.; Choi, W. Y.; Cha, D. S.; Chinnan, M. J.; Park, H. J.; Lee, D. S.; Park, J. M. *LWT- Food Sci Technol* **2005,** *38,* 417-423.

(300) Rabea, E. I.; Badawy, M. E.; Stevens, C. V.; Smagghe, G.; Steurbaut, W. *Biomacromolecules* **2003,** *4,* 1457-1465.